IN-SITU RESPONSE TIME TESTING OF PLATINUM RESISTANCE THERMOMETERS

EPRI NP-459
(Research Project 503-3)

Key Phase Report

January 1977

Prepared by

THE UNIVERSITY OF TENNESSEE
Nuclear Engineering Department
Knoxville, Tennessee

PRINCIPAL INVESTIGATORS
T. W. Kerlin
L. F. Miller
J. E. Mott
B. R. Upadhyaya
H. M. Hashemian
J. S. Arendt

Prepared for

Electric Power Research Institute
3412 Hillview Avenue
Palo Alto, California 94304

EPRI Project Manager
David G. Cain

FOREWORD

This key phase report summarizes the first of a two year effort by the University of Tennessee to develop techniques for verifying resistance temperature detector (RTD) time response capability in-situ. EPRI support for this project is motivated by requirements for checking sensor time responses in nuclear plant safety systems and lack of a practical means of doing so.

In the report three methods for verifying (RTD) response capabilities are described: (1) loop current step response; (2) static self-heating; and (3) noise analysis. Theory, application and initial experimental results establish the strength and weaknesses of each method.

The loop current step response (LCSR), which provides an equivalent step response by transformation, is relatively simple to carry out. Although this report (p. 52) states that the LCSR method will not work for Rosemount 176 KF Temperature sensors, laboratory and in-plant testing subsequent to preparation of this report indicates this conclusion is in error. The problem has been traced to the software used in digital reduction of the test data. Recent results suggest that estimates of (63%) time constants for plunge test using the LCSR approach are accurate to within approximately 0.1 sec.

The self-heating approach is the simplest of all methods but does not provide an absolute measurement of RTD response. Moreover, the measurement is static, providing no information as to variation in sensor heat capacity.

Noise analysis is completely passive and can be done on-line. However, data processing and statistical estimation are complex procedures. The technique may be limited by inability to reliably distinguish between sensor and process dynamics.

Subsequent project work will seek to refine both the self-heating and the loop current step response methods to facilitate plant application by utility personnel. Test instrumentation design and test procedures will be provided along with results from additional in-plant tests at Westinghouse, Babcock and Wilcox, and Combustion Engineering units. The in-plant data, augmented by laboratory calibrations, should enable ready comparison and confirmation of field test results.

Two related projects concerned with sensor response time have been undertaken by EPRI. The Nuclear Services Corporation has completed a project concerned with safety-related pressure transducers. Results were published as EPRI report NP-267. A project with Babcock and Wilcox Company is devoted exclusively to response verification of pressure and temperature sensors using the process noise approach. The work by Babcock and Wilcox is on-going and will be documented by a final report when completed.

D.G. Cain
Project Manager

ABSTRACT

This report provides interim results of Research Project 503-3, concerned with in-situ resistance temperature detector (RTD) time response verification. The report covers the theoretical bases, laboratory experimentation, and limited in-plant testing of three prospective methods. Sensors employed in this project represent those which are presently employed in safety-related applications in the field, namely Rosemount models 176KF, 177GY, and 104AFC.

ACKNOWLEDGEMENT

The help of a number of individuals and organizations is gratefully acknowledged.

R. L. Shepard and R. M. Carroll of Oak Ridge National Laboratory contributed significantly through their discussions and by arranging for equipment loans.

Florida Power and Light and Duke Power Company permitted testing in their nuclear power plants.

Combustion Engineering, Inc., Florida Power and Light Company, and Duke Power Company provided platinum resistance thermometers for laboratory testing.

TABLE OF CONTENTS

1.0 INTRODUCTION

1.1 Historical Background

The response time has been considered an important property of resistance temperature detectors (RTD's) since their early use for industrial temperature measurement. Classically, the response was measured prior to installation in the plant utilizing a measurement that involved plunging the sensor into flowing water. The time constant was usually defined as the time required to reach 63.2 per cent of the final response following a step change in fluid temperature.

The Nuclear Regulatory Commission added a new dimension to sensor response time measurement when it recommended that utilities operating nuclear power plants make in-situ time response measurements of sensors installed in the plant. This recommendation was promulgated in U. S. Nuclear Regulatory Guide 1.118.

1.2 Objectives of This Research

The research reported herein has the objective of developing a method for in-situ response time testing of platinum resistance thermometers of the type used in modern pressurized water reactors. The test is only required to show that the response time is less than a specified maximum allowable value; but, of course, actual determination of the response time is also acceptable. In addition, the testing method should have these characteristics:

1. Technical acceptability so as to receive Nuclear Regulatory Commission approval
2. Minimal cost for special equipment
3. Minimal complexity.

1.3 Approaches for In-Situ Testing

Several methods are plausible for in-situ testing of resistance temperature detectors (RTD's). The two broad categories are: (1) fluid temperature perturbations external to the RTD, and (2) internal perturbations of the RTD by ohmic heating in the sensing wire. Applicable methods related to fluid temperature perturbations involve:

1. analysis of the fluctuations in the sensor output during normal operation (noise analysis)
   a. using time series analysis
   b. using frequency domain analysis
   c. using correlation function analysis[1]
2. analysis of induced temperature fluctuations
   a. using control rod motions to cause power changes and concomitant temperature changes
   b. using steam valve or feedwater valve perturbations to induce primary fluid temperature changes
   c. using special local devices near the sensor such as fluid injection ports or small electrical heating elements.

Those related to internal perturbations include the analysis of:

1. a transient sensor output induced by above-normal current that causes ohmic heating of the sensor filament (usually called a loop current step response test)[2,3]
2. the steady state measurement of temperature rise vs. ohmic heating level in the sensor filament (usually called a self heating test).

In this report, the methods considered are:

1. noise analysis (using time series analysis)
2. the self-heating test
3. the loop current step response (LCSR) test.

These methods are used since they require no system modification and can be accomplished with a modest investment for test equipment. Induced fluid temperature perturbations are omitted because: (a) transients induced with control rods, steam valves or feedwater valves involve test complexity that is probably unnecessary for sensor response measurement (though these methods may be useful for measuring lags due to by-pass lines used for some sensor installations), and (b) special in-pipe hardware would involve an expensive plant modification that is unwarranted. Furthermore, testing by a remove-and-test procedure or a simple periodic replacement is ruled out because these methods ignore the important effects of the environment in the pipe where the measurement is to be made.

Noise analysis is a well established diagnostic procedure. It is used herein to identify the sensor dynamics so that an impulse response can be obtained. Knowing the impulse response, one can readily determine the step response. Consequently, the time constant associated with a plunge test can be identified. Details relating to the application of noise analysis for this research are given in Section 7.0.

The physical basis for the self-heating test is that the temperature rise in a system with a given internal heat generation rate is inversely proportional to the overall heat transfer coefficient. Thus, the slope of the curve of temperature rise versus heat generation rate due to ohmic heating in the sensor element (the self-heating curve) is inversely

proportional to the heat transfer coefficient. A change in the slope of the self-heating curve indicates a change in the heat transfer resistance. A change in effective heat capacity of the RTD system would change the response time, but would not change the slope of the self-heating curve. However, only a change in the heat transfer resistance is considered plausible. Additional details pertaining to the self-heating method are given in Section 6.0.

The loop current step response (LCSR) test exploits the fact that heat transfer resistances and heat capacities are independent of the direction of heat flow. Thus, the same heat transfer characteristics control the transient response following a change in ohmic heating in the sensor that control the transient response following a change in fluid temperature change. Of course, the transients are not the same for both perturbations. For a fluid temperature change, the heat must diffuse through the assembly to the sensing wire. For an ohmic heating change, the heat is generated exactly at the point of measurement, then it diffuses through the sensor assembly to the fluid.

Since the response to a fluid temperature change is desired and the response to a change in ohmic heating is feasible in an installed RTD, there is a need to transform the ohmic heating transient into the transient that would occur if the fluid temperature changes. This has been done for the case of a step change in ohmic heating and is referred to as the loop current step response transformation.[4] The transformation may be performed analytically for RTD's that meet two conditions necessary in the theoretical development (predominately one-dimensional heat transfer and a centrally located sensing wire). For sensors that do not meet these

conditions, empirical transformations obtained from laboratory results may be used. Details of the LCSR method appear in Section 5.

2.0 RESISTANCE THERMOMETRY

2.1 Material Requirements

Resistance thermometry exploits the temperature dependence of metals to monitor temperature. Desirable properties of materials for resistance thermometry are:

1. large temperature coefficient of resistance
2. linear curve of temperature vs. resistance
3. chemical inertness
4. ductility
5. mechanical strength.

Platinum is an excellent material to provide these characteristics, and most industrial resistance thermometers use platinum wire as the sensing element.

2.2 RTD Characteristics

An RTD usually consists of a fine platinum wire wound on a support structure mounted inside a metal sheath (usually stainless steel) that is back filled with magnesium oxide. The support structure is designed to minimize stress on the wire because stress affects the sensor performance. Magnesium oxide is used to provide electrical isolation of the sensing wire from the sheath and to provide thermal coupling between the wire and the sheatn. The magnesium oxide is compacted, often by centrifuging after filling the sheath with magnesium oxide powder during construction.

RTD's may be designed for direct immersion into a fluid stream (wet type) or for installation into a well in the stream (well type). To improve the heat transmission in well-type sensors, a thermal bounding material is often used in the gap between the sheath and the well.

The sensors found in pressurized water reactors manufactured by different vendors are quite different. Table 2.1 gives specifications on some of the commonly-used sensors. Figures 2.1 through 2.4 show these sensors and X-rays to reveal their internal characteristics.

The resistance element is connected to lead wires that connect to appropriate instrumentation. Sensors may be constructed with the lead wire configurations shown in Figure 2.5. The multiple lead and dummy wire configurations are used in measurement systems to compensate for lead wire resistance to obtain accurate temperature measurements. RTD's are made with single sensing elements per sheath and with dual elements that allow two independent measurements with the same sensor.

The temperature coefficient of resistance of pure annealed platinum wire is 0.003925 $\frac{\text{ohms}}{\text{ohm}}$/°C (0.002181 $\frac{\text{ohms}}{\text{ohm}}$/°F). By selecting the wire length and diameter, one can obtain various values of absolute resistance at any temperature. Standard sensors have 100 ohms at 0°C or 200 ohms at 0°C. Temperature coefficients depend on platinum purity, and commercial sensors usually have slightly smaller temperature coefficients than pure platinum. A pure platinum 100 ohm sensor would have a temperature coefficient of 0.3925 ohms/°C (.2181 ohms/°F), and a pure platinum 200 ohm sensor would have a temperature coefficient of 0.7850 ohms/°C (0.4361 ohms/°F). Temperature coefficients for commercial sensors are typically 80 to 90 percent as large as for those with pure platinum elements.

TABLE 2-1

Sensor Manufacturer	Model Number	Plants Where Used	Wet Type Or Well Type	Sensor Sheath O.D.	Well O.D.	Number of Sensing Elements Per RTD	2 Wire 3 Wire or 4 Wire	Dummy Wire?	Resistance at 0°F $R_o(\Omega)$
REC*	177-GY	B&W	wet	.335"	---	2	4	no	100
REC	177HW	B&W	well	.290"	.410"	2	4	no	100
REC	104-AFC	C.E.	well	**---	.281"	1	2	yes	200
REC	176-KF	Westinghouse	wet	.375"	---	4	4	no	200

*Rosemount Engineering Company.

**Measurement not available.

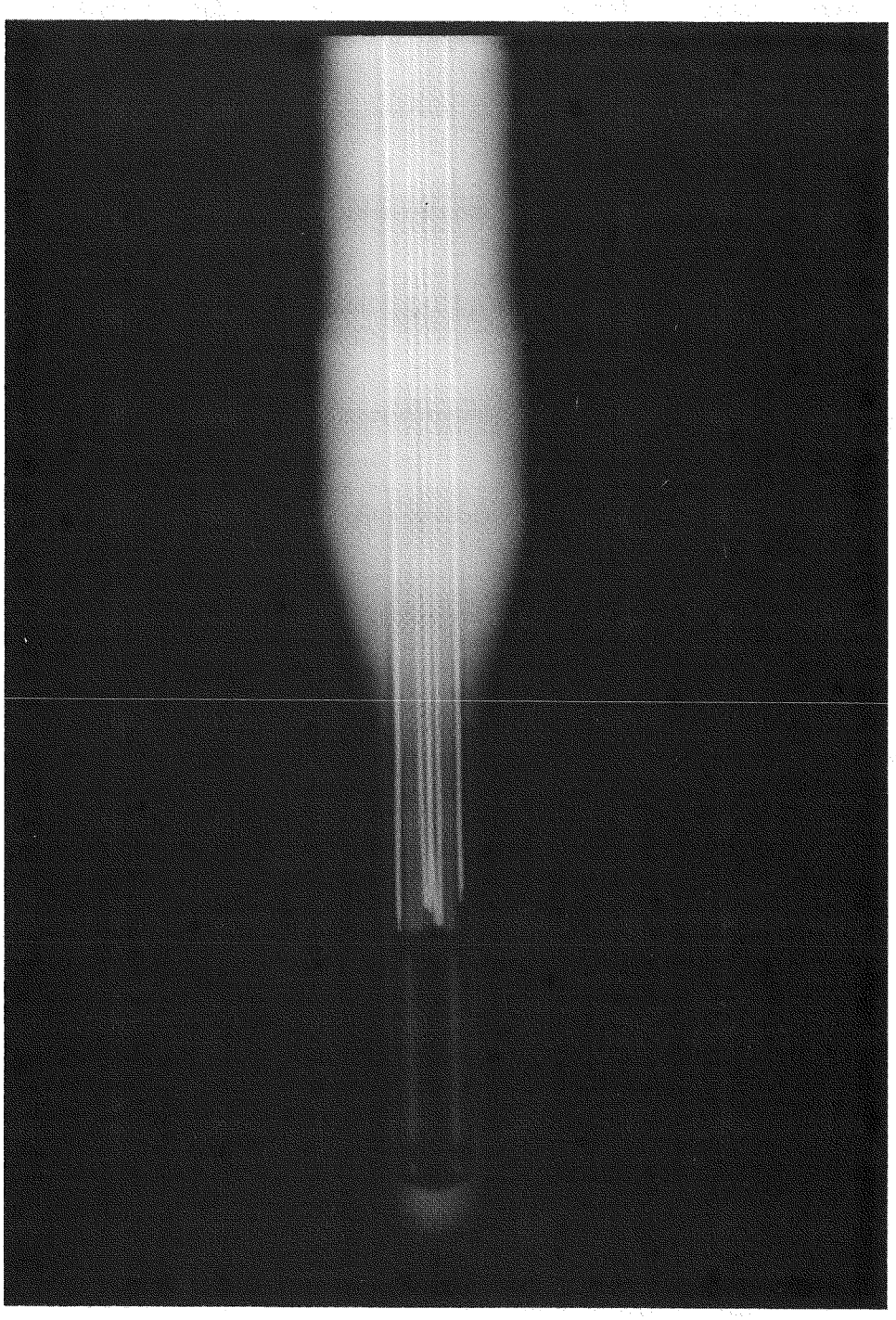

Figure 2.1a X-Ray of the Rosemount 177GY Sensor.

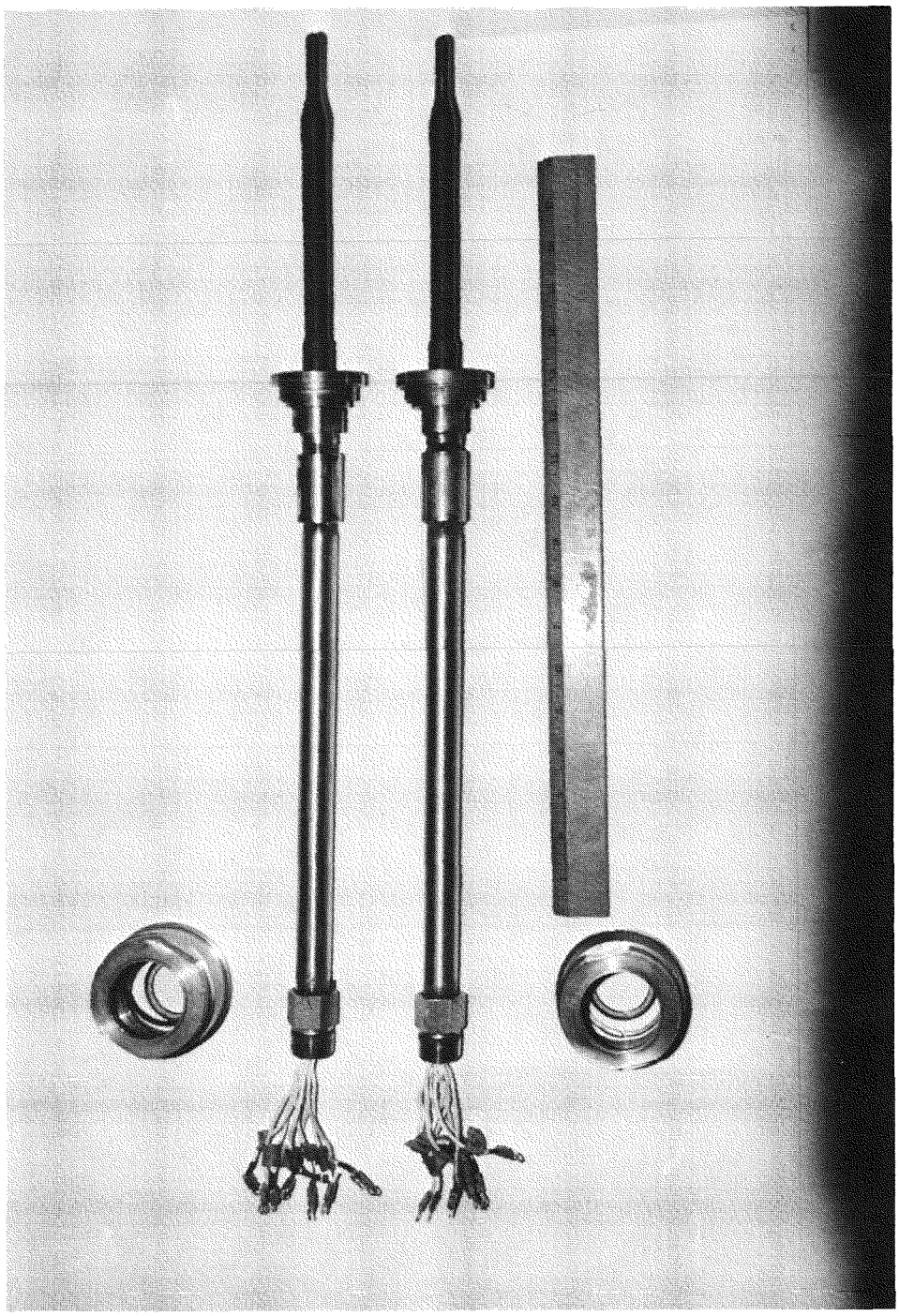

Figure 2.1b Picture of the Rosemount 177GY Sensor.

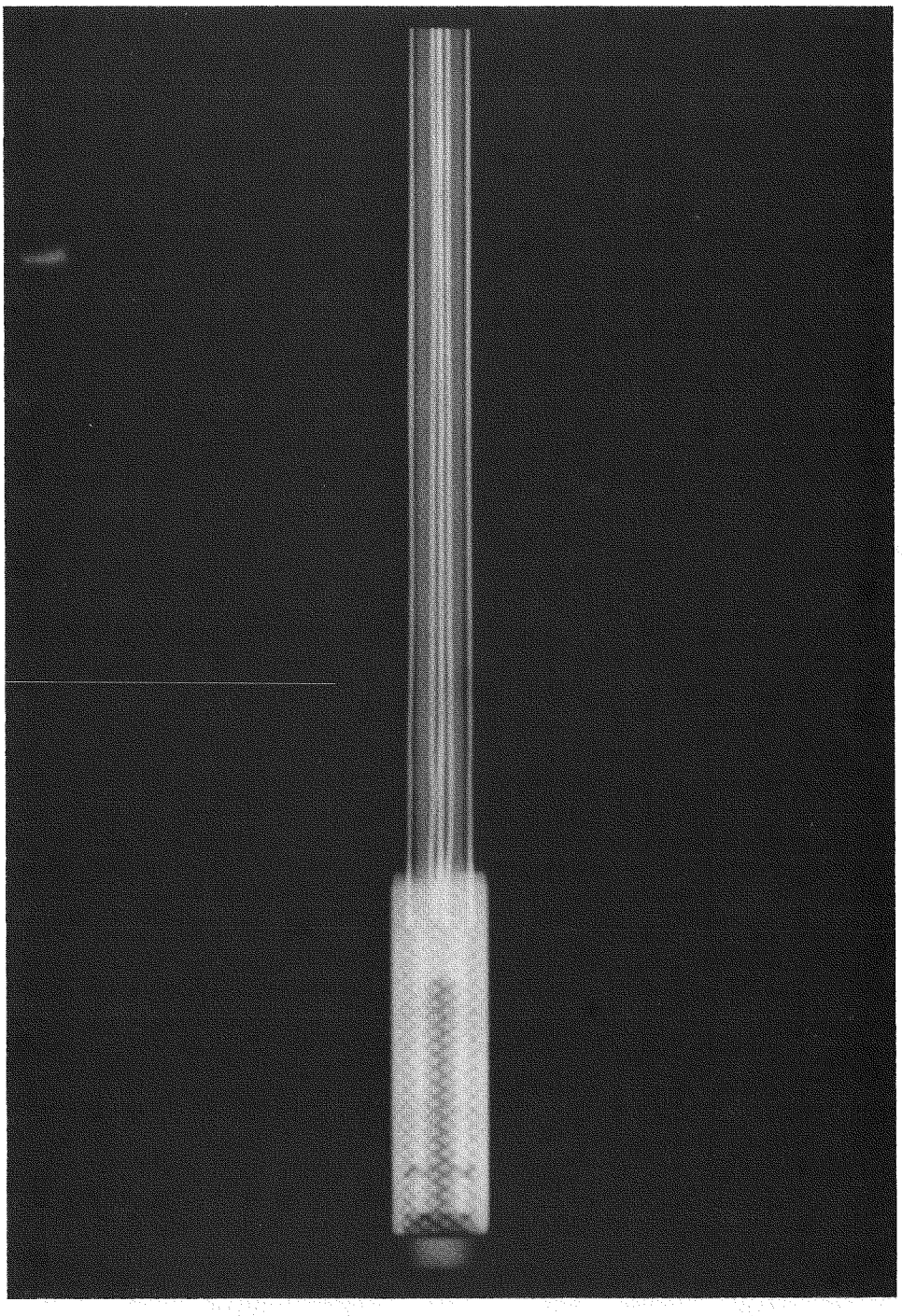

Figure 2.2a X-Ray of the Rosemount 177-HW Sensor.

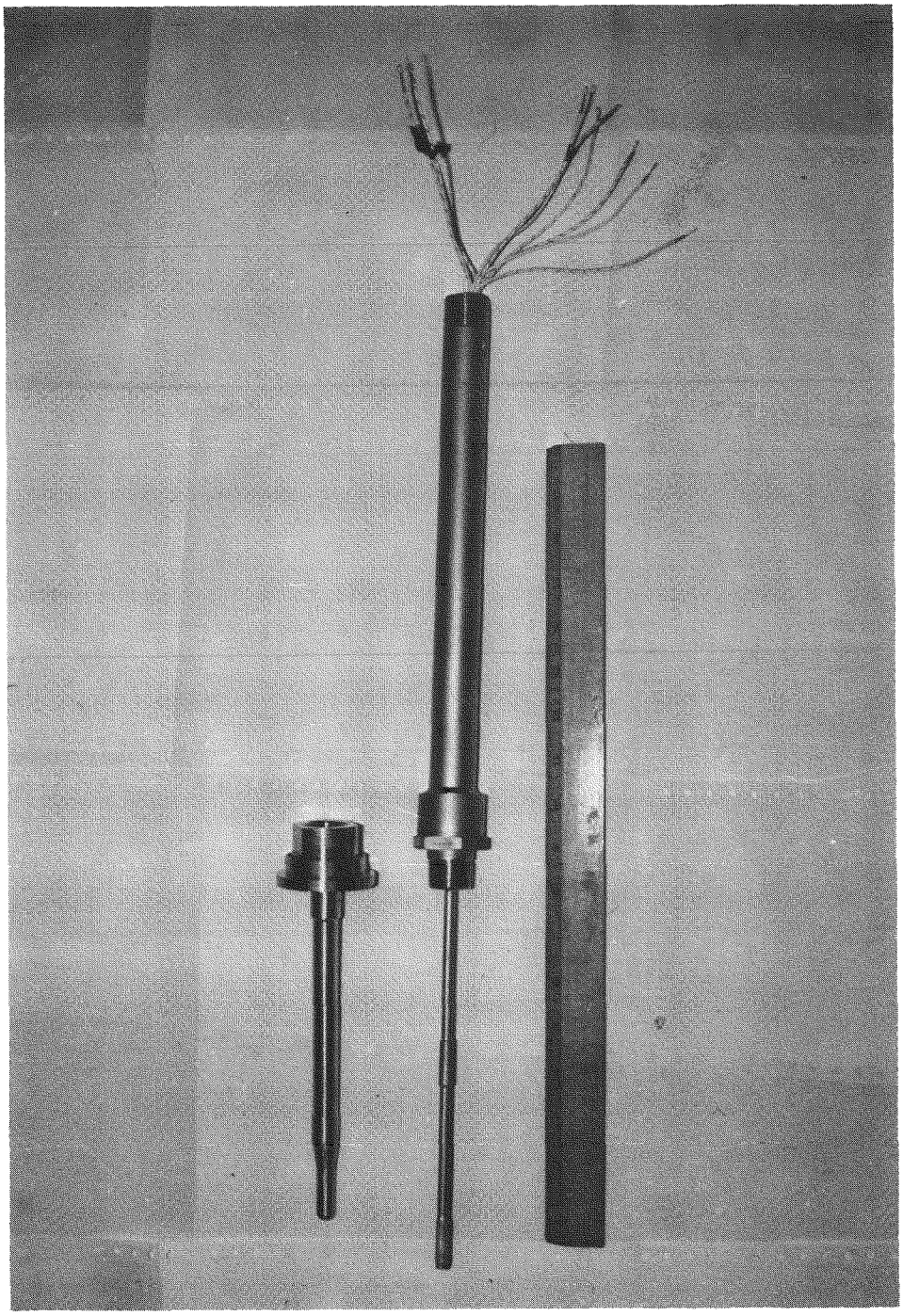

Figure 2.2b Picture of the Rosemount 177-HW Sensor.

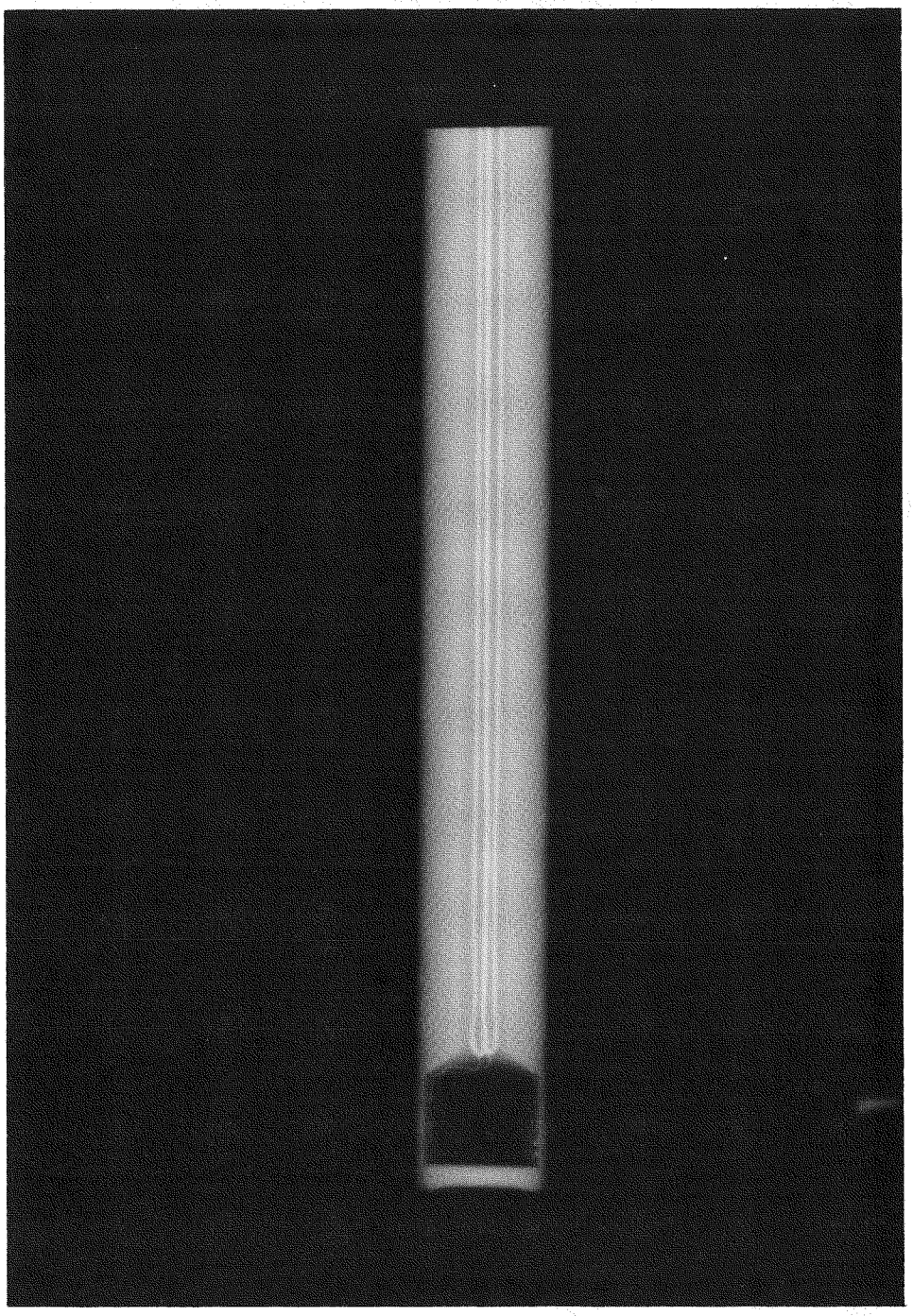

Figure 2.3a X-Ray of the Rosemount 177-KF Sensor

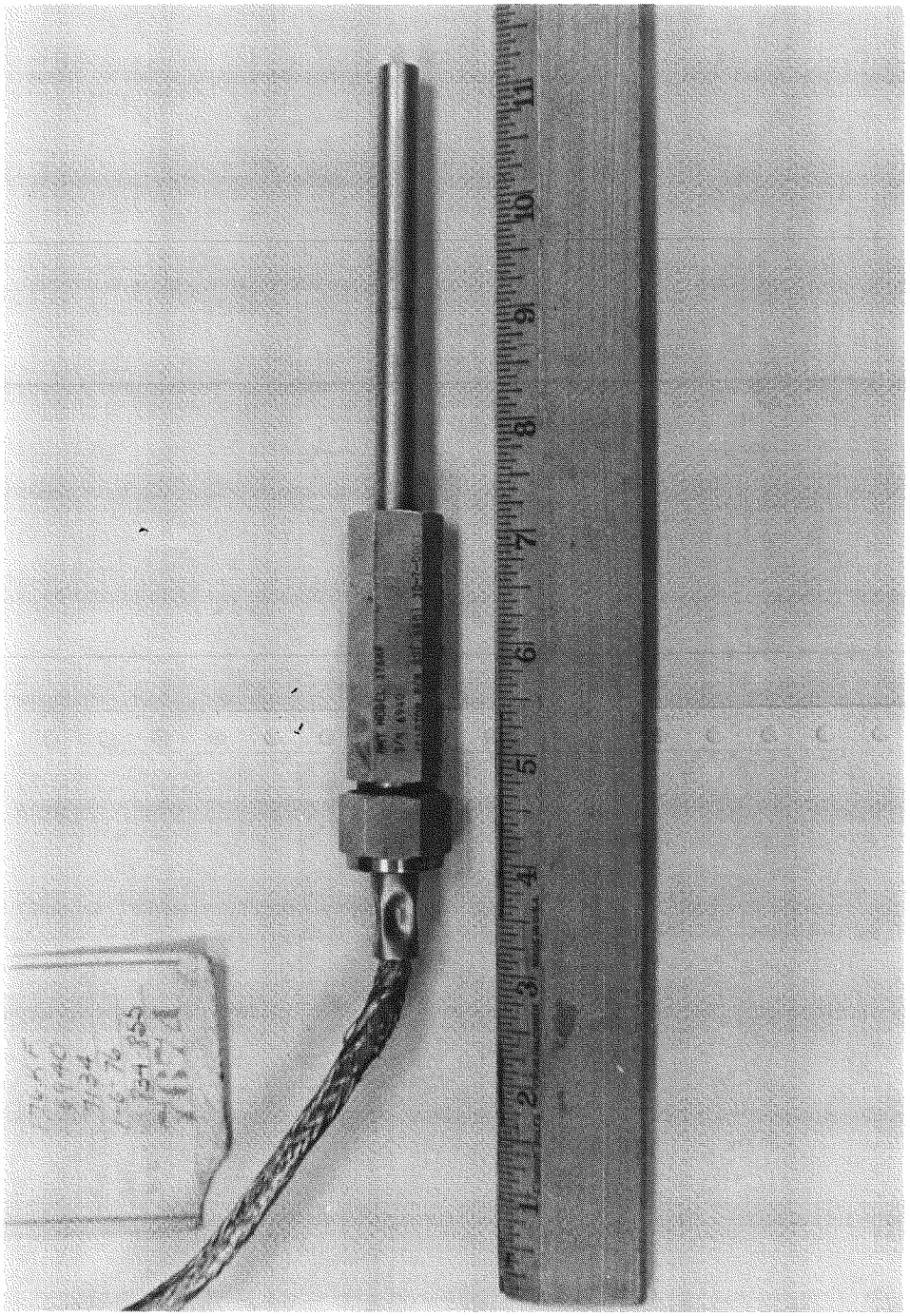

Figure 2.3b Picture of the Rosemount 177-KF Sensor.

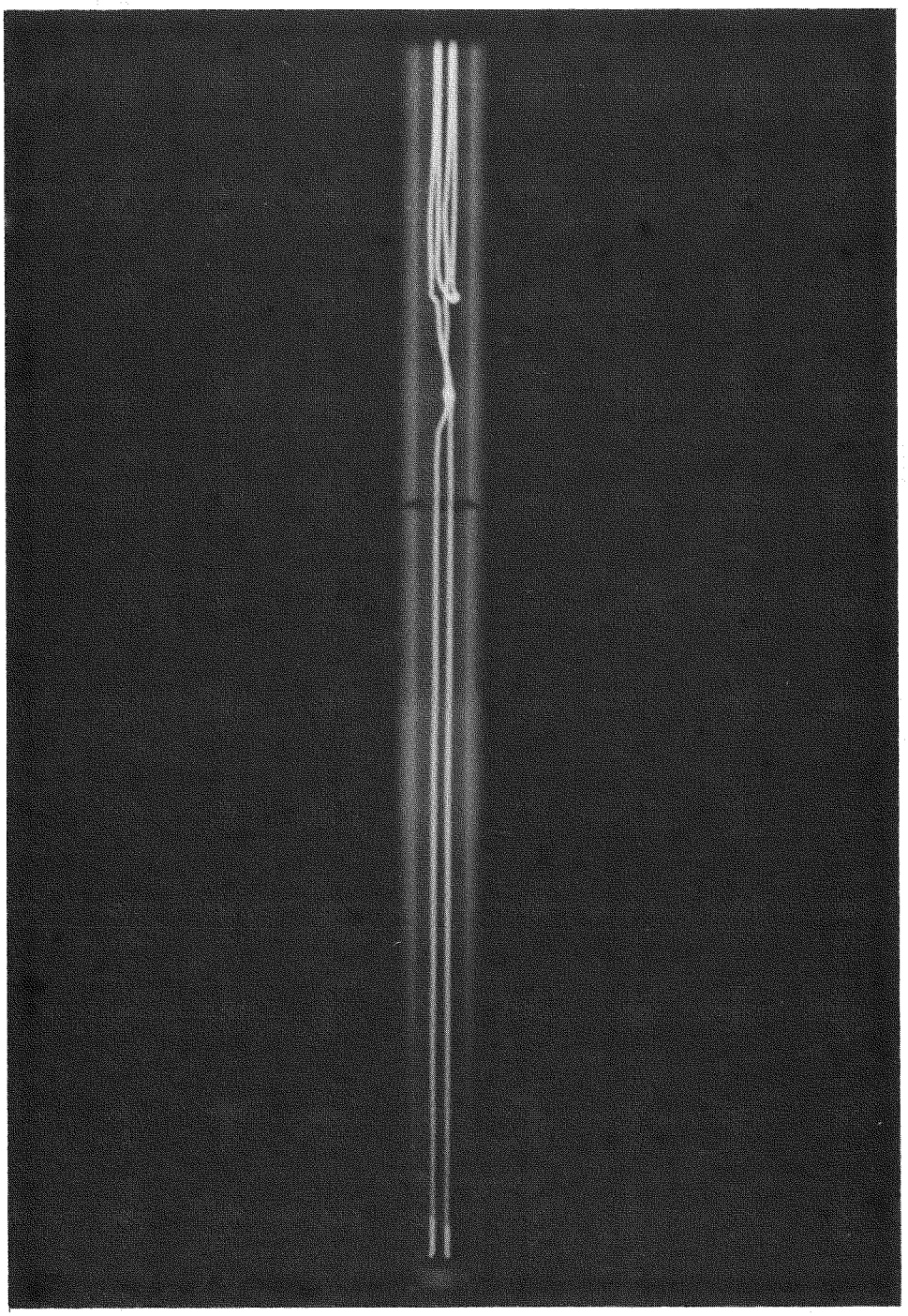

Figure 2.4 X-Ray of the Rosemount 104-AFC Sensor.

a) 2 Wire

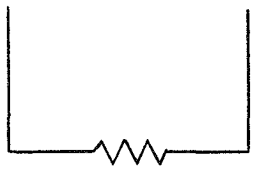

b) 3 Wire

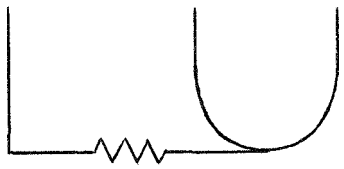

c) 4 Wire

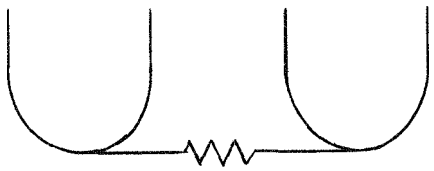

d) 2 Wire with Dummy

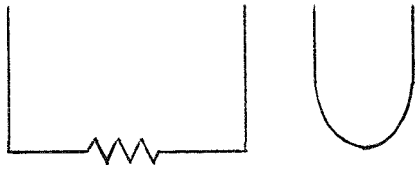

Figure 2.5 Possible Lead Wire Configurations for RTDs.

2.3 RTD Instrumentation

The instrumentation used in resistance thermometry is usually a bridge circuit as shown in Figure 2.6. Various special methods for connecting multiple-wire RTD's are available, but all use the same basic Wheatstone bridge circuit. If the two fixed resistors have the same resistance, R_a, then the RTD resistance can be determined by finding the value for the variable resistance, R_d, that nulls the voltage drop, ΔV. If the bridge is used in the non-nulling mode then changes in the RTD resistance are related to the voltage drop across the two arms of the bridge by

$$\Delta V = \frac{(R_d - R_{RTD})\, R_a}{(R_a + R_d)\,(R_a + R_{RTD})}\quad E. \tag{2.1}$$

Note that the voltage drop is approximately linearly related to the RTD resistance for bridges in which the change in the sensor resistance is small compared to the sum of the original RTD resistance and the fixed resistance, R_a.

The voltage, E, used in normal applications is selected to give insignificant ohmic heating in the RTD. The self heating effect is quantified by the self heating coefficient expressed in ohms/mw. A typical value is 8×10^{-3} ohms/mw for a 100 ohm sensor. For such a sensor with a 2 ma sensing current, the heat generation rate is 0.4 mw. This gives a resistance change of 3.2×10^{-3} ohms with a resulting temperature measurement error of 8.15×10^{-3}°C. Similar calculations show that a 50 ma current would give a temperature increase of 5.62°C (10.1°F).

3.0 THE LOOP CURRENT STEP RESPONSE TRANSFORMATION

3.1 Introduction

The result of interest is the time constant associated with a step change in fluid temperature external to the sensor. The time

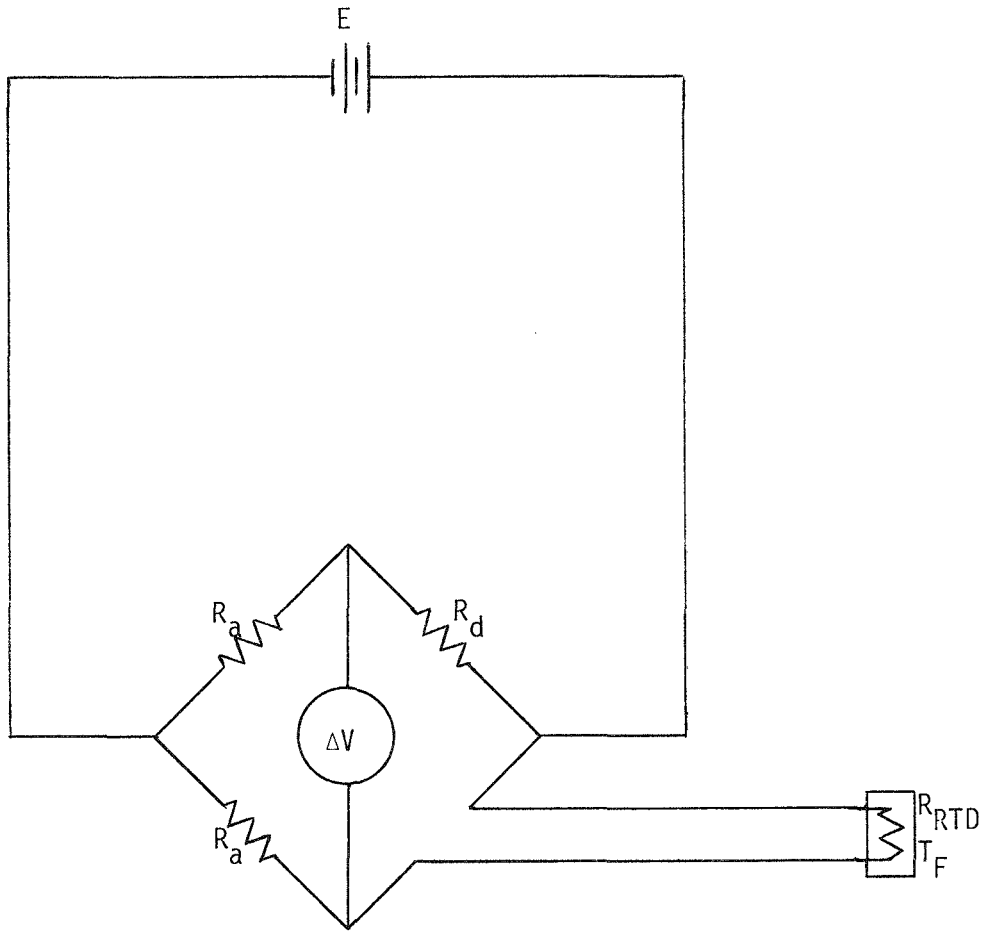

Figure 2.6 A Typical Bridge Circuit Used in Conjunction with an RTD.

constant is defined to be the time required for the sensor output to reach 63.2 percent of its final steady-state value after a step change in fluid temperature. This time constant is usually obtained from a plunge test in a laboratory environment. Since the plunge test cannot be used to obtain the time constant of an installed RTD, the LCSR test is proposed as one method to obtain an estimate of the desired plunge test time constant.

A transformation is needed to convert LCSR data into a prediction of the response that would occur following a fluid temperature step change. The transformation may be developed using a general nodal model for sensor heat transfer. The development is independent of the number of nodes included in the model, so use of this approach does not imply any restrictive assumptions. The following sections give some details on RTD heat transfer that permit formulation of a transformation and that define the conditions for validity of the transformation.

3.2 Mathematical Development of the LCSR Transformation

An analytical transformation for converting loop current step response (LCSR) test results into plunge test results may be developed using a general nodal model for sensor heat transfer. Consider first a system with predominantly one-dimensional heat transfer. In this case, the nodal model may be represented schematically as shown in Figure 3.1. The accuracy of such a model may be made as great as desired by using enough nodes.

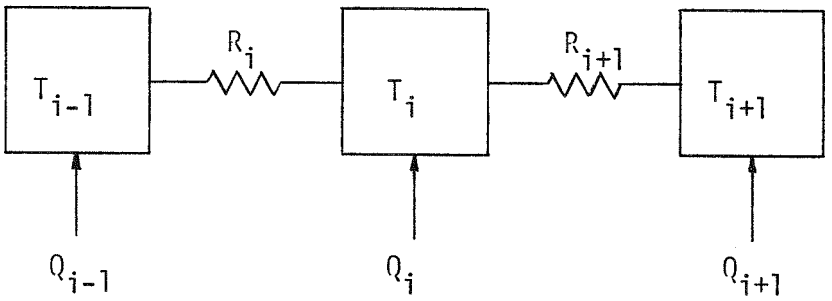

Figure 3.1 Schematic of a One-Dimensional Node-to-Node Heat Transfer Model.

The dynamic heat transfer equation for node i is:

$$(MC)_i \frac{dT_i}{dt} = \frac{1}{R_{i-1}} (T_{i-1} - T_i) - \frac{1}{R_i} (T_i - T_{i+1}) + Q_i \qquad (3.1)$$

where Q_i = heat generation rate in node i

M_i = mass of material in node i

C_i = specific heat capacity of material in node i

R_i = heat transfer resistance for node i-1 to node i

T_i = temperature of node i.

Dividing through by $(MC)_i$ and defining constants gives

$$\frac{dT_i}{dt} = a_{i,i-1} T_{i-1} - a_{i,i} T_i + a_{i,i+1} T_{i+1} + b_i Q_i \qquad (3.2)$$

where

$$a_{i,i-1} = \frac{1}{(MC)_i R_{i-1}}$$

$$a_{i,i} = \frac{1}{(MC)_i} \left(\frac{1}{R_{i-1}} + \frac{1}{R_i}\right)$$

$$a_{i,i+1} = \frac{1}{(MC)_i R_i}$$

$$b_i = \frac{1}{(MC)_i} .$$

The nodal equations may be applied to a series of nodes, starting at the node closest to the center (i=1) and ending with the node closest to the surface (i=N). The equations have the form:

$$\frac{dT_1}{dt} = -a_{11} T_1 + a_{12} T_2 + b_1 Q_1$$

$$\frac{dT_2}{dt} = a_{21} T_1 - a_{22} T_2 + a_{23} T_3 + b_2 Q_2$$

$$\frac{dT_3}{dt} = a_{32}\, T_2 - a_{33}\, T_3 + a_{34}\, T_4 + b_3\, Q_3$$

.

.

.

$$\frac{dT_N}{dt} = a_{N,N-1}\, T_{N-1} - a_{N,N}\, T_N + C_{N,F} T_F + b_N\, Q_N$$

where

T_F = fluid temperature.

These equations may be written in matrix form:

$$\frac{d\bar{x}}{dt} = A\,\bar{x} + B\,\bar{q} + \bar{c}\,T_F \qquad (3.3)$$

where

$$\bar{X} = \begin{bmatrix} T_1 \\ T_2 \\ T_3 \\ . \\ . \\ . \\ T_N \end{bmatrix} \qquad A = \begin{bmatrix} -a_{11} & a_{12} & 0 & 0 & \cdots & \\ a_{21} & -a_{22} & a_{23} & 0 & \cdots & \\ 0 & a_{32} & -a_{33} & a_{34} & \cdots & \\ . & & & & & \\ . & & & & & \\ . & & & & & \\ & & & & & a_{N,N-1} - a_{N,N} \end{bmatrix}$$

$$B = \begin{bmatrix} b_1 & 0 & 0 & \cdots & \\ 0 & b_2 & 0 & \cdots & \\ 0 & 0 & b_3 & \cdots & \\ & & & & b_N \end{bmatrix} \qquad \bar{q} = \begin{bmatrix} Q_1 \\ Q_2 \\ Q_3 \\ . \\ . \\ . \\ Q_N \end{bmatrix}$$

Laplace transformation gives:

$$[sI-A]\ \bar{x}(s) = \bar{c}\ T_F(s) + B\ \bar{q}(s). \tag{3.4}$$

The Laplace transform solution for the response of any node, x_i, may be found using Cramer's rule. Let us consider several cases:

1--central node, no heat generation in any nodes, fluid temperature perturbation, one dimensional heat transfer

$$T_1(s) = \frac{F(s)}{|sI-A|} \tag{3.5}$$

where

$$F(s) = \begin{vmatrix} 0 & -a_{12} & 0 & 0 & \cdots & \\ 0 & (s+a_{22}) & -a_{23} & 0 & \cdots & \\ 0 & -a_{32} & (s+a_{33}) & -a_{34} & \cdots & \\ 0 & 0 & -a_{34} & (s+a_{44}) & \cdots & \\ \cdot & \cdot & \cdot & \cdot & \cdots & \\ \cdot & \cdot & \cdot & \cdot & \cdots & \\ \cdot & \cdot & \cdot & \cdot & \cdots & \\ C_{N,F}T_F(s) & \cdot & \cdot & \cdot & \cdots & -a_{N,N-1} \quad (s+a_{N,N}) \end{vmatrix} \tag{3.6}$$

This may be written

$$F(s) = C_{N,F}\ T_F(s)\ (-1)^{(N+F)} \begin{vmatrix} -a_{12} & 0 & 0 & \cdots & \\ (s+a_{22}) & -a_{23} & 0 & \cdots & \\ -a_{32} & (s+a_{33}) & -a_{34} & \cdots & \\ \cdot & \cdot & \cdot & \cdots & \\ \cdot & \cdot & \cdot & \cdots & \\ \cdot & \cdot & \cdot & & -a_{N-1,N-1} \end{vmatrix} \tag{3.7}$$

This determinant is for a matrix in lower triangular form (All elements above the diagonal are zero). The determinant is given by the product of the diagonals, all of which are constants. Therefore, for a fluid temperature perturbation in a one-dimensional heat transfer system, the response of the central node is characterized by a transfer function with no zeroes. If the sensing element in an RTD is centrally located, then this type of transfer function describes the response characteristics of the sensor.

The transfer function may be written

$$\frac{T_1(s)}{T_F(s)} = \frac{K}{|sI-A|}$$

$$= \frac{K}{(s-p_1)\ (s-p_2)\ \ldots} \tag{3.8}$$

where

p_i = poles (identical to eigenvalues of A).

For a unit step change in T_F, $T_F(s) = \frac{1}{s}$, and we may write:

$$T_1(s) = \frac{K}{s(s-p_1)\ (s-p_2)\ \ldots}\ . \tag{3.9}$$

Inversion of this Laplace transform using the residue theorem gives:

$$T_1(t) = K\left[\frac{1}{(-p_1)\ (-p_2)\ \ldots\ (p_N)} + \frac{e^{p_1 t}}{(p_1)\ (p_1-p_2)\ \ldots}\right.$$

$$\left. + \frac{e^{p_2 t}}{(p_2)\ (p_2-p_1)\ \ldots} + \ldots\right]. \tag{3.10}$$

Thus, we make the following important observation:

For an RTD with predominantly one dimensional heat transfer and a centrally located sensing element,

the poles alone (no zeroes) are adequate to characterize the response to a fluid temperature change.

The implication is that if one can identify the poles by some other test (such as the LCSR), then he can construct the response to a fluid temperature step.

2--non-central node, no heat generation in any nodes, fluid temperature perturbation, one dimensional heat transfer.

This case may be analyzed for the response of any non-central node, but for notational simplicity, let us consider the response of the second node. In this case

$$T_2(s) = \frac{F(s)}{|sI-A|} \tag{3.11}$$

where

$$F(s) = \begin{vmatrix} (s+a_{11}) & 0 & 0 & 0 & \cdots \\ -a_{21} & 0 & -a_{23} & 0 & \cdots \\ 0 & 0 & (s+a_{33}) & -a_{34} & \cdots \\ \cdot & \cdot & \cdot & \cdot & \cdots \\ \cdot & \cdot & \cdot & \cdot & \cdots \\ \cdot & \cdot & \cdot & \cdot & \cdots \\ \cdot & C_{N,F}T_F(s) & \cdot & \cdot & \cdots \end{vmatrix} \tag{3.12}$$

This may be written

$$F(s) = C_{N,F}\, T_F(s)\, (-1)^{(2+N)} \begin{vmatrix} (s+a_{11}) & 0 & 0 & 0 \ldots \\ -a_{21} & -a_{23} & 0 & 0 \ldots \\ 0 & (s+a_{33}) & -a_{34} & 0 \ldots \\ . & . & . & . \ldots \\ . & . & . & . \ldots \\ . & . & . & . \ldots \end{vmatrix} \qquad (3.13)$$

Again, we observe that the matrix is triangular, but the diagonals are not all constant. In this case, the transfer function will have one zero. For the response of nodes further from the center, there will be more zeroes. Thus, the poles alone are not adequate to construct the response for an RTD if the sensing element is not located at the center.

3--central node, heat generation in central node, constant fluid temperature, one-dimensional heat transfer

$$T_1(s) = \frac{F(s)}{|sI-A|} \qquad (3.14)$$

where

$$F(s) = \begin{vmatrix} b_1\ Q_1 & -a_{12} & 0 & 0 & \ldots \\ 0 & (s+a_{22}) & -a_{23} & 0 & \ldots \\ 0 & -a_{32} & (s+a_{33}) & -a_{34} & \ldots \\ . & . & . & . & \ldots \\ . & . & . & . & \ldots \\ . & . & . & . & \ldots \end{vmatrix} \qquad (3.15)$$

This may be written

$$F(s) = b_1 Q_1 \begin{vmatrix} (s+a_{22}) & -a_{23} & 0 & 0 & \cdots \\ -a_{32} & (s+a_{33}) & -a_{34} & 0 & \cdots \\ 0 & -a_{43} & (s+a_{44}) & -a_{45} & \cdots \\ \cdot & \cdot & \cdot & \cdot & \cdots \\ \cdot & \cdot & \cdot & \cdot & \cdots \\ \cdot & \cdot & \cdot & \cdot & \cdots \end{vmatrix} \qquad (3.16)$$

In this case, the matrix is not triangular, and the transfer function will have zeroes.

The transfer function may be written:

$$\frac{T_1(s)}{Q_1(s)} = K^1 \frac{(s-z_1)\ (s-z_2)\ \ldots\ (s-z_M)}{(s-p_1)\ (s-p_2)\ \ldots\ (s-p_N)} . \qquad (3.17)$$

For a unit step change in $Q_1(Q_1(s) = \frac{1}{s})$, we obtain

$$T_1(s) = \frac{K^1(s-z_1)\ (s-z_2)\ \ldots\ (s-z_M)}{s(s-p_1)\ (s-p_2)\ \ldots\ (s-p_N)} . \qquad (3.18)$$

Inversion by the residue theorem gives:

$$T_1(t) = K^1\left[\frac{(-z_1)\ (-z_2)\ \ldots\ (-z_M)}{(-p_1)\ (-p_2)\ \ldots\ (-p_N)} + \frac{(p_1-z_1)\ (p_1-z_2)\ \ldots\ (p_1-z_M)}{(p_1)\ (p_1-p_2)\ \ldots\ (p_1-p_N)} e^{p_1 t}\right.$$

$$\left. + \frac{(p_2-z_1)\ (p_2-z_2)\ \ldots\ (p_2-z_M)}{(p_2)\ (p_2-p_1)\ \ldots\ (p_2-p_N)} e^{p_2 t} + \ldots\right]. \qquad (3.19)$$

Note that the response is determined by the zeroes as well as the poles. However, the poles are the same as for the fluid temperature change case. Thus, if we can identify the poles from a LCSR test, we can construct the equivalent fluid perturbation response using Equation (3.10).

4--central node, no heat generation in any nodes, fluid temperature perturbation, multi-dimensional heat transfer.

In this case, there is branching in the heat transfer (see Figure 3.2). This means that the temperature of a node may be influenced by more than just two neighboring nodes as in the one-dimensional case. In the one-dimensional case, all of the elements of the A matrix are on the diagonal or in the position adjacent to the diagonal. In the multi-dimensional case, coupling terms appear in other positions (always symmetrically positioned around the diagonal). Thus F(s) may be written

$$F(s) = \begin{vmatrix} 0 & -a_{12} & * & * & \cdots \\ 0 & (s+a_{22}) & -a_{23} & * & \cdots \\ \cdot & -a_{32} & (s+a_{33}) & -a_{34} & \cdots \\ \cdot & * & * & * & \cdots \\ \cdot & \cdot & \cdot & \cdot & \cdots \\ \cdot & \cdot & \cdot & \cdot & \cdots \\ \cdot & \cdot & \cdot & \cdot & \cdots \\ C_{N,F}T_F(s) & \cdot & \cdot & \cdot & \cdots \end{vmatrix} \qquad (3.20)$$

where

* = possible new coupling terms.

In this case, the matrix is not triangular and zeroes can occur. This means that the availability of the poles through some sort of measurement is not sufficient for construction of the response to a fluid temperature step.

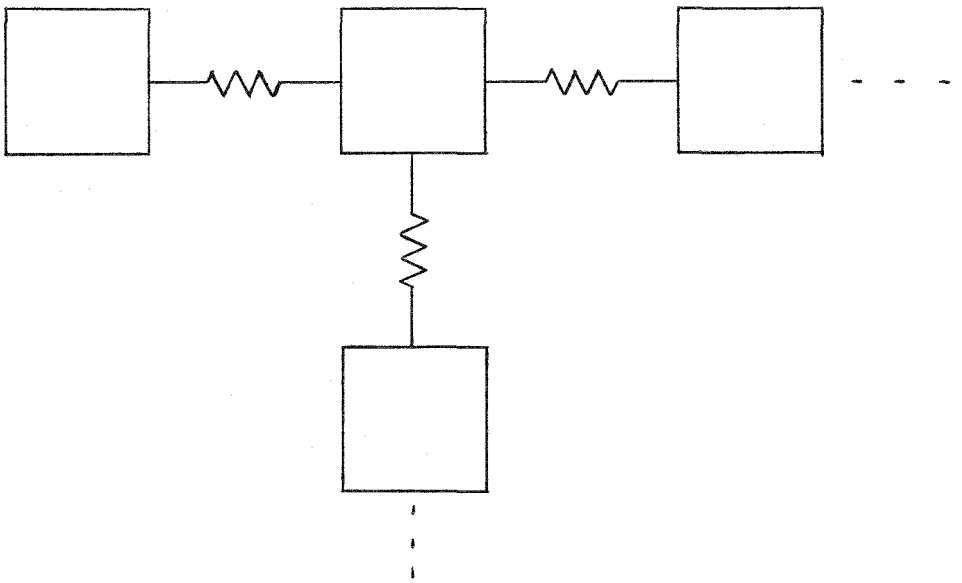

Figure 3.2 Schematic of a Multi-Dimensional Node-to-Node Heat Transfer Model.

3.3 Steps in Implementing the LCSR Transformation

The steps for obtaining the plunge test time constant are:

1. perform a LCSR test
2. identify the poles associated with the LCSR data
3. construct the step response for a fluid temperature perturbation using Equation (3.10).

A key element is identification of the poles by analysis of the LCSR transient data. This is a classical fitting problem that has been investigated extensively in the past. Techniques such as exponential peeling are widely used, but, in general, identification of exponential coefficients from transient data is a difficult numerical problem.

A computer program for the PDP-11 has been written that estimates the poles then constructs an estimate of the plunge time constant. This program is operational, but development is continuing to find the most suitable pole-fitting procedure.

One method to help in the pole-fitting problem has been proposed by Carroll of Oak Ridge National Laboratory. He observed that for a centrally located sensor in a cylindrical sensor with small surface heat transfer resistance compared to internal heat transfer resistance, the following relation approximately defines the poles:

$$p_i = p_1[1 + (i-1)\ R]^2. \qquad (3.21)$$

This relation is useful because it allows one to estimate higher poles using fitted values for only two parameters (p_1 and R). Some of the limitations of this approach are discussed in Section 3.4.3.

3.4 Theoretical Considerations Regarding the LCSR Transformation

In this section, some restrictions on the LCSR transformation are examined. First, the theory of the homogeneous RTD is presented and second, parametric effects on RTD time response are evaluated. Next, the affect of the adiabatic inner surface assumption on RTD's that have the filament near the outer surface is considered. Also, a homogeneous RTD is analyzed considering: (1) the error in the time constant due to limiting the number of terms in the solution, and (2) the error in the time constant due to errors in estimates of poles. These considerations allow one to determine: (1) regions where the LCSR transformation is valid, (2) constraints on the determination of the poles, and (3) error estimates on the results of the LCSR method.

3.4.1 Homegeneous RTD Theory

In this section, solutions will be presented for two cases: (1) a homogeneous RTD subjected to a step in heat generated in the filament, and (2) a homogeneous RTD plunged into a fluid path. The temperature data obtained from the first case may be transformed using the LCSR transformation and the results of this transformation can then be compared with the answer provided by the second analysis. The plunge test is treated in most textbooks on conduction and is not derived herein. The loop-current step response is derived to illustrate the similarities and differences with the plunge test.

The solution given by Equation (3.22) is for the plunge test considering: (1) a uniform homogeneous RTD, (2) the outer radius to be R, (3) the filament located at R*, (4) the sensor at an initial

temperature of T_o, (5) a bath temperature of T_∞, and (6) a surface heat transfer coefficient of h.

$$\frac{T(t) - T_\infty}{T_o - T_\infty} = \sum_{n=1}^{\infty} B_n J_0(M_n r/R) e^{-M_n^2 \alpha t/R^2} \tag{3.22}$$

where

$$\frac{J_1(M_n)}{J_0(M_n)} = \frac{hR/k}{M_n}$$

and

$$B_n = \frac{2 J_1(M_n) T_o}{M_n[J_0^2(M_n) + J_1^2(M_n)]} \tag{3.23}$$

k = thermal conductivity

ρ = density

C_p = specific heat capacity.

The sensor response is obtained by evaluating Equation (3.22) at r = R*.

The solution for the temperature in the sensor prior to the start of the LCSR test can be obtained from

$$\frac{1}{r}\frac{d}{dr} r \frac{dT_i}{dr} = - \frac{\dot{Q}_o \delta(R^*-r)}{2\pi R^*} \quad * \tag{3.24}$$

subject to boundary conditions

$T_i(r=0)$ is finite (3.25)

$$- k \frac{dT_i}{dr} (r=R) = h(T_i(R) - T_\infty) \tag{3.26}$$

where

$\dot{Q}_o$ is the heat generation rate for t < 0

R* is the radial location of the filament.

---

*δ is the Dirac delta function.

At time $t = 0$, the heat generation rate is changed to $\dot{Q}_\infty$. Note that as $t \to \infty$ the final temperature T_f may be obtained from

$$\frac{1}{r}\frac{d}{dr}\left(r\frac{dT_f}{dr}\right) = -\frac{\dot{Q}_\infty\,\delta(R^* - r)}{2\pi R^*} \tag{3.27}$$

subject to the same boundary conditions as T_i. Thus, the temperature varies from T_i to T_f as time goes from zero to infinity.

The solutions to these equations are

$$T_i(r) = T_\infty + \frac{\dot{Q}_o}{2\pi}\left[\frac{1}{Rh} - \frac{\ell n(R^*/R)}{k}\right] \qquad (r \le R^*) \tag{3.28}$$

$$T_i(r) = T_\infty + \frac{\dot{Q}_o}{2\pi}\left[\frac{1}{Rh} - \frac{\ell n(r/R)}{k}\right] \qquad (r > R^*) \tag{3.29}$$

and

$$T_f(r) = T_\infty + \frac{\dot{Q}_\infty}{2\pi}\left[\frac{1}{Rh} - \frac{\ell n(R^*/R)}{k}\right] \qquad (r \le R^*) \tag{3.30}$$

$$T_f(r) = T_\infty + \frac{\dot{Q}_\infty}{2\pi}\left[\frac{1}{Rh} - \frac{\ell n(r/R)}{k}\right] \qquad (r > R^*). \tag{3.31}$$

The transient is given as the solution to

$$\frac{1}{r}\frac{\partial}{\partial r}\left(r\frac{\partial T}{\partial r}\right) + \frac{\dot{Q}(t)\,\delta(R^* - r)}{2\pi R^* K} = \frac{\rho C}{k}\frac{\partial T}{\partial t} \tag{3.32}$$

where $\dot{Q}(t) = \dot{Q}_\infty$ for $t \geq 0$. By defining $\psi = T - T_f$ one obtains

$$\frac{1}{r}\frac{\partial}{\partial r}\left(r\frac{\partial \psi}{\partial r}\right) = \frac{\rho C}{k}\frac{\partial \psi}{\partial t} \tag{3.33}$$

subject to boundary conditions

ψ is finite at $r = 0$

$$-k\frac{\partial \psi}{\partial r} = h\psi \text{ at } r = R$$

$$\psi = T_i - T_f \text{ at } t = 0.$$

The solution to (3.33) is

$$\psi = \sum_{n=1}^{\infty} C_n J_0(M_n r/R)\, e^{-M_n^2 \alpha t/R^2} \tag{3.34}$$

where again

$$\frac{J_1(M_n)}{J_0(M_n)} = \frac{hR/k}{M_n} \tag{3.35}$$

and

$$C_n = \frac{\dot{Q}_0 - \dot{Q}_\infty}{\pi k}\,\frac{J_0(M_n R^*/R)}{M_n^2[J_0^2(M_n) + J_1^2(M_n)]} \tag{3.36}$$

was obtained from the orthogonality condition

$$\int_0^R (T_i - T_f)\, J_0(M_m\, r/R)\, 2\pi r dr =$$

$$\int_0^R \sum_{n=1}^{\infty} C_n\, J_0(M_n\, r/R)\, J_0(M_m\, r/R)\, dr. \tag{3.37}$$

Evaluating both series (Equations (3.22) and (3.34)) at $r = R^*$, one obtains for the plunge test response

$$T_p(t) - T_f = \sum_{n=1}^{\infty} K_n\, e^{-\lambda_n t} \tag{3.38}$$

and for the loop current step

$$T_{LCS}(t) - T_f = \sum_{n=1}^{\infty} L_n\, e^{-\lambda_n t} \tag{3.39}$$

where $\lambda_n = M_n^2 \alpha / R^2$ and is the same for both cases. The expansion coefficients are given by

$$K_n = \frac{2\, T_o\, J_1(M_n)\, J_0(M_n\, R^*/R)}{M_n [J_0^2(M_n) + J_1^2(M_n)]} \tag{3.40}$$

and

$$L_n = \frac{\dot{Q}_o - \dot{Q}_\infty}{\pi k}\, \frac{J_0^2(M_n\, R^*/R)}{M_n^2 [J_0^2(M_n) + J_1^2(M_n)]}\,. \tag{3.41}$$

Note that all the L_n's have the same sign (determined by $\dot{Q}_0 - \dot{Q}_\infty$) whereas the K_n's may be of the same sign (e.g., when $R^* = R$) or may be of alternating sign (when $R^* = 0$). Note that the LCSR transformation produces alternating signs.

One is now in a position to: (1) choose hR/k and R^*/R and solve Equation (3.38) for the plunge time constant τ_p, (2) evaluate Equation

(3.39) and use these temperatures to find the poles using a fitting algorithm, (3) perform the LCSR transformation, and (4) compare the results of the time constant obtained from this transformation with these theoretical results. This then gives one the opportunity to evaluate the entire LCSR procedure with data from a theoretical sensor with a known plunge time constant.

The solutions presented in this section demonstrate that the two principal parameters are R*/R (the ratio of sensor radius to outer radius) and the Biot modulus, hR/k (the ratio of conductive resistance to convective resistance). For RTD's filled with MgO, the Biot modulus can vary from 33 (for water at 70°F and a velocity of 4 ft/sec) to 200 for water at 500°F and 40 ft/sec velocity (typical reactor conditions). Thus, the relative convection resistance is extremely small and conduction is the principal heat transfer mechanism.

Figure 3.3 is a plot of the ratio of the plunge time constant at selected radial positions to the value at the center (obtained from Equation (3.38)) for two values of Biot modulus. Note that for the small Biot modulus, τ is approximately independent of filament position, while for a large Biot modulus, the time constant is strongly dependent on filament position.

One result should be noted. The eigenvalues, λ_i, are functions of hR/k only, and the LCSR transformation (see Section 3.2) uses only these eigenvalues (poles) to determine the time constant. Thus, no matter where the sensor is located, the transformation will produce a time constant that presumes a central location. This appears to be a conservative result since the transformation gives an estimate of the time

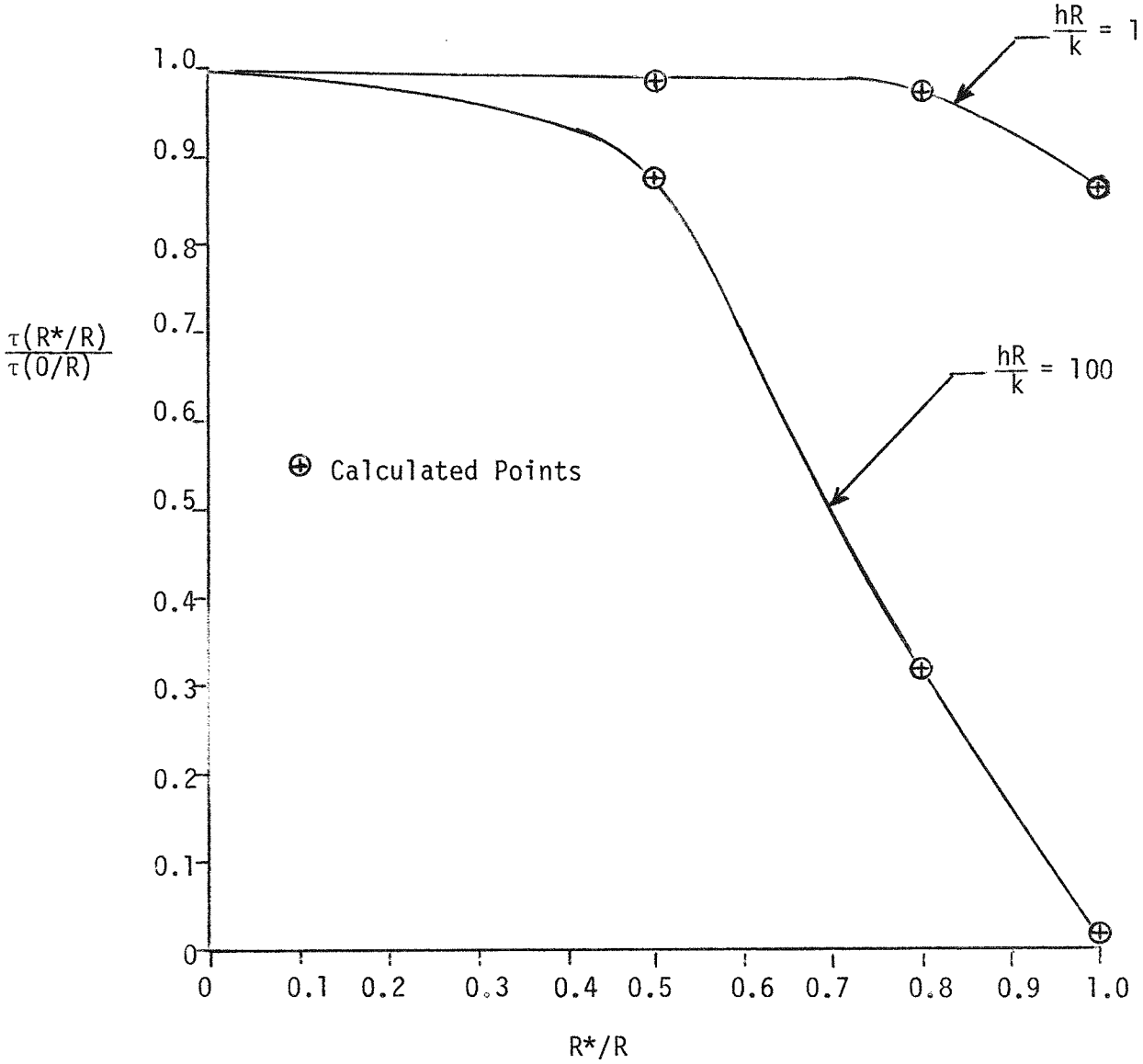

Figure 3.3 Ratio of the Time Constant Evaluated at R*/R ($\tau(R^*/R)$) to the Time Constant Evaluated at 0/R Versus the Ratio of Filament Radius to Sensor Radius.

constant that is too large, however, analytical corrections should not be made since the time constant for non-central filament depends on the Biot modulus, and it is imperfectly known.

3.4.2 Effect of Non-Homogenieties on Time Response

One of the more probable causes of sensor degradation is cracking of the MgO filler material and subsequent separation from the sensor. Because analytical solutions to the multiregion non-uniform problem are quite complex, a lumped parameter model is used to study these effects. The RTD is divided into four lumps: (1) an inner MgO solid cylinder, (2) the filament, (3) an outer MgO cylinder, and (4) a steel casing. Provision is made to insert a resistance, to simulate a gap: (1) between the center cylinder and the filament, (2) between the filament and the outer cylinder, and (3) between the outer MgO cylinder and the case. The solution is then obtained: (1) with no gap, (2) with a gap at each of the above mentioned positions, and (3) with no gap but the surface heat transfer coefficient reduced a factor of ten.

The lumped parameter equations are

$$\rho_1 \nu_1 C_1 \frac{dT_1}{dt} = \frac{1}{R_{12}} (T_2 - T_1) \tag{3.42}$$

$$\rho_2 \nu_2 C_2 \frac{dT_2}{dt} = \frac{(T_1 - T_2)}{R_{12}} + \frac{(T_3 - T_2)}{R_{23}} + \dot{Q} \tag{3.43}$$

$$\rho_3 \nu_3 C_3 \frac{dT_3}{dt} = \frac{(T_2 - T_3)}{R_{23}} + \frac{(T_4 - T_3)}{R_{34}} \tag{3.44}$$

$$\rho_4 \nu_4 C_4 \frac{dT_4}{dt} = \frac{(T_3 - T_4)}{R_{34}} + \frac{(T_5 - T_4)}{R_{45}} \tag{3.45}$$

where T_5 = fluid temperature

$$R_{12} = \frac{1}{2\pi}\left[\frac{1}{k_m}\ln\left(\frac{r_1}{r_{1m}}\right) + \frac{\Delta_1}{k_a r_1}\right]$$

$$R_{23} = \frac{1}{2\pi}\left[\frac{\Delta_2}{k_a r_2} + \frac{1}{k_m}\ln\left(\frac{r_{3m}}{r_2}\right)\right]$$

$$R_{34} = \frac{1}{2\pi}\left[\frac{\Delta_3}{k_a r_3} + \frac{1}{k_m}\ln\left(\frac{r_3}{r_{3m}}\right) + \frac{1}{k_s}\ln\left(\frac{r_{um}}{r_3}\right)\right]$$

$$R_{45} = \frac{1}{2\pi}\left[\frac{1}{k_s}\ln\left(\frac{r_4}{r_{um}}\right) + \frac{1}{hr_u}\right]$$

$$r_{1m} = r_1/\sqrt{2},\ r_{3m} = \sqrt{\frac{r_3^2 + r_2^2}{2}},\ r_{4m} = \sqrt{\frac{r_4^2 + r_3^2}{2}}$$

$$\nu_1 = \pi r_1^2,\ \nu_2 = \pi(r_2^2 - r_1^2)$$

$$\nu_3 = \pi(r_3^2 - r_2^2),\ \nu_4 = \pi(r_4^2 - r_3^2)$$

k_m = thermal conductivity of the MgO

k_a = thermal conductivity of the air

k_s = thermal conductivity of the steel

$\dot{Q}$ = heat generation rate in the filament.

These equations are further simplified by setting ν_2, the filament volume, equal to zero. This assumption appears physically reasonable because the sensor is significantly smaller than other components, and it simplifies the solution for the eigenvalues.

These equations are next solved in the following fashion: (1) Equations (3.42) through (3.45) are written in the matrix form

$$\frac{d\bar{T}}{dt} = \bar{\bar{A}}\,\bar{T} + \bar{B} \qquad (3.46)$$

and (2) the eigenvalues of the A matrix found. These are the same eigenvalues that would be found from analysis of a loop current step test. These eigenvalues (poles) are then used in the LCSR transformation to obtain a time constant. Next, Equations (3.42) through (3.45) are solved (using a forward difference technique) subject to initial condition T = 1 for all nodes and for T_5 (set to zero). The solution procedes until the filament temperature drops to e^{-1} at which point the time reaches the plunge time constant. This simulates: (1) an RTD plunged into a bath, and (2) the results of a loop current step and LCSR transformation.

Table 3.1 presents the results for a 0.25" diameter RTD. Two sensor locations, R* = 0 and R* = 0.8R, are presented and a gap 10 mils thick is used. Note that for the case where the sensor is located at the center, the plunge and the transformation give results which are the same within the precision of the calculation, and that for the sensor placed near the outside of the RTD, the transformation results are always conservative. Similar calculations with different gap sizes and different sensor locations yield equivalent results.

The results of this calculation together with that for the homogeneous sensor lead to the following conclusions:

1. The results of a loop current step test and subsequent LCSR transformation are valid only for the case where the filament is located at the center of the RTD.
2. It is not valid to use analytically derived factors to correct the time constant for filament location since the correction factor is not constant.

TABLE 3.1

$R^*/R = 0$

RTD Geometry	τ_{plunge}	$\tau_{transformation}$
No Gap	7.11	6.85
Gap Inside Sensor	6.82	7.07
Gap Outside Sensor	6.90	6.90
Gap Inside Sheath	11.20	10.85
No Gap - h = h/10	8.26	7.95

$R^*/R = 0.8$

RTD Geometry	τ_{plunge}	$\tau_{transformation}$
No Gap	.68	7.63
Gap Inside Sensor	.12	10.78
Gap Outside Sensor	3.40	10.11
Gap Inside Sheath	4.32	11.01
No Gap (h reduced by factor of 10)	1.93	8.60

3. The time constant obtained from the loop current step response test and transformation may be used (uncorrected for geometry) for all sensors and will produce conservative results. This procedure may penalize some RTDs severely.

3.4.3 Effect of the Number of Eigenvalues on Solution Accuracy

In this section, the validity of the empirical expression of Equation (3.21) used to estimate higher poles (eigenvalues) is examined. This empirical expression, $P_i = P_1[1 + (i - 1) R]^2$, utilizes the first two eigenvalues P_1 and P_2 to obtain R, and then subsequent eigenvalues are obtained from this expression. Table 3.2 presents the results when this procedure is attempted on the eigenvalues produced in the non-homogeneous calculation. Examination of the last two columns clearly indicates that this procedure is invalid when the sensor is non-homogeneous.

Since the above empirical expression for higher eigenvalues is not valid, it is necessary to determine the number of eigenvalues which must be obtained from the fit of the loop current step data. In order to estimate this number, the following procedure is adopted:

1. Evaluate the plunge time constant from the homogeneous solution.
2. Using eigenvalues from the homogeneous model, perform the LCSR transformation with N eigenvalues and obtain a transformation time constant.
3. Compare these results.

TABLE 3.2

Case	λ_1	λ_2	R	λ_3	$\lambda_1(1+2R)^2$
1	-.15	-8.5	6.5	-15.1	-48.6
2	-.15	-3.1	3.6	-15.1	-10.0
3	-.15	-6.3	5.5	-15.1	-21.6
4	-.09	-8.8	8.9	-15.0	-31.8
5	-.14	-1.8	2.6	-8.5	-5.33

Table 3.3 presents the results of this computation for two Biot numbers hR/k = 1 and hR/k = 100. Two items are noteworthy. First, all predictions are too small and progressively increase to the true value, and second, it requires approximately four terms to produce an estimate within 10% of the true value for hR/k = 100.

TABLE 3.3

	hR/k = 1	hR/k = 100
N	$\tau_{transform}/\tau_{true}$	$\tau_{transform}/\tau_{true}$
1	.84	.69
2	.93	.83
3	.95	.88
4	.97	.91
5	.97	.93
10	.99	.96

4.0 LABORATORY FACILITIES

4.1 Laboratory Capability

A Thermometry Laboratory was established at The University of Tennessee to test the procedures and equipment for in-situ response time testing of RTD's. One or more of each of the RTD models used in modern PWR's have been available for testing in the Thermometry Laboratory.

4.2 Equipment

A brief description of available laboratory equipment follows:

1. A rotating tank (diameter = 22 inches, height = 13 inches) is used for laboratory response time testing. The fluid velocity varies from zero at the center of the tank to 4 feet/sec at the edge. Most tests are performed in the region where the velocity is about 3 feet/sec. The system is shown in Figure 4.1.
2. A bridge with capability of switching from one current level to another was built (see Figure 4.2). The switching is by a relay that can be switched manually or by computer control. The adjustable balancing resistance is a seven element decade box. The fixed resistors in the bridge are 500 ohm resistors rated at 25 watts. This avoids error due to heating in the fixed resistors when high currents are used.
3. Appropriate amplifiers are used for obtaining useful voltage levels.
4. A strip chart recorder is used for recording transient data.
5. A PDP-11 computer system is available for transient data storage and analysis. The computer, which is located in a separate room, communicates with the instrumentation in the Thermometry Laboratory via a permanently installed data link.

Figure 4.1 Rotating Tank.

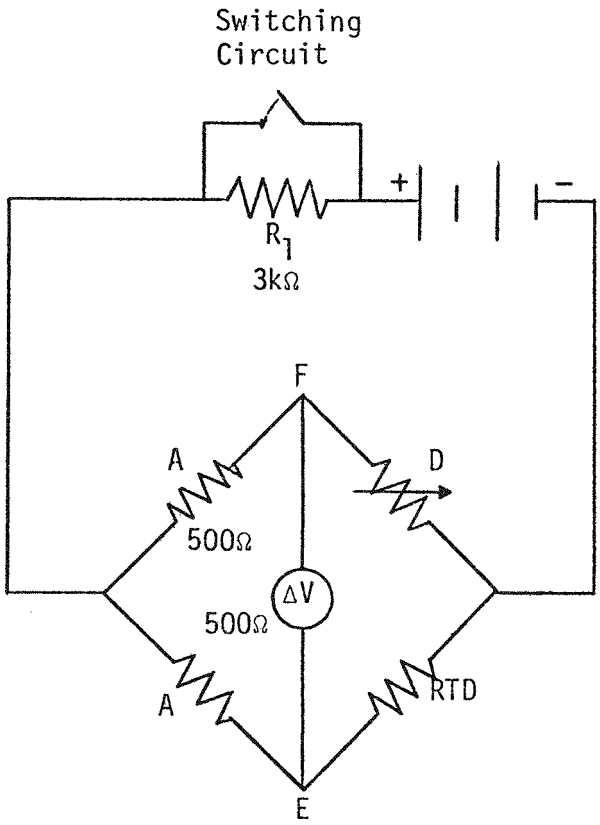

Figure 4.2 Laboratory Testing Bridge Circuit Schematic.

4.3 Data Collection and Analysis

The LCSR test can be run remotely from the computer room. A computer program is available that causes the system to switch the relay, digitize the transient data, and store it in the computer memory. The transient data may be examined on a CRT display, then transferred to a disk file if it is to be saved. Subsequently, the LCSR data on the disk can be transformed to give an estimate of the response that would occur after a fluid temperature step. This involves estimation of the system poles using the LCSR data, then constructing the estimate of the response to a fluid temperature step using Equation (3.10).

5.0 THE LOOP CURRENT STEP RESPONSE TEST

5.1 Brief Description of the Testing Method

During normal operation of a resistance temperature detector (RTD) a small sensing current, typically 1-5 mA, is passed through the resistance element, and fluid temperature changes are determined by measuring the change in resistance of the element. The Loop Current Step Response (LCSR) test procedure involves imposing a step change in the sensing current from the steady state value of 1-5 mA to 20-60 mA. This effectively increases the sensor internal temperature a few degrees above ambient temperature through ohmic heating. After a steady state condition is reached, the resistance heating is terminated by returning the sensing current to its original steady state value. The sensor output is monitored throughout the transient.

5.2 LCSR Test Procedure

The LCSR test is implemented by switching the supply voltage from a lower value to a higher value. Figure 5.1 depicts a typical signal measured during a LCSR test. If the bridge is exactly balanced initially, $R_d = R_{RTD}$. The initial voltage output is given by

$$\Delta V = \left[\frac{(R_d - R_{RTD})\ R_a}{(R_a+R_d)\ (R_a+R_{RTD})}\right]_0 E_0 = 0 \qquad (5.1)$$

where the subscript, 0, denotes conditions during initial low current operation.

When the current is stepped up, there should be an exponential change in the voltage output as a function of time. The new steady state condition is given by,

$$\Delta V \tilde{=} C\ \Delta R_{RTD}\ E_N \qquad (5.2)$$

where

$$C = -\frac{R_a}{(R_a+R_d)\ (R_a+R_{RTD})} \quad \text{(assumed } \sim \text{ constant)}$$

ΔV = change in ΔV

E_N = voltage drop across the bridge.

When the bridge voltage, E, is stepped down to its original value at t_2, the voltage output decays exponentially to its original value.

5.3 Development of an Empirical Transformation Using the LCSR

For cases when the assumptions apply, the analytical transformation developed in Section 3 predicts the sensor response to a fluid temperature step perturbation accurately. If either the analytical transformation fails for a particular sensor, or the method for implementing it fails because of difficulties in identifying the poles, another method is

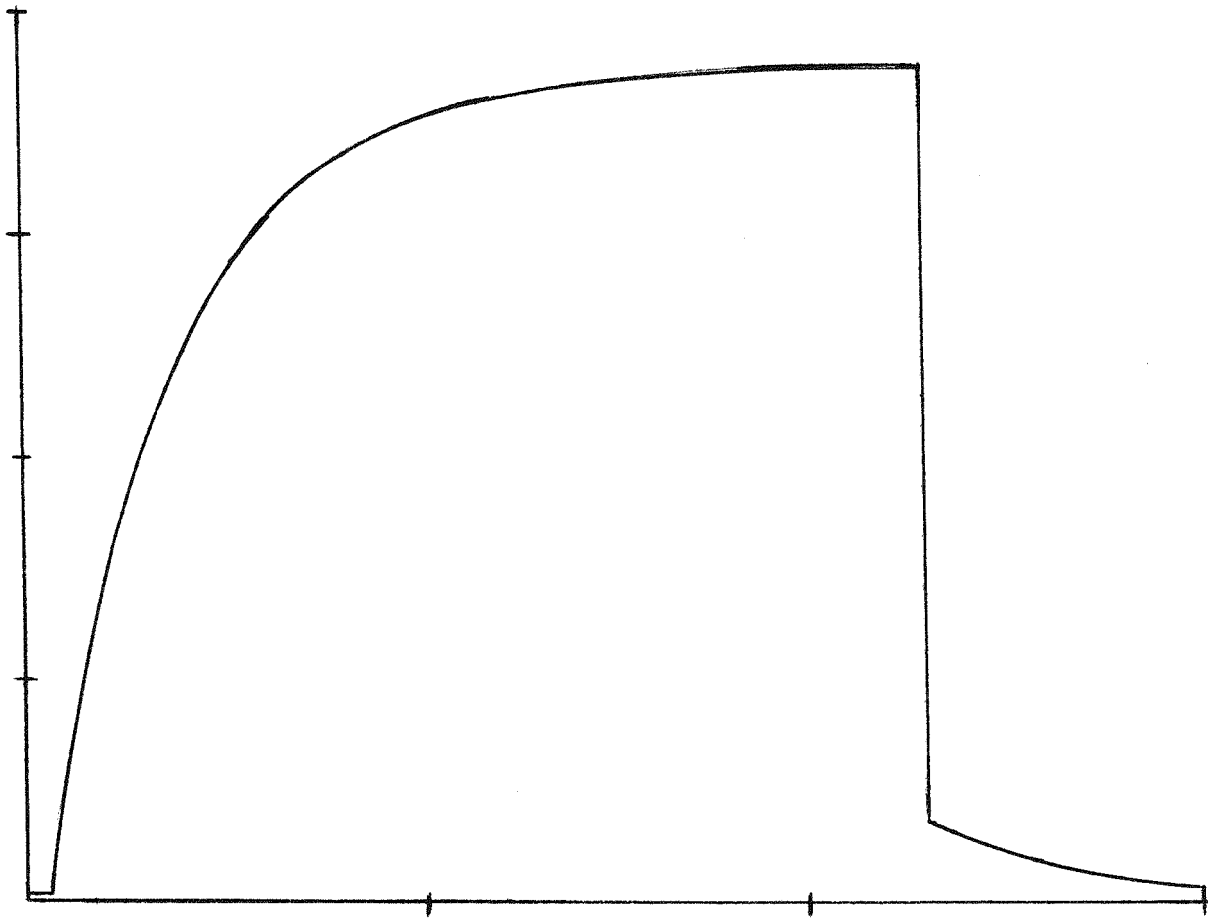

Figure 5.1 LCSR Test Result with $R_D = R_{RTD}$ Initially.

needed to interpret LCSR results. Because one of the objectives of this research was to develop an in-situ test usable on all types of sensors, an effort was made to discover an empirical correlation to be used in cases where the analytical transformation does not apply.

Experimental results were investigated to determine whether a unique relationship exists between the fluid temperature step response and the response to a step increase in internal heating of the sensor. The two parameters of interest were the time constants in the LCSR test and in the plunge test. The LCSR time constant, τ_{LCSR}, is defined as the time required for the sensor to attain 63.2% of its final output after a step change in the internal heating in the sensor. The plunge test time constant, τ_{PL}, is defined as the time required by the sensor to attain 63.2% of its final output following the plunging of the sensor into a fluid at a temperature different from the original steady state temperature before the plunge.

As previously mentioned, the time response of a sensor is dependent upon the heat transfer properties and characteristics of its environment. When the heat transfer resistance of a sensor increases, it follows that the response time of the sensor will increase. Likewise, when the heat transfer resistance of the sensor decreases, the response time of the sensor will decrease. It is possible to simulate heat transfer changes artifically in the sensor environment by placing insulating material of varying thicknesses around the thermometer. LCSR and plunge tests can be performed in the laboratory and the resulting time constants measured.

The tests may be repeated under many differing simulated heat transfer environments. The associated time constants measured at each configuration constitute a point on an empirical curve. When the resulting points are plotted, they yield an experimental correlation curve. From this empirical relationship, it is possible to predict the fluid temperature step response time constant given the LCSR time constant for a range of surface heat transfer conditions. With this empirical transformation, it is possible to conduct LCSR tests throughout the life of the plant, determine the LCSR time constant, and verify whether the plunge test time constant has changed by using this correlation.

5.4 Laboratory Results from LCSR Tests

LCSR tests were performed in the Thermometry Laboratory for PWR-type RTD's. Figures 5.2 through 5.4 show LCSR data obtained for sensors in flowing water (3 ft/sec) at room temperature.

The transformation was applied to LCSR data collected by the computer. For laboratory work, the sensor may be subjected to actual plunge tests to check the validity of the transformation. A typical plunge test result is shown in Figure 5.5. The results of the transformation and the actual plunge test results for one sensor appear in Figure 5.6. The transformation gave good results for this sensor, but this was not universally true for all sensors. The predictions for the 176KF sensor were especially bad. *This is attributed to the sensor configuration, which violates the assumption of a centrally located filament as required for validity of the transformation.

---

*Refer to statement in report Summary, taking exception to this conclusion.

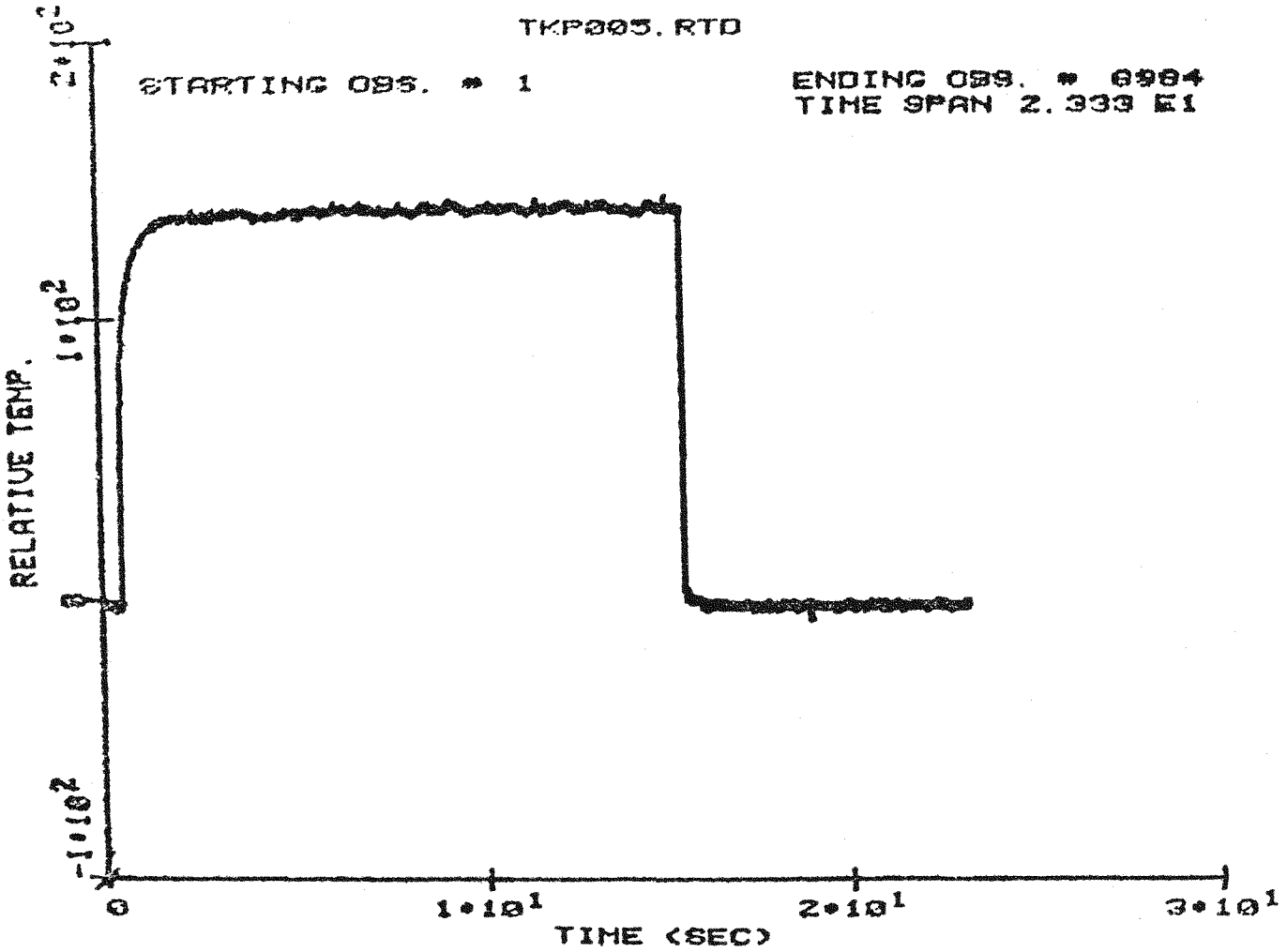

Figure 5.2 Loop Current Step Response Test Data for a Sensor in Water Flowing 3 ft/sec (Rosemount Model 176-KF).

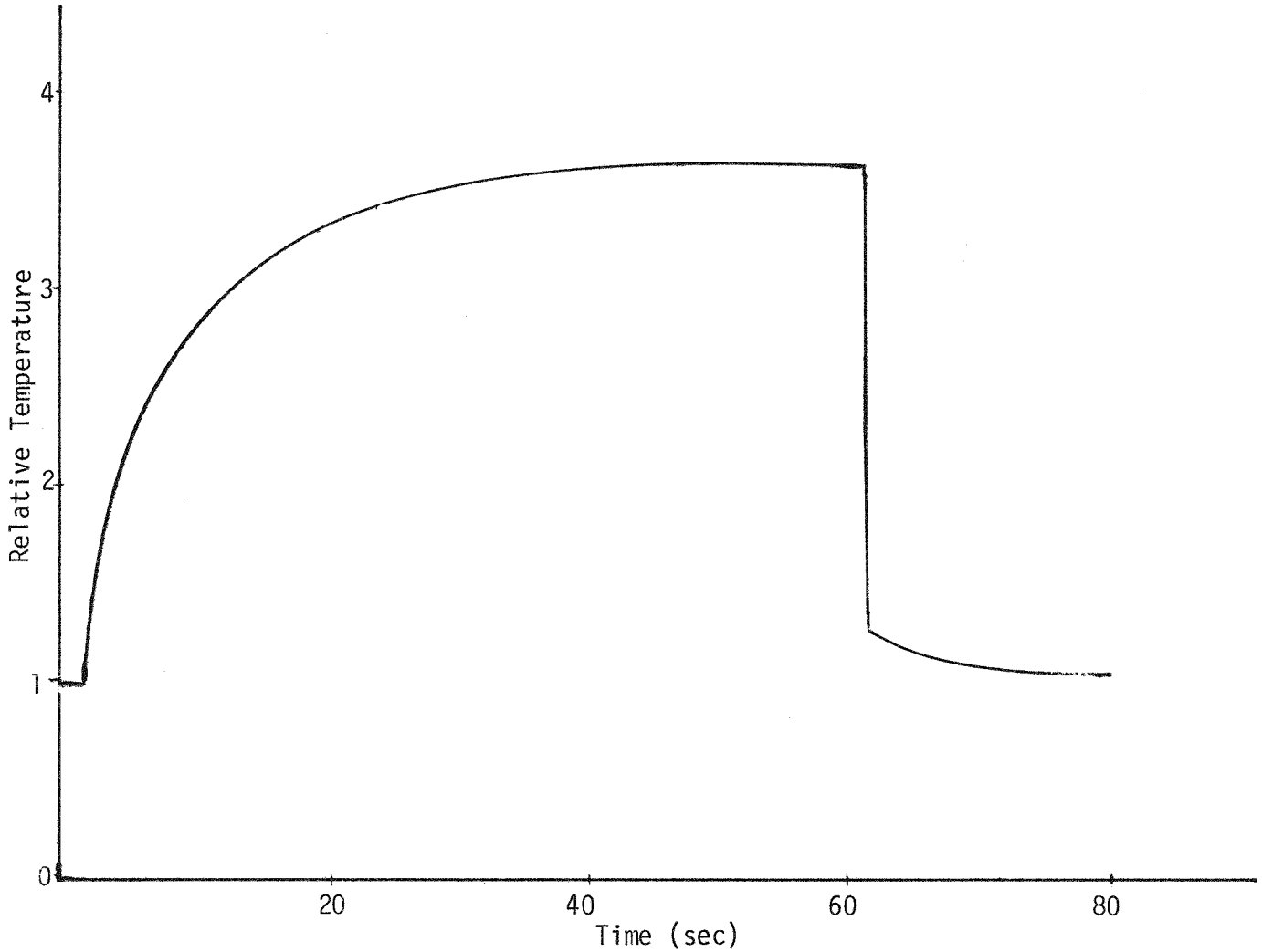

Figure 5.3 Loop Current Step Response Test Data in Water Flowing at 3 Ft/Sec (Rosemount Model 104AFC).

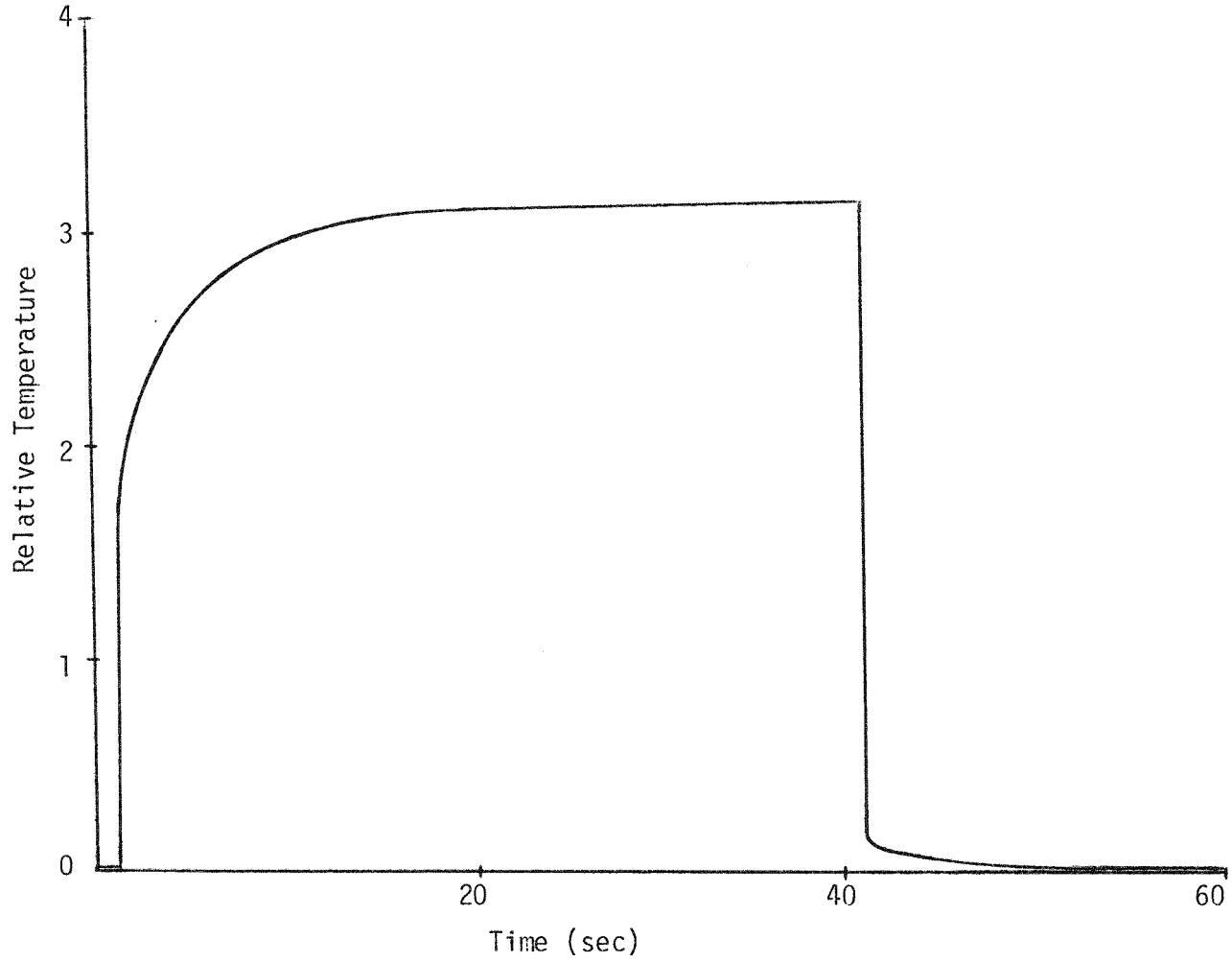

Figure 5.4 Loop Current Step Response Test Data in Water Flowing at 3 Ft/Sec (Rosemount Model 177-GY).

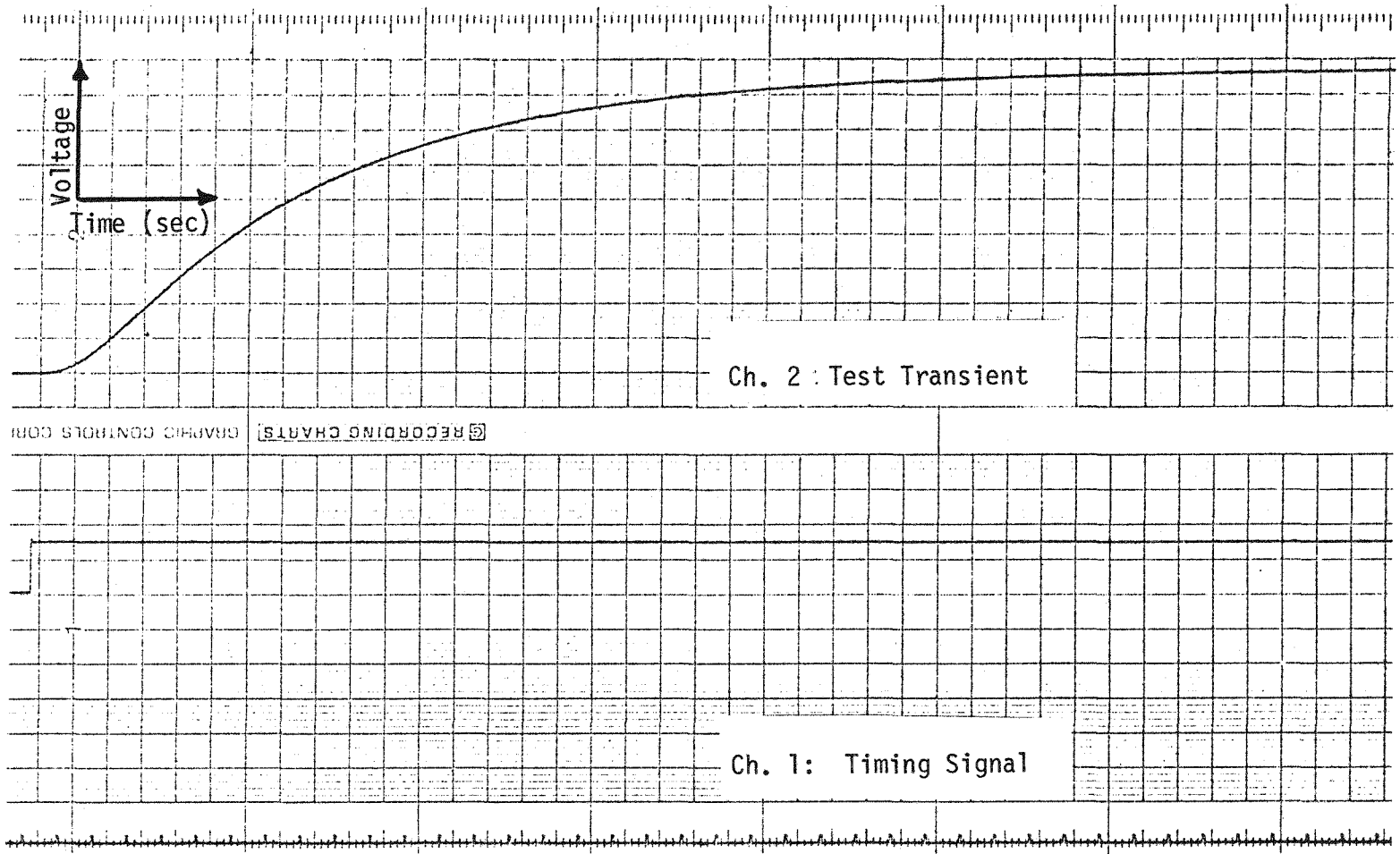

Figure 5.5 A Typical Plunge Test Output. Sensor is Plunged From Air into a Moderately Stirred Water Tank (Rosemount Model 104AFC).

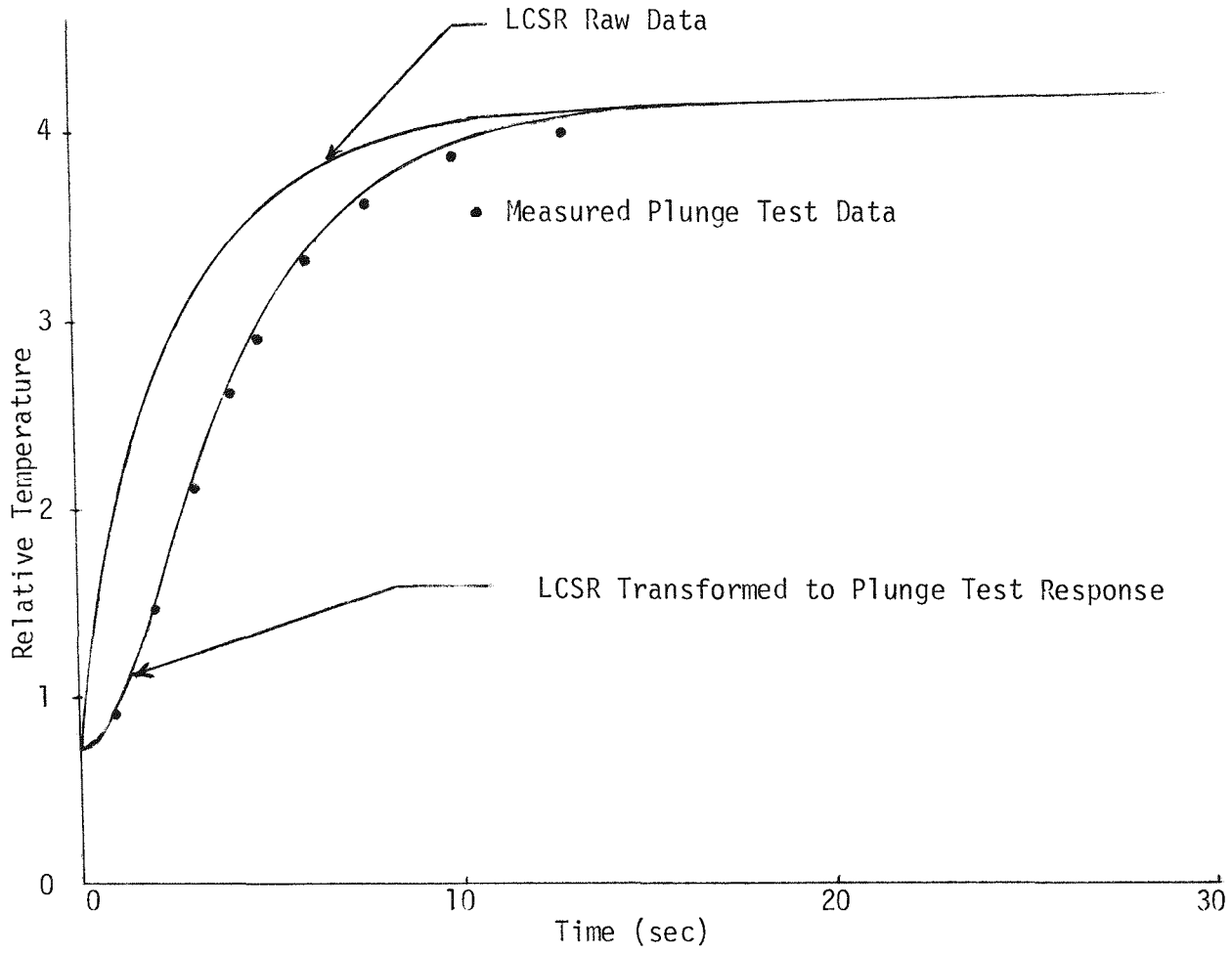

Figure 5.6 Transformed Loop Current Step Response Test for Rosemount Model 104AFC.
Note: A Heat Transfer Fluid (Neverseize) was Used in the Well.

Numerous tests were performed to collect data to obtain an empirical relation between the LCSR time constant and the plunge time constant. For empirical correlation, it is necessary to obtain data for the sensor with its characteristics altered so as to cause it to have varying response characteristics. In the laboratory, this was accomplished by augmenting the surface heat transfer resistance by adding sections of adhesive tape or rubber tubing to the surface of the RTD. Different values of resistance change were achieved by varying the amount and position of material added at the surface. For each configuration, three tests were performed: plunge test, LCSR test, and self heating test (see Section 6.0).

Figures 5.7a, 5.7b, 5.8a, and 5.8b show the empirical correlations for LCSR data. These could be used to convert in-plant LCSR test data into the desired τ_{plunge} needed for satisfying Nuclear Regulatory Commission requirements if the following assumptions are valid:

1. Laboratory tests involving augmentation of surface heat transfer resistance adequately simulate actual degradation that might occur in an in-plant sensor.
2. Differences between temperature and fluid velocity conditions in the laboratory and the plant have insignificant effects.

These questions are being explored in current work.

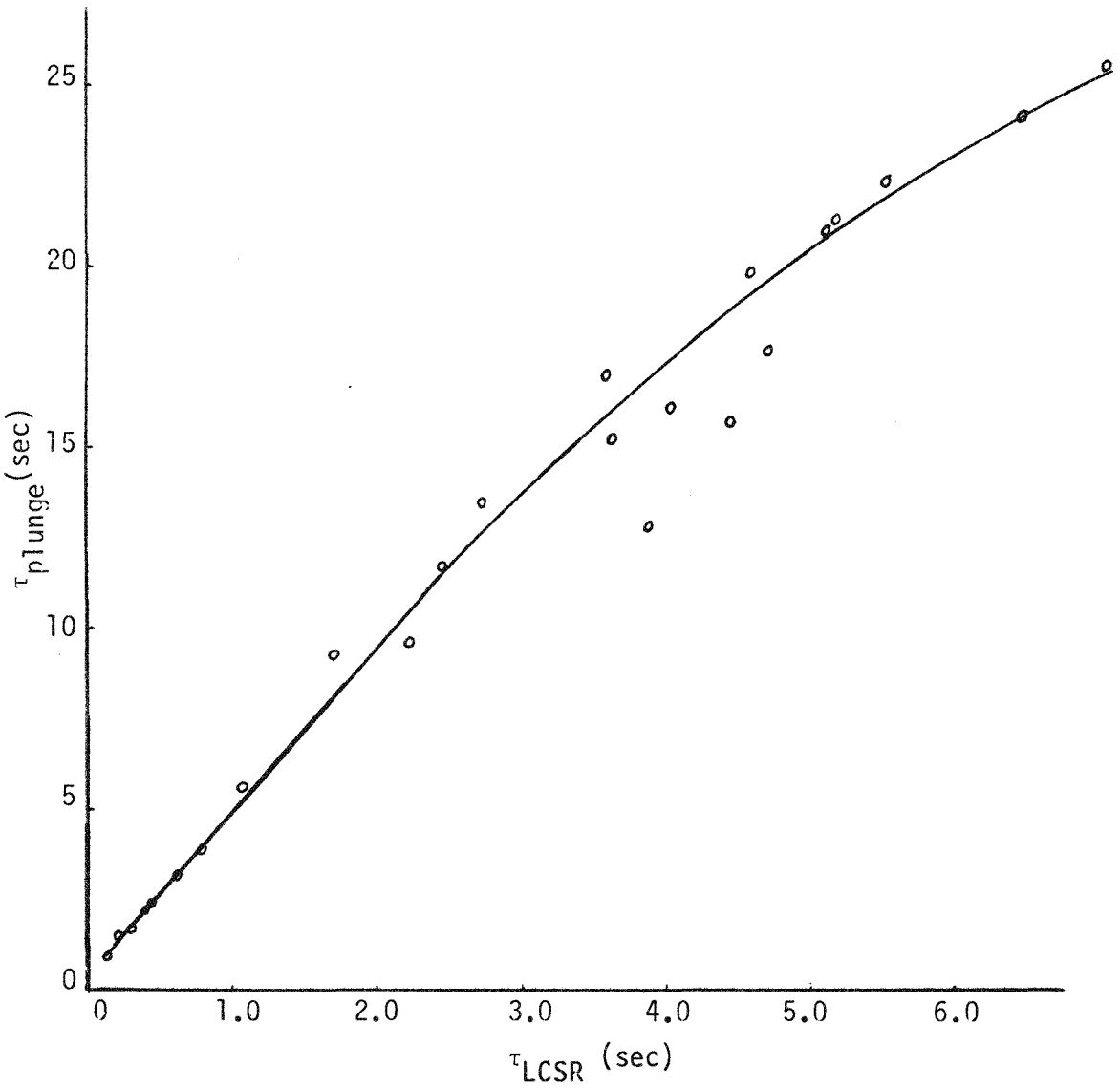

Figure 5.7a An Empirical Correlation Between a Plunge Test Time Constant, τ_{plunge}, and a Loop Current Step Response Test Time Constant, τ_{LCSR} (Wide Range). The Correlation is for the Rosemount Model 176-KF Sensor.

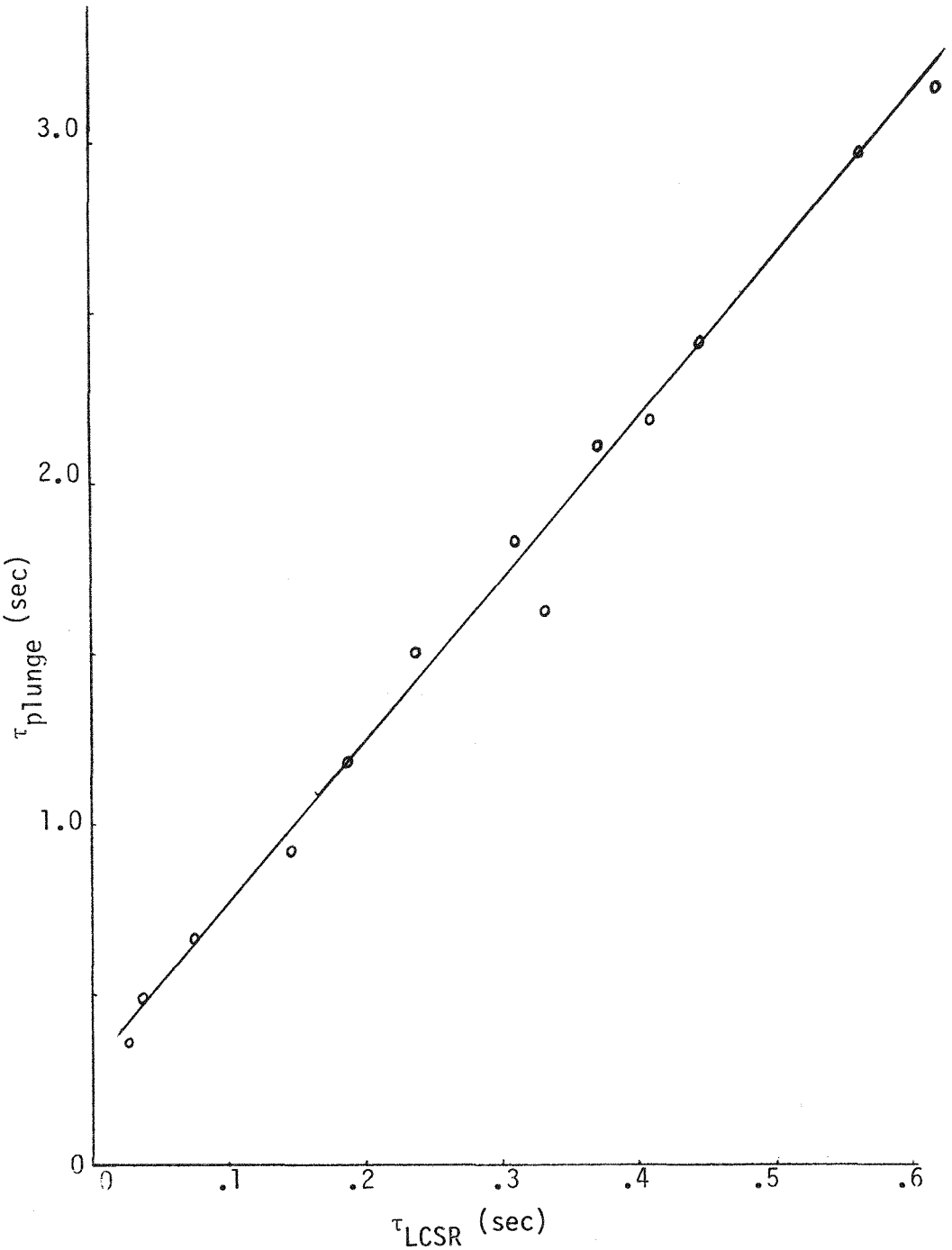

Figure 5.7b An Empirical Correlation Between a Plunge Test Time Constant, τ_{plunge}, and a Loop Current Step Response Test Time Constant, τ_{LCSR} (Narrow Range). The Correlation is for Rosemount Model 176-KF Sensor.

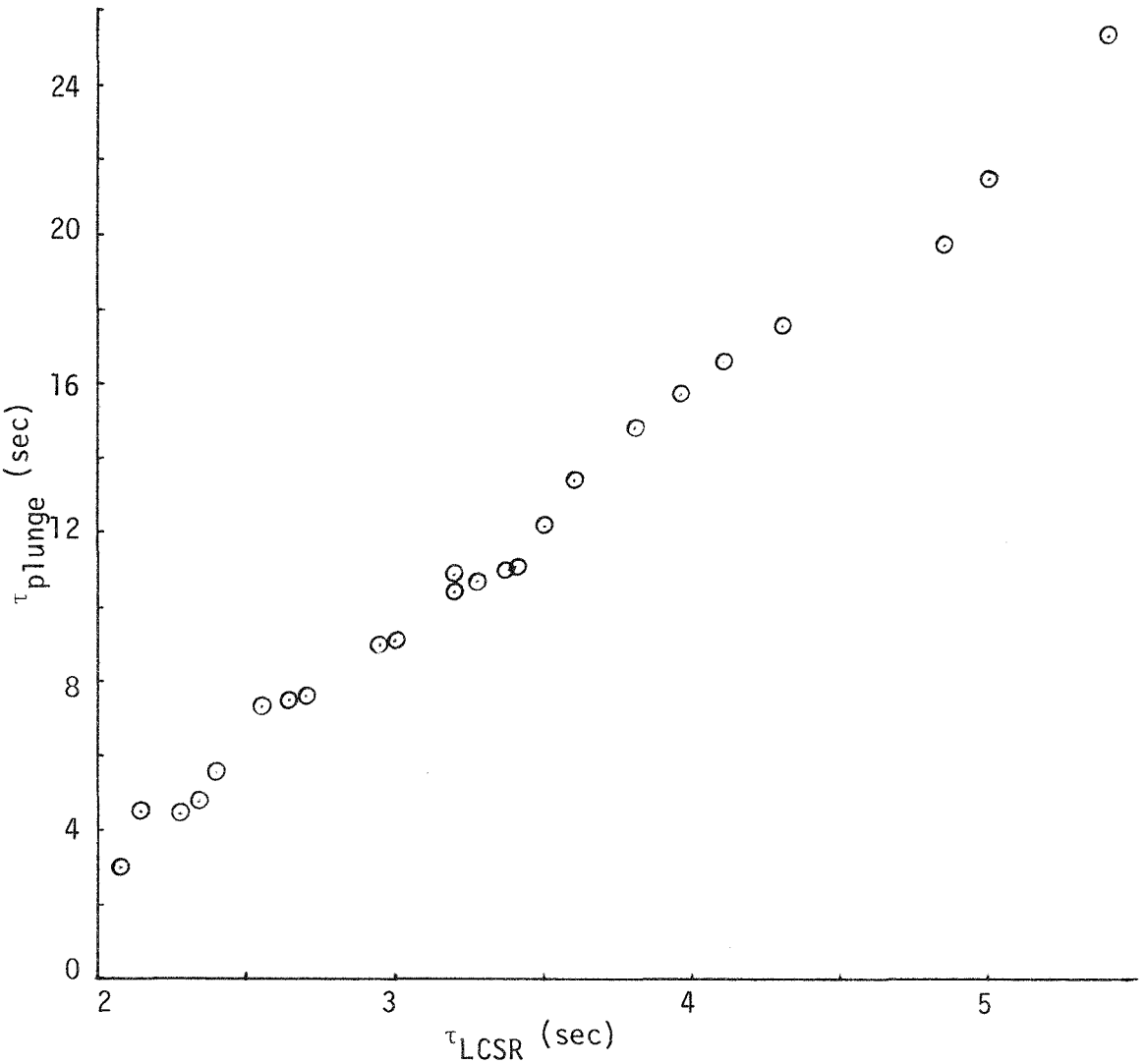

Figure 5.8a Empirical Correlation Between a Plunge Test Time Constant τ_{plunge}, and a Loop Current Step Test Time Constant, τ_{LCSR} (Wide Range) Rosemount Model 104AFC.

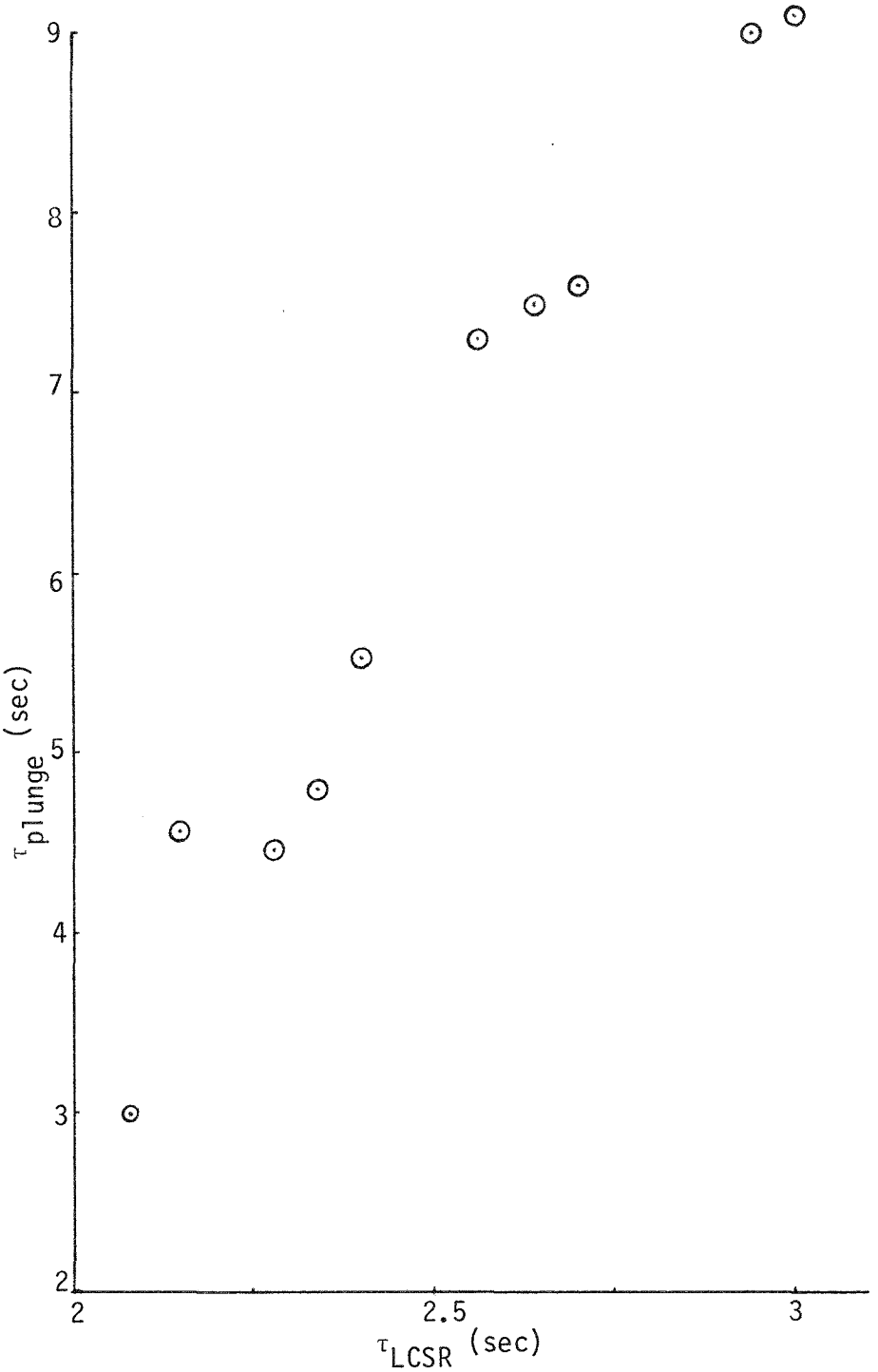

Figure 5.8b Empirical Correlation Between a Plunge Test Time Constant, τ_{plunge}, and a Loop Current Step Response Test Time Constant, τ_{LCSR} (Narrow Range) Rosemount Model 104AFC.

5.5 In-Plant Results from LCSR Tests

Loop current step response measurements have been performed in two operating pressurized water reactors. Tests were performed at Turkey Point (a 760 MWe Westinghouse plant that is owned and operated by Florida Power and Light Company) and at Oconee Unit 3 (an 886 MWe Babcock and Wilcox plant that is owned and operated by Duke Power Company). Both tests were performed while the plants were operating at full power.

The first in-plant test was performed at Turkey Point. Because of instrumentation problems, the results were of poor quality. Subsequent laboratory investigation revealed the cause of the problem. A voltmeter that was connected across one of the fixed resistors in the bridge to measure the current was responsible for the problem. The effect on the data was a large spike immediately after the current switching for the LCSR test. This is shown in Figure 5.9.

If one ignores the spike and assumes a smoother curve through the section where the spike occurs, then he can obtain a transient suitable for analysis. However, this questionable procedure serves more to find out whether the estimate is in the expected range rather than to obtain a reliable response time.

The smoothed data were used in the analytical transformation (see Figure 5.10 for a smoothed response). It was expected that this would not provide a correct response time because laboratory experience had already shown that the analytical transformation does not apply for Westinghouse sensors. Thus, the obviously incorrect response time results ranging from 0.0113 to 10.84 seconds were not surprising. There

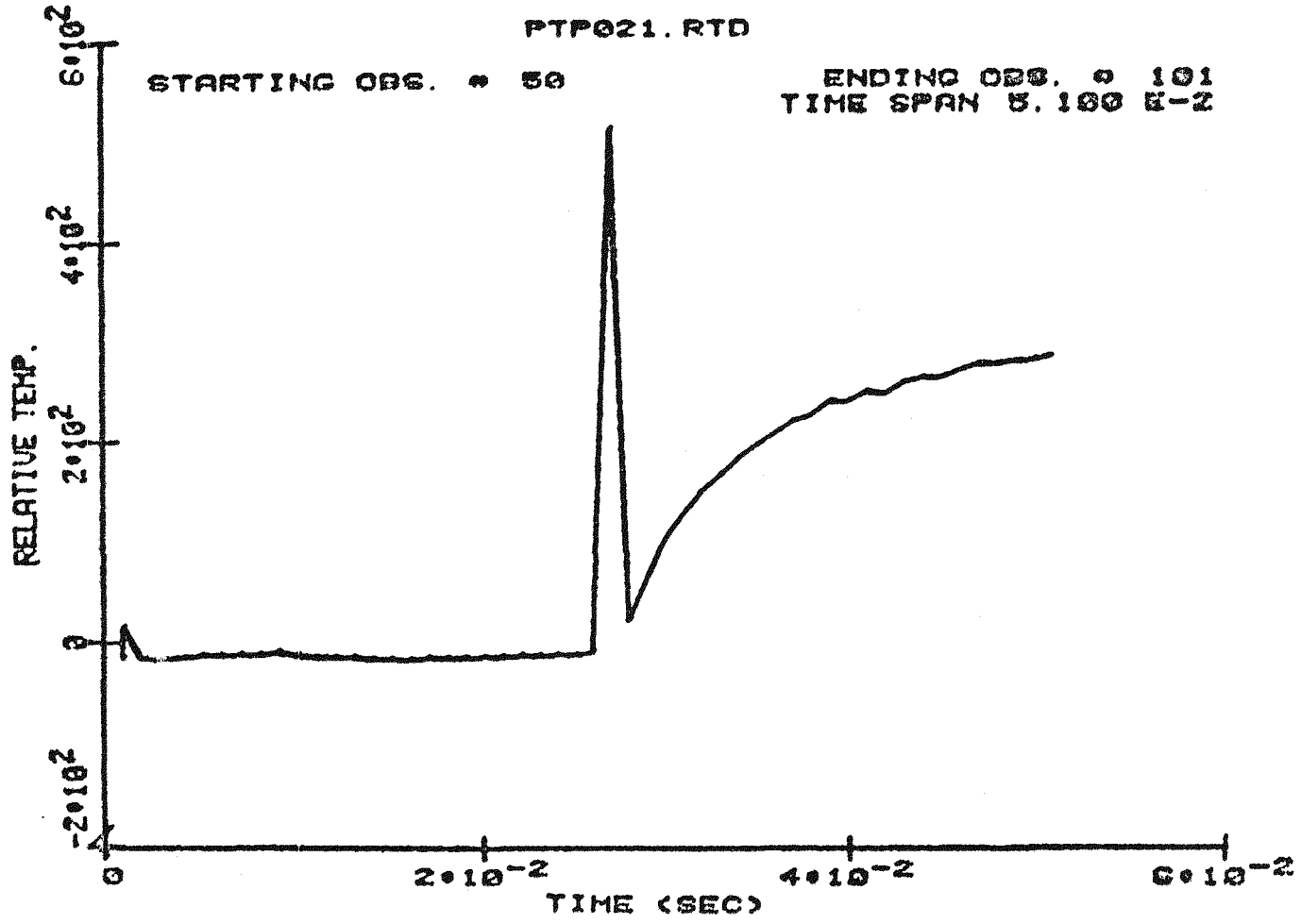

Figure 5.9 LCSR Test Data Showing Spike Encountered at Turkey Point.

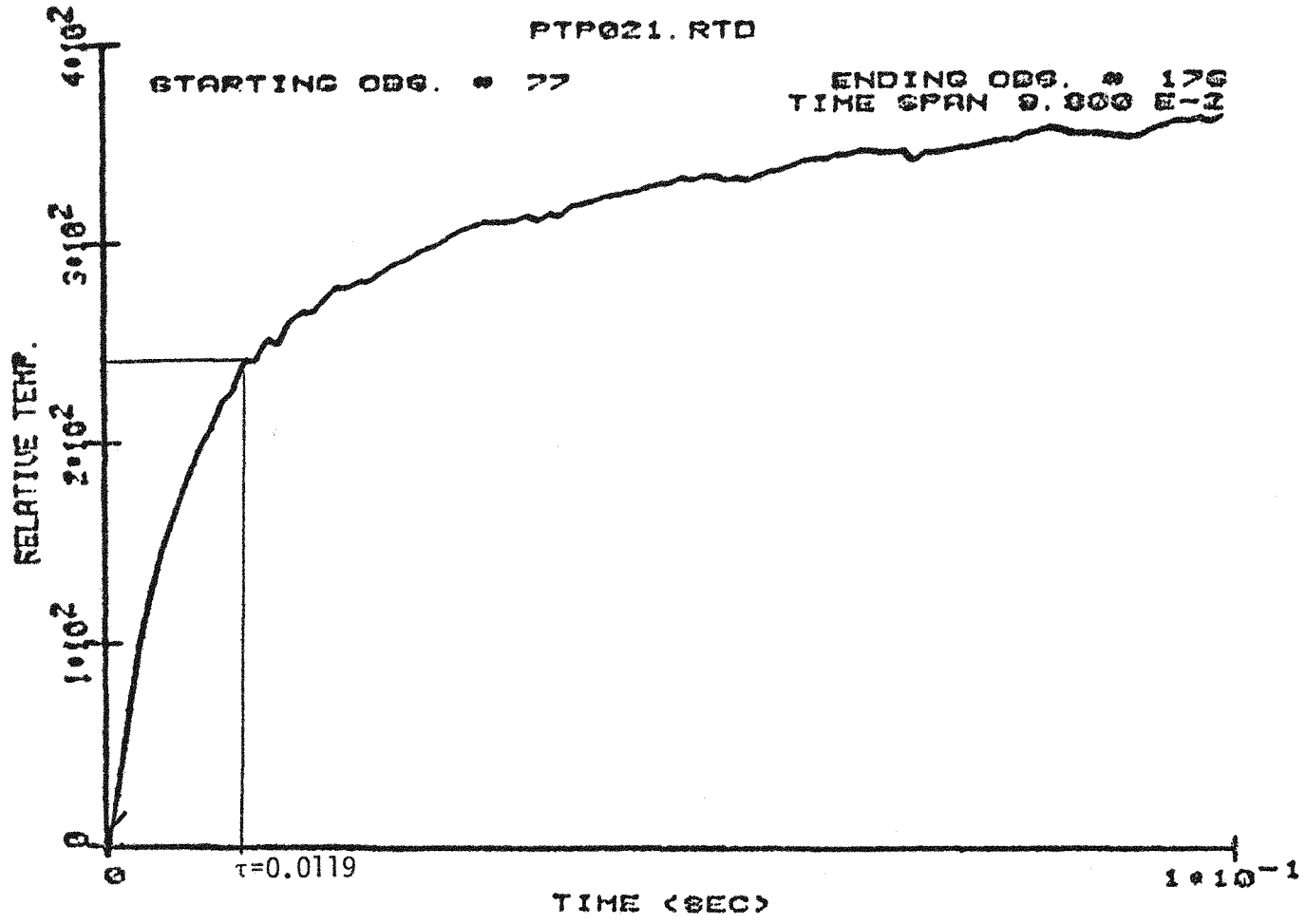

Figure 5.10 LCSR Test with Smoothed Curve.

is more confidence in the empirical correlation. The value obtained for τ_{LCSR} was 0.0142 second. The empirical transformation (see Figure 5.7) gives a time constant (τ_{plunge}) of 0.26 second. The time constant measured for a similar sensor in the laboratory is 0.4 second. Thus, the results are in the same range, but the poor quality of the test data makes it unwise to read very much into this result.

The second in-plant test was made at Oconee. This test benefitted from lessons learned at Turkey Point and from progress made in the laboratory after the Turkey Point tests. At Oconee, there were no experimental difficulties. LCSR tests were performed on three different RTDs (two in the cold legs and one in a hot leg), and two types: one was a Rosemount model 177-GY (direct immersion type), and one was a Rosemount model 177HW (well type). The LCSR transients were as expected (see Figures 5.11 through 5.13). In these tests, the current during the high-current phase of the test was 40 ma, giving a temperature rise of about 12.6°F (177-GY) and 10.6°F (177-HW).

Data analysis has been delayed because the computer has been unavailable and because the empirical correlation data for these sensors have not yet been collected in the laboratory. A very preliminary analytical transformation analysis gave an estimate of τ_{plunge} of 6.2 seconds for the 177-GY. This is close to the plunge test result of 6.0 seconds that has been measured in the laboratory. In general, the Oconee test data looks very good, and successful determination of the time constant is anticipated.

5.6 Conclusions

The loop current step response method appears to be a good candidate for performing in-situ response time measurements in RTDs. The

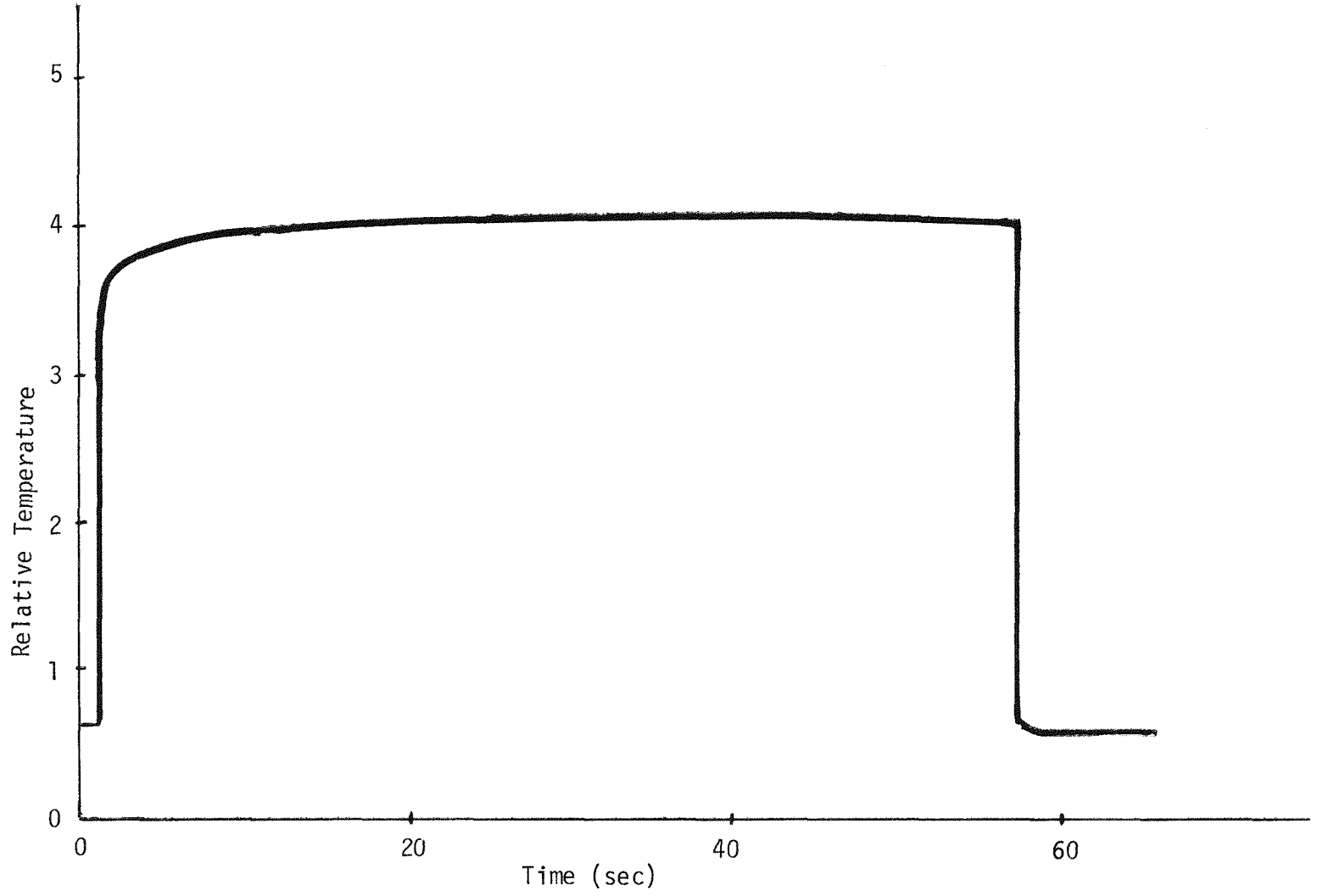

Figure 5.11 LCSR Data for Oconee Sensor No. 1.

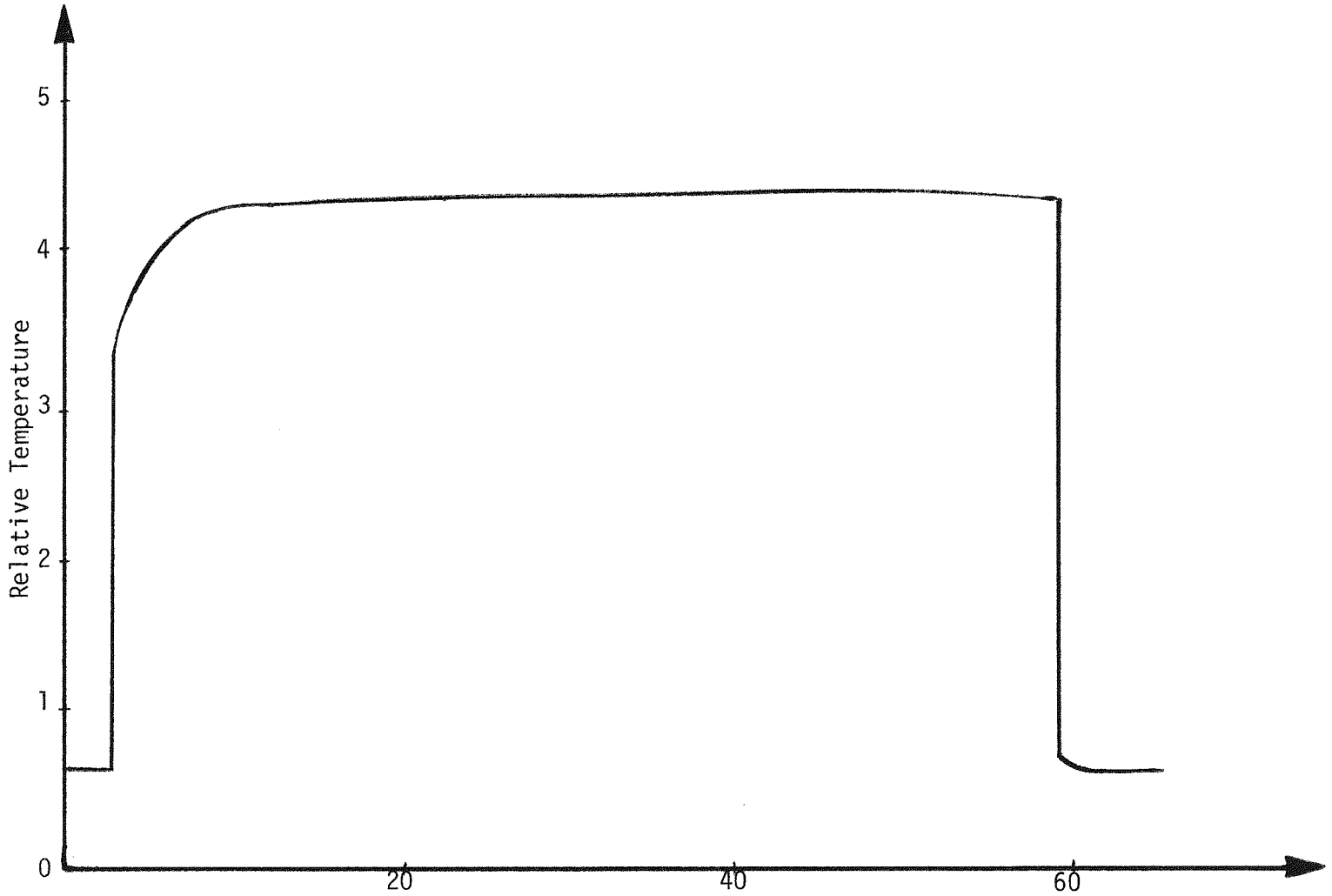

Figure 5.12 LCSR Data for Oconee Sensor No. 2.

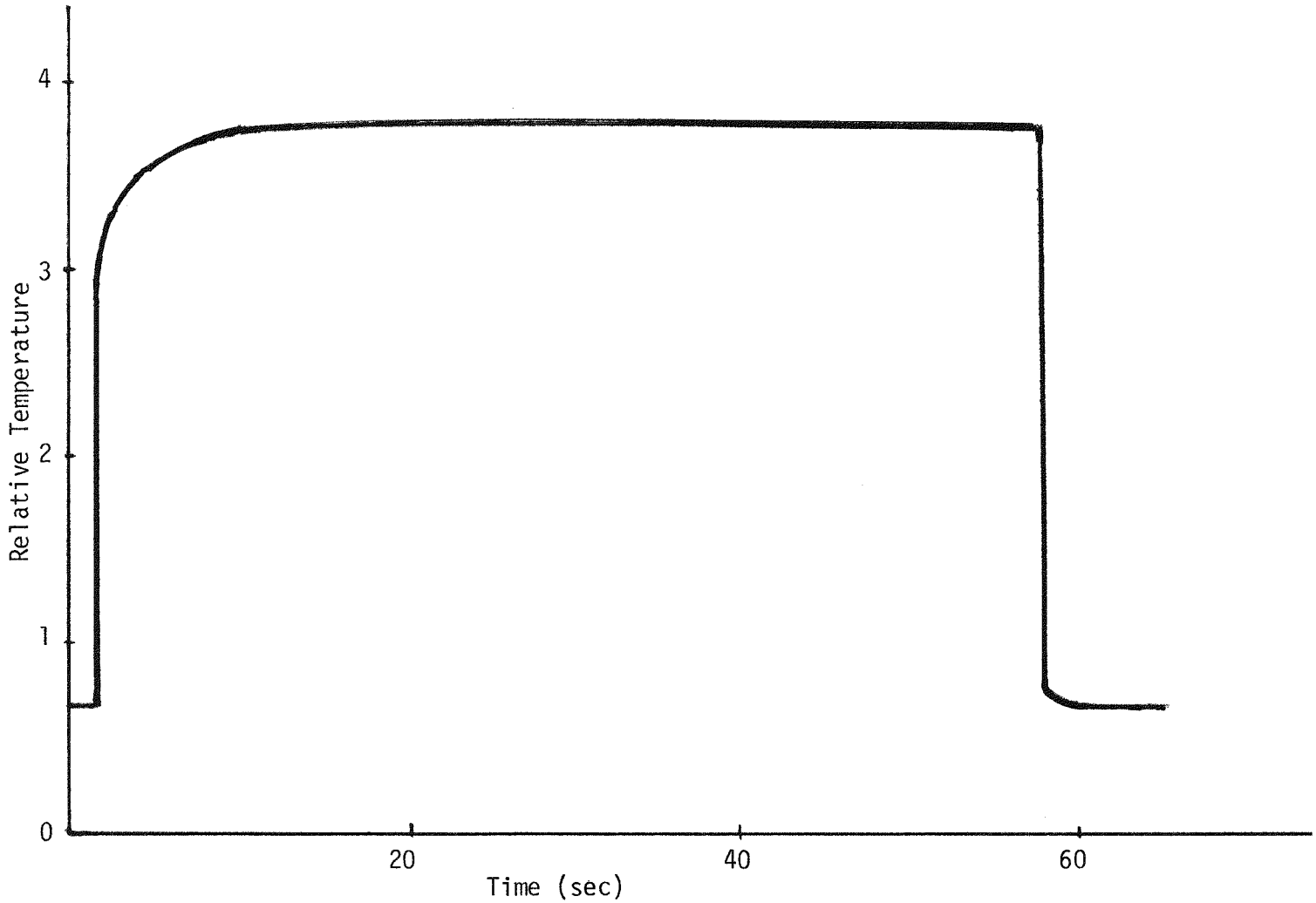

Figure 5.13 LCSR Data for Oconee Sensor No. 3.

analytical transformation provides a method for interpreting the data for sensors that satisfy the conditions for validity of the transformation. For other sensors, an empirical transformation seems to be adequate. Testing methods have been established through a great deal of laboratory experience. In-plant test experience now indicates that the LCSR test is suitable for measurements in the environment of an operating plant.

6.0 THE SELF-HEATING TEST

6.1 Brief Description of the Self-Heating Testing Method

The self-heating test exploits the dependence between temperature rise in an RTD during steady state internal ohmic heating and the sensor-to-fluid heat transfer resistance. This dependence makes it possible to detect changes in heat transfer characteristics. The temperature rise in the sensor is a function of both the heat generated and the ability of the sensor to dissipate heat to its surroundings.

The normal sensing current passing through the resistance element is usually 1-5 mA. During the self-heating test, the current is incrementally increased from 1-5 mA to a significantly higher value (20-100 mA). The electrical resistance of the element is measured at steady state conditions for a set of points and the power generated in the sensor is computed for each point.

The result is a curve that shows the change in resistance of the sensing element as a function of the power generated in the sensor. The resistance change is proportional to the change in temperature of the resistance element. For elements made of platinum, the self-heating curve is linear.

6.2 Theory and Principle of the Self-Heating Method

The resistance measurement needed for a normal temperature measurement involves the use of an electrical bridge circuit. A small current passes through the RTD and the bridge resistors so that a temperature change in the RTD is indicated by a voltage drop across two arms of the bridge. The current used for normal measurements is set at a small enough value (1 to 5 ma) to avoid significant ohmic heating of the RTD and concomitant temperature measurement errors. The self heating test involves increasing the current incrementally to higher values (20 - 100 ma) in order to cause enough ohmic heating to give a significant increase in the temperature of the sensing wire in the RTD. The steady state heat transfer is defined by

$$Q = UA(T-\theta) \tag{6.1}$$

where

Q = heat generation rate in the RTD

U = overall heat transfer coefficient

A = heat transfer area

T = sensor temperature

θ = fluid temperature.

If the fluid temperature remains constant, the temperature rise, ΔT, is related to a change in heat generation rate, ΔQ, as follows:

$$\Delta T = \frac{\Delta Q}{UA} . \tag{6.2}$$

Since the resistance of an RTD is proportional to its temperature,

$$\frac{1}{UA} \propto \frac{\Delta R}{\Delta Q} . \tag{6.3}$$

This motivates one to make steady state measurements of the RTD resistance for several values of I^2R power generated in the sensor. The slope of the curve of ΔR vs. ΔQ is proportional to $\frac{1}{UA}$.

The response time[2] is proportional to the heat capacity of the sensor and inversely proportional to UA. If it may be assumed that the heat capacity of a sensor will not change after construction, the response time, τ, is related to the slope of the self-heating curve as follows:

$$\tau \propto \frac{\Delta R}{\Delta Q} . \qquad (6.4)$$

That is, degradation of the response time could be detected by measuring an increase in $\Delta R/\Delta Q$.

6.3 Development of an Empirical Transformation Using the Self-Heating Test

It is possible to simulate changes in the sensor heat transfer resistance in laboratory tests. This is done by adding artificial heat transfer resistance (such as adhesive tape or short sections of rubber tubing) to the surface of the RTD. In doing so, an empirical relation can be obtained by performing plunge tests and self-heating tests on a set of heat transfer configurations.

The plunge test time constant is computed along with the value of the slope of the self-heating curve for various surface heat transfer conditions obtainable in the laboratory. After installation in a reactor, the fluid temperature step response can be predicted by: performing a self-heating test in-situ, computing the value for $\Delta R/\Delta Q$ for that environment, and determining the corresponding plunge test time constant from the empirical curve.

6.4 Laboratory Results from Self-Heating Tests

Self-heating tests were performed in the laboratory for PWR-type RTD's. Results were obtained for bare sensors and for all of the augmented surface resistance configurations used in developing the LCSR empirical correlation (see Section 5.3).

Self heating curves for bare sensors are shown in Figures 6.1 through 6.3. Note the strong linearity of the relation. Curves such as these (each involving twenty to thirty points for different current levels) were obtained for each augmented surface resistance configuration. The slope of the self heating curve was determined for each case. Figures 6.4a, 6.4b, 6.5a, and 6.5b show the empirical correlation between the slope of the self heating curve and the measured plunge time constant. These curves make it possible to use an in-plant self-heating test to provide the plunge test time constant provided the following assumptions are satisfied (as with the LCSR empirical transformation):

1. Laboratory tests involving augmentation of surface heat transfer resistance adequately simulate actual degradation in an in-plant sensor.
2. Differences between temperature and fluid velocity conditions in the laboratory and the plant have insignificant effects.

The validity of these assumptions is being evaluated.

6.5 In-Plant Results from Self-Heating Tests

Self-heating tests were not performed at Turkey Point because this test had not been conceived at the time of that test. However, the self-heating tests were performed at Oconee for all three RTD's. The measured self-heating curves are shown in Figures 6.6 through 6.8.

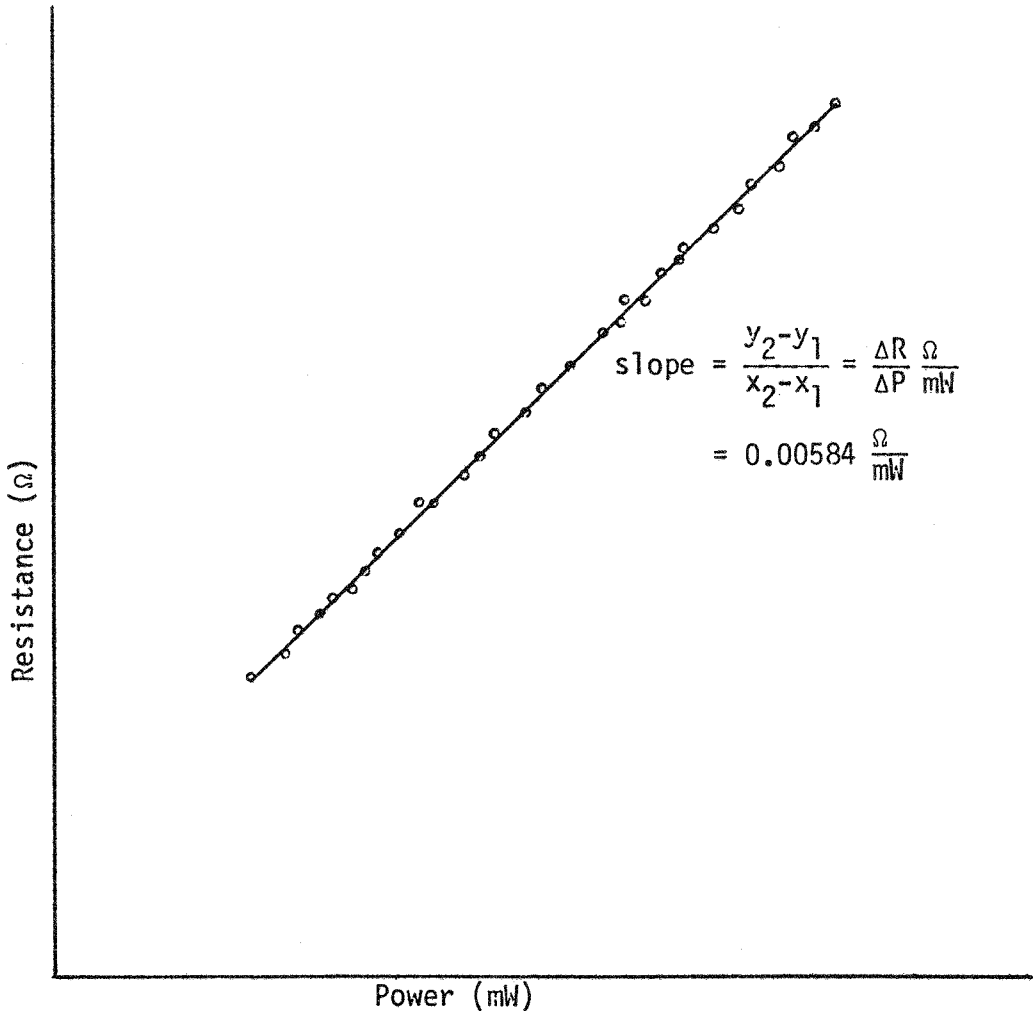

Figure 6.1 Self-Heating Curve for the 176-KF Sensor.

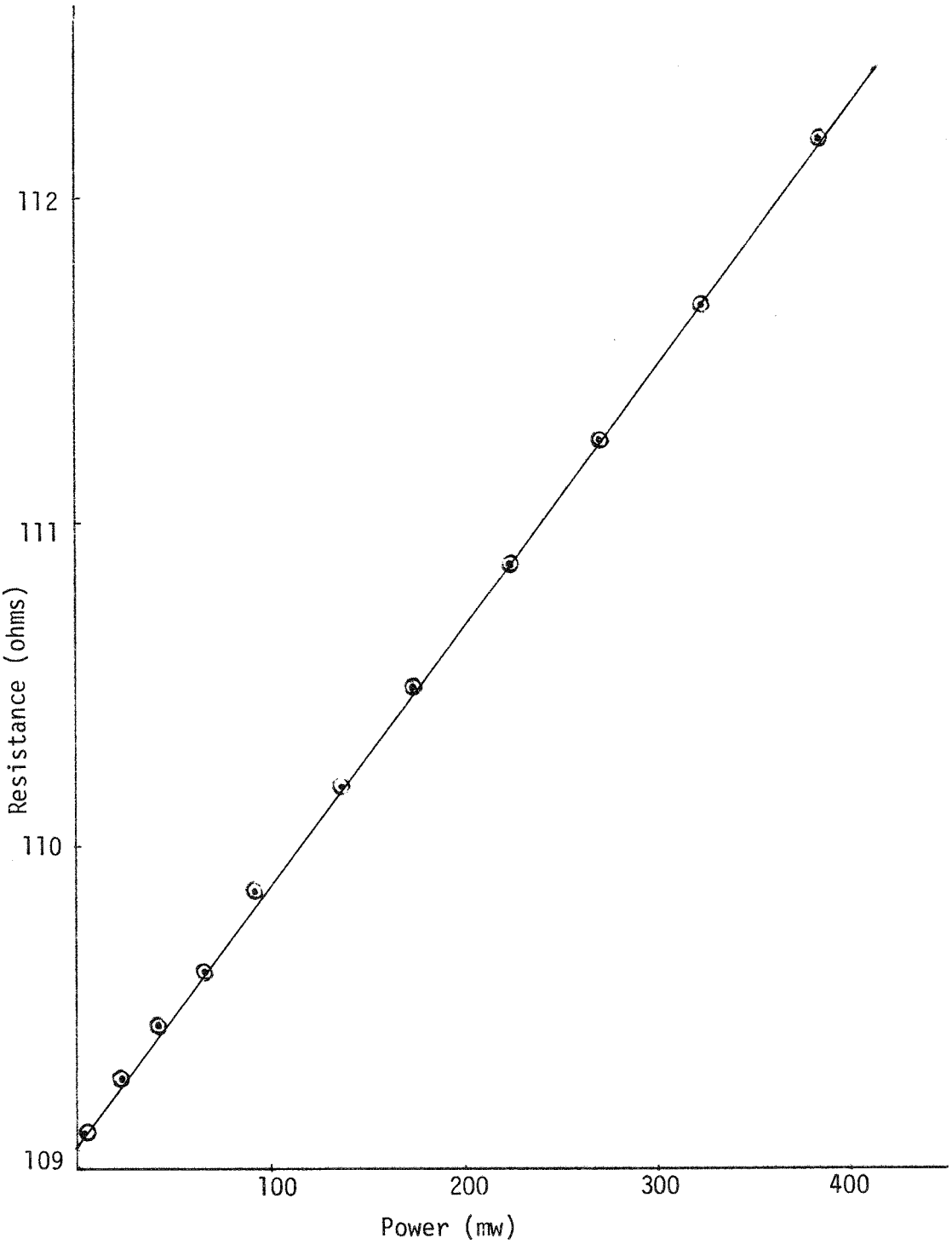

Figure 6.2 Self-Heating Curve for Rosemount Model 177GY.

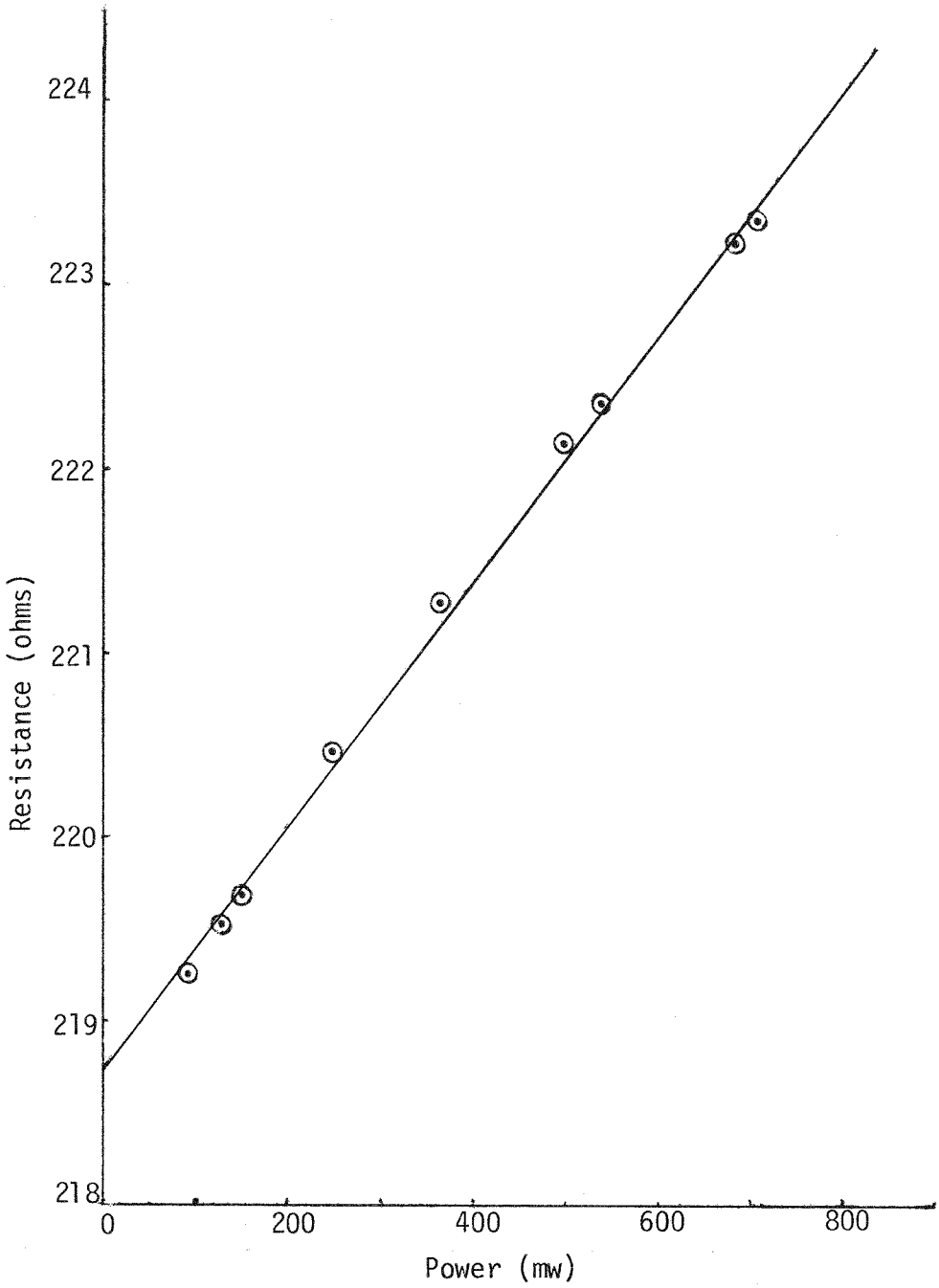

Figure 6.3 Self-Heating Curve for Rosemount Model 104AFC.

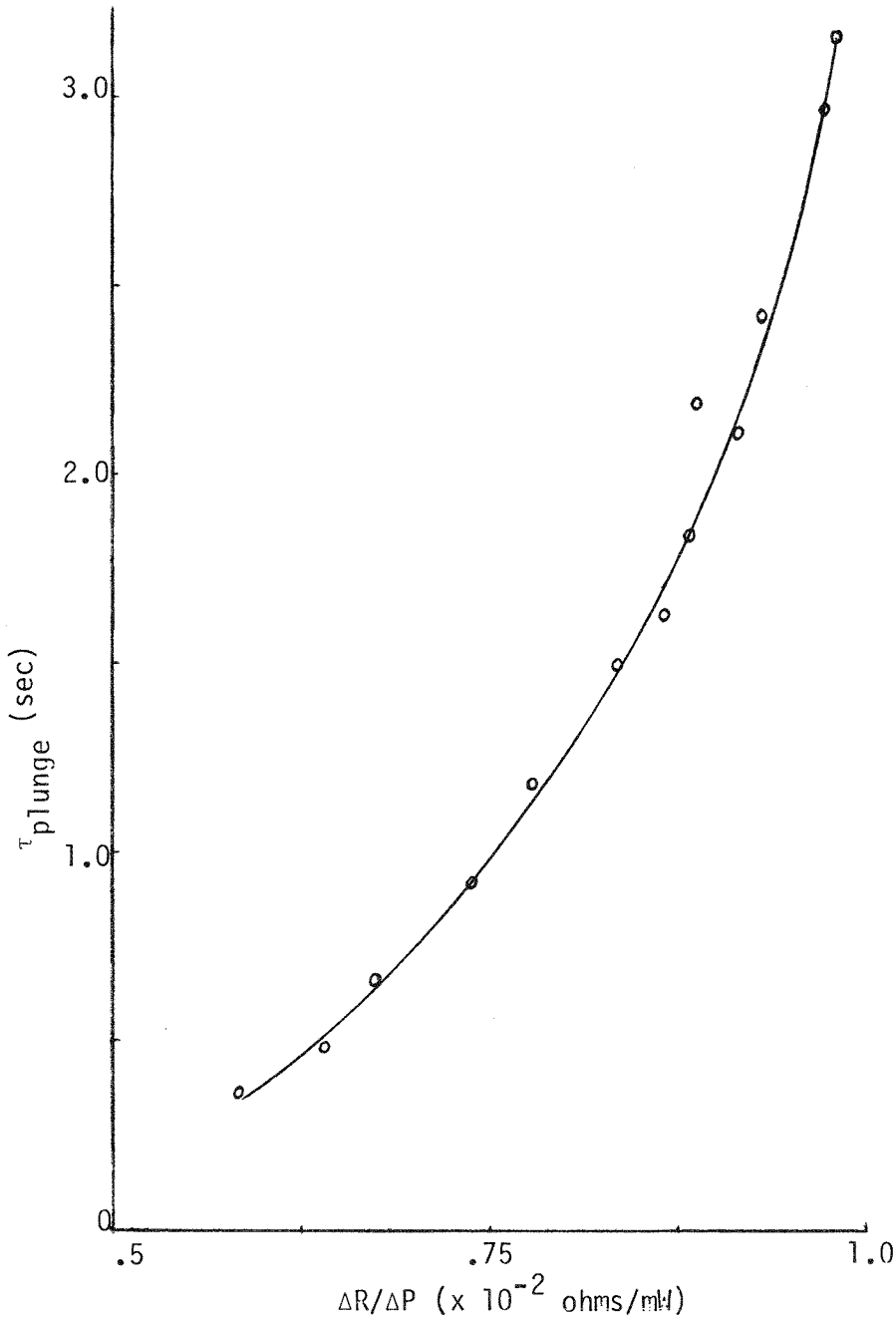

Figure 6.4a Empirical Correlation Between the Slope of the Self-Heating Curve and the Measured Plunge Test Time Constant. This Correlation is for the 176-KF Sensor.

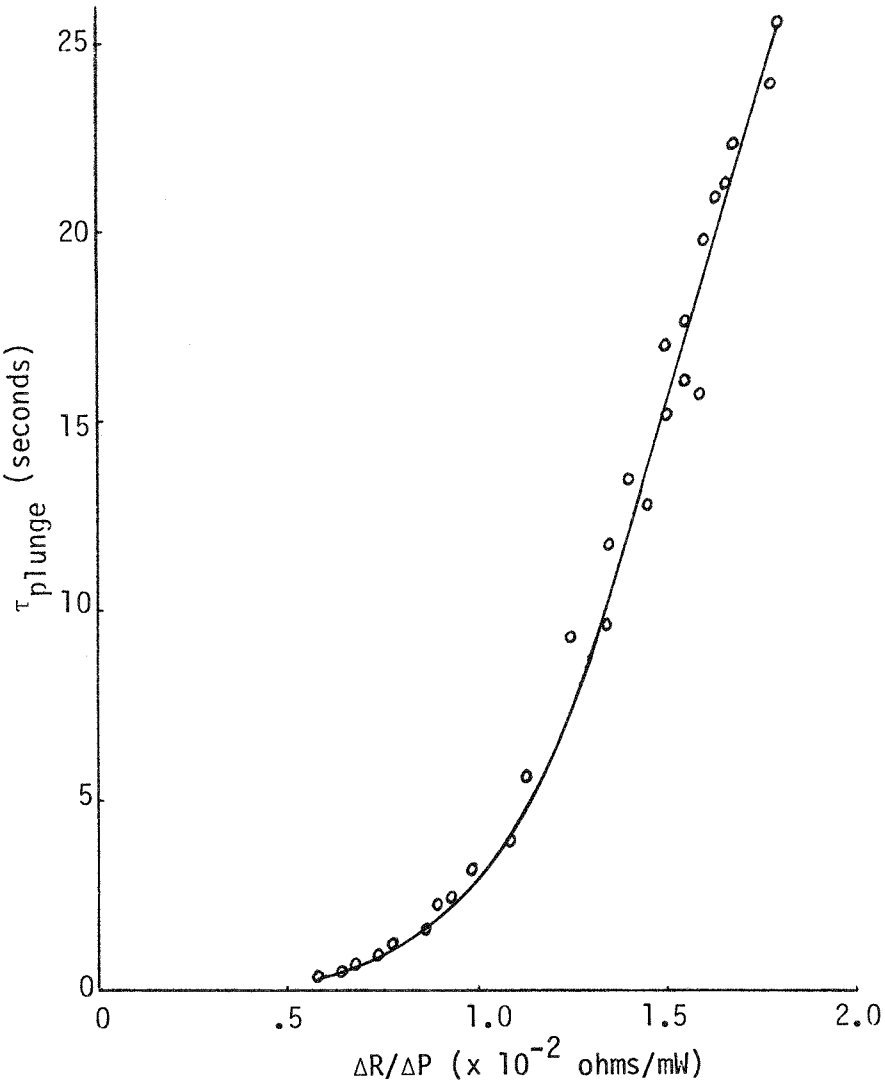

Figure 6.4b Empirical Correlation Between the Slope of the Self-Heating Curve and the Measured Plunge Test Time Constant. This Correlation is for the 176-KF Sensor.

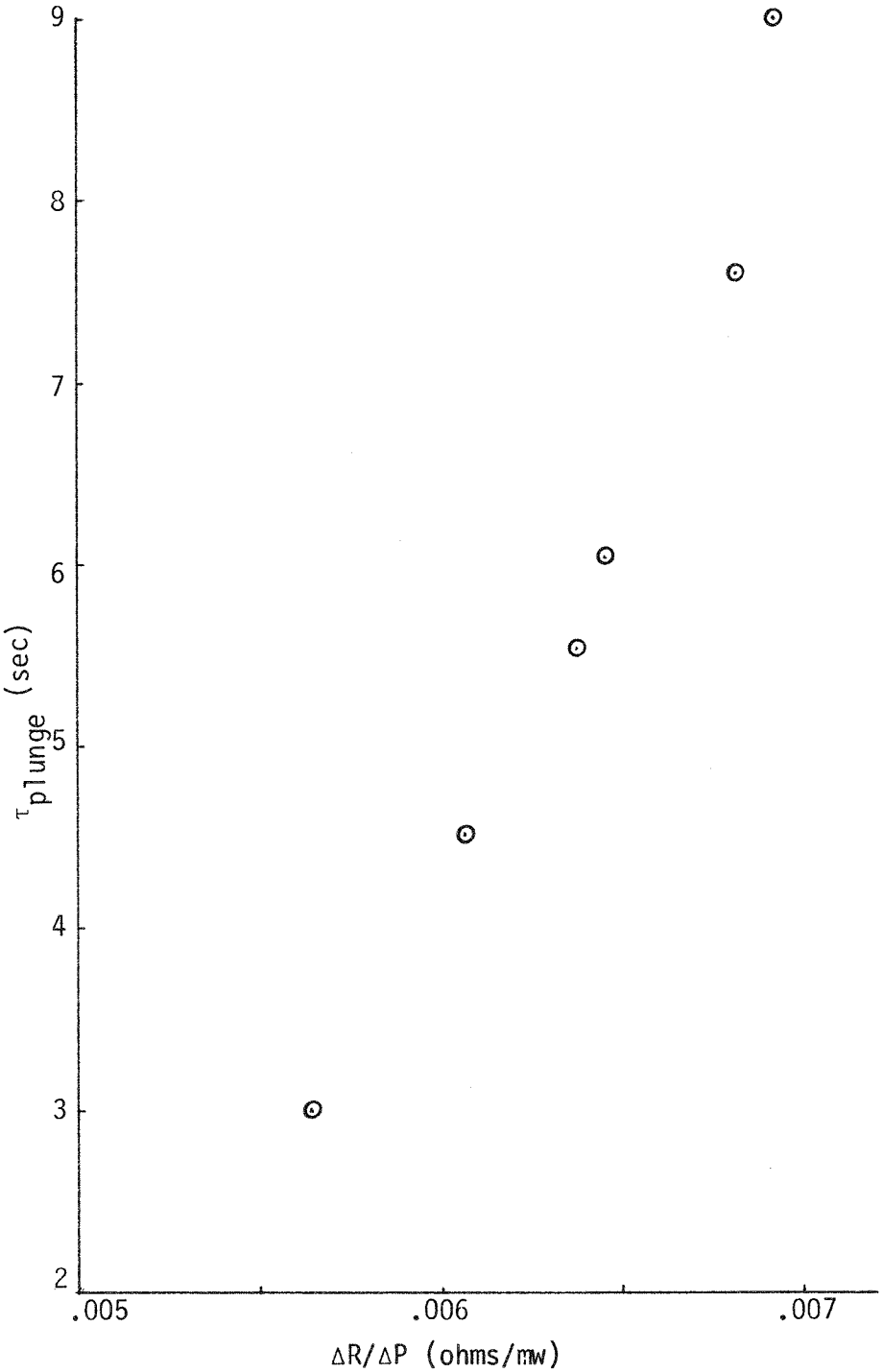

Figure 6.5a Empirical Correlation Between the Slope of the Self-Heating Curve and the Measured Plunge Test Time Constant (Narrow Range) Rosemount Model 104AFC.

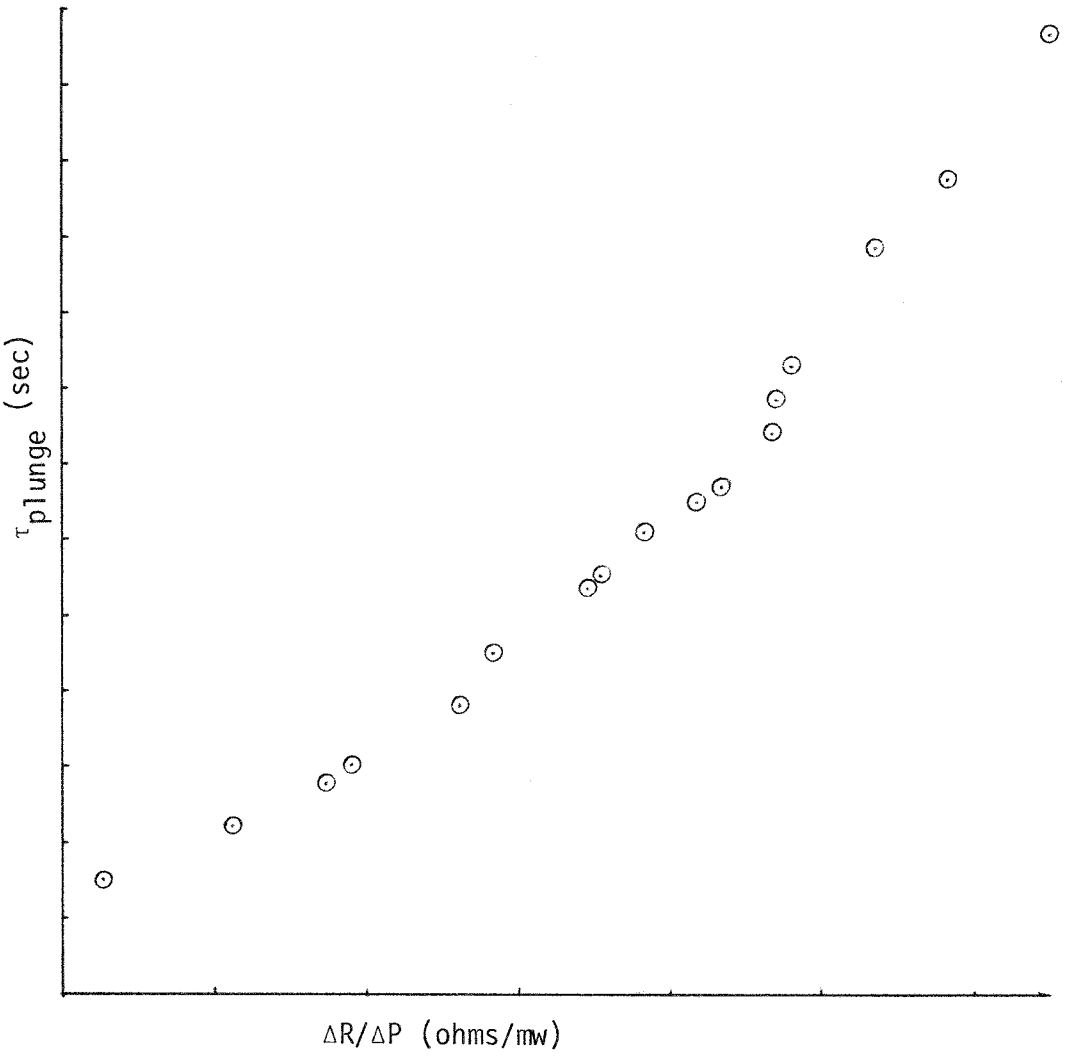

Figure 6.5b Empirical Correlation Between the Slope of the Self-Heating Curve and the Measured Plunge Test Time Constant (Wide Range) Rosemount Model 104AFC.

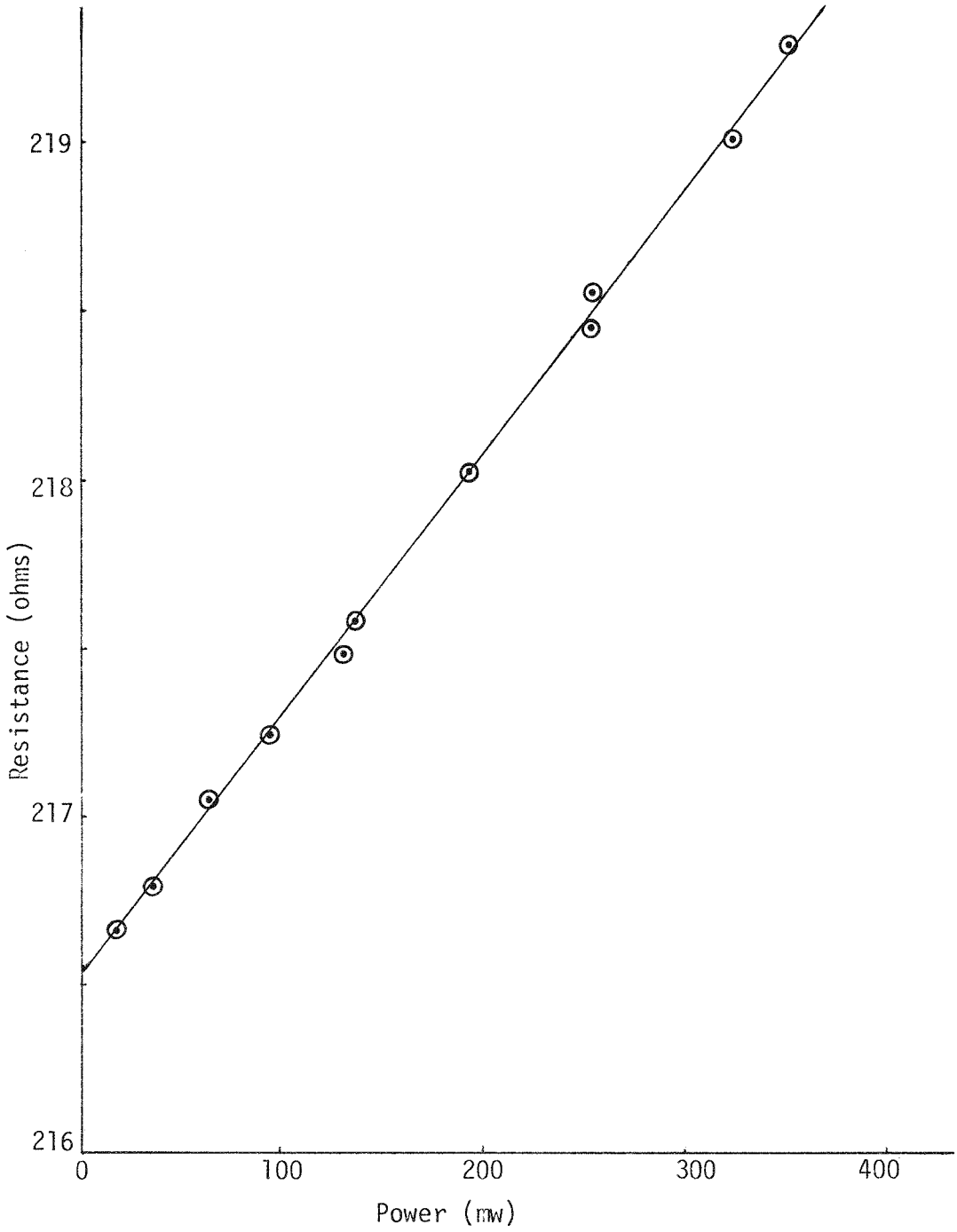

Figure 6.6 Self-Heating Curve for Oconee Sensor No. 1.

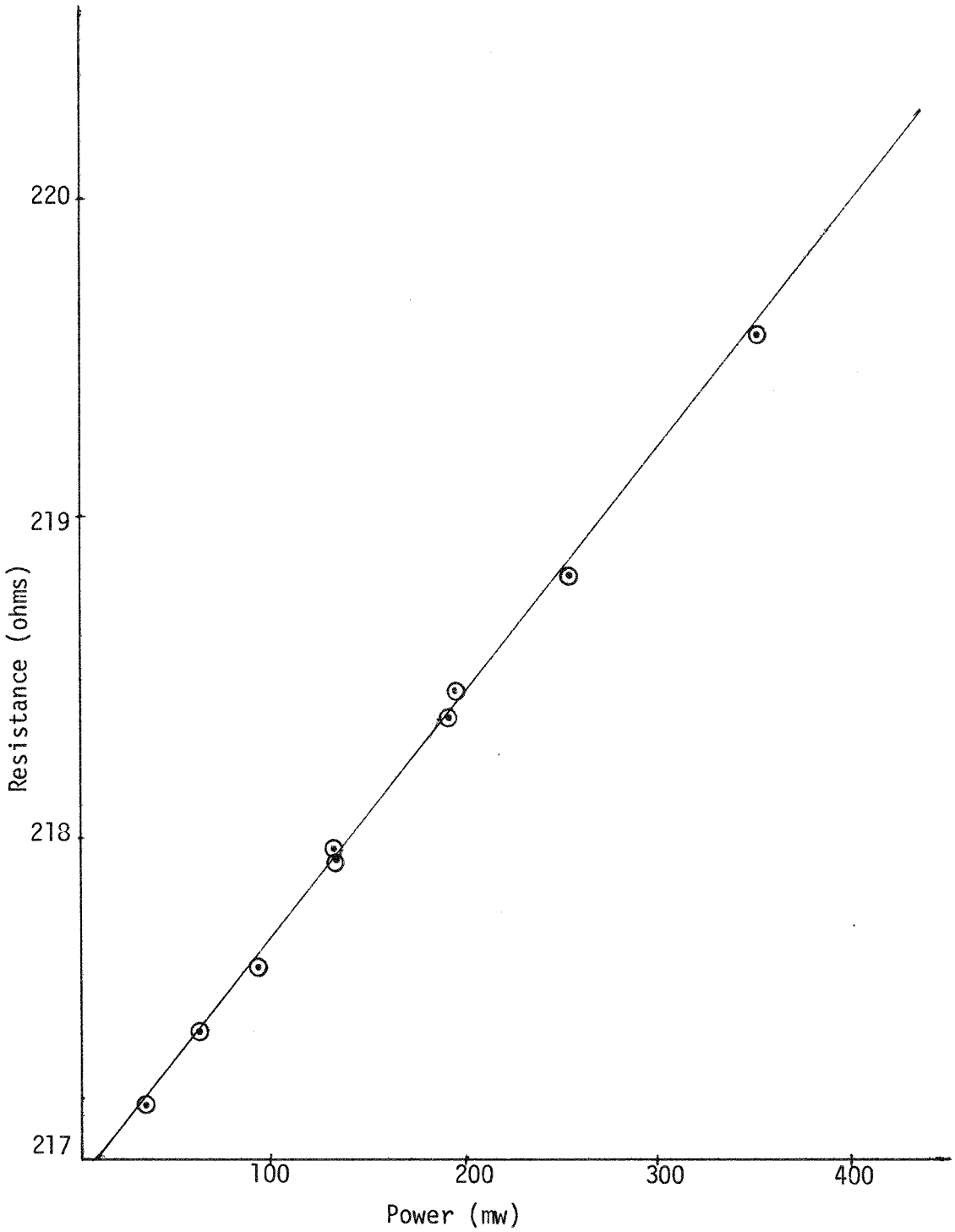

Figure 6.7 Self-Heating Curve for Oconee Sensor No. 2.

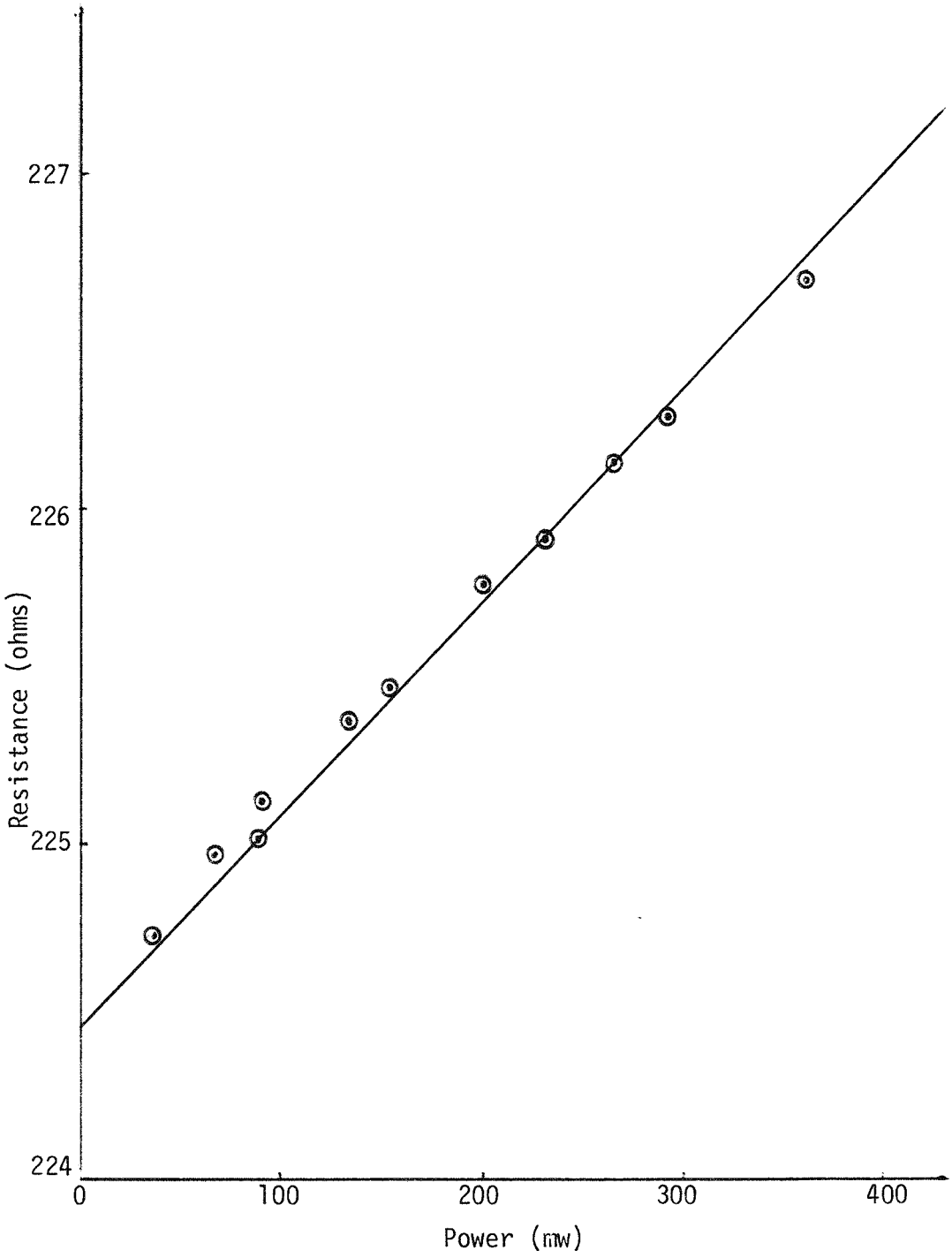

Figure 6.8 Self-Heating Curve for Oconee Sensor No. 3.

According to information obtained from Oconee plant personnel, sensors number 2 and 3 are Rosemount model 177GY and sensor number 1 is a Rosemount model 177-HW. Laboratory data for the self-heating empirical correlations have not been obtained for these sensors, but a single self-heating curve for a bare 177GY has been measured in the laboratory. The results for the Oconee sensors and for the laboratory results on a model 177GY are shown in Table 6.1.

TABLE 6.1

SELF-HEATING DATA FOR OCONEE SENSORS AND FOR ROSEMOUNT 177GY IN THE LABORATORY

Sensor	Slope of Self Heating Curve
Oconee # 1	7.83×10^{-3} Ω/mw
Oconee # 2	7.66×10^{-3} Ω/mw
Oconee # 3	6.37×10^{-3} Ω/mw
Laboratory 177GY	8.07×10^{-3} Ω/mw

From this, it appears that the sensor specification obtained from Oconee personnel was incorrect and that sensors number 1 and 2 are Rosemount 177GY. If this is true, the self-heating curve measured at Oconee indicates that the model 177GY sensors in the plant have nearly the same time constant as was observed for that sensor in the laboratory (~6 seconds).

7.0 THE NOISE ANALYSIS APPROACH FOR SENSOR RESPONSE TIME MEASUREMENT

7.1 Introduction

In this chapter, the sensor time response characteristics are evaluated using a time series analysis of noise signals. The method described in the following sections is based on the fact that the response of a linear system due to background noise disturbance can be modeled adequately by a finite order autoregressive (AR) model. The optimal estimated model can also provide the power spectrum of the time series without using Fourier transform methods.

In Section 7.2, the representation of the time series models is described. The discussions are brief and the reader is referred to appropriate references for details. The estimation of autoregressive parameters using Yule-Walker equations and the determination of an optimal model order are discussed in Section 7.3. Also, power spectrum estimation through use of an autoregressive model is discussed in Section 7.3. Verification procedures for model adequacy are given in Section 7.4.

Section 7.5 describes how one can obtain the impulse response and the step response of the dynamic system using the autoregressive model. These techniques, based on the exact solution to a continuous

system and a recursive estimation from the AR model, are tested by simulating known systems of order two and five. These results are presented in Section 7.6. Evaluation of the response time of RTD's used in the Millstone 2 PWR from noise data is presented in Section 7.7. Concluding remarks are given in Section 7.8.

7.2 Time Series Models for Noise Analysis

Let $\{y_k\}$ be a sequence of measurements of a random, weakly stationary process generated from a white noise disturbance $\{V_k\}$. The linear prediction model of $\{y_k\}$ can be written as

$$y_k = \sum_{i=1}^{\infty} a_i y_{k-i} + \sum_{i=1}^{\infty} b_i V_{k-i} + V_k. \tag{7.1}$$

An infinite representation Eq. (7.1) is not feasible and often may be incorrect. A finite order autoregressive moving average (ARMA) model is given by (see Box and Jenkins)[5]

$$y_k = \sum_{i=1}^{n} a_i y_{k-i} + \sum_{i=1}^{m} b_i V_{k-i} + V_k. \tag{7.2}$$

If the response y_k is to be represented only in terms of the past and present disturbances, then the one-sided moving average representation is

$$y_k = \sum_{i=1}^{\infty} b_i V_{k-i} + V_k. \tag{7.3}$$

Thus, we see that the space of observations generated by $\{V_i,\ i \leq k\}$ is equal to that generated by $\{y_i:\ i \leq k\}$. Accordingly, y_k can be approximated by the autoregressive model[6]

$$y_k = \sum_{i=1}^{n} a_i y_{k-i} + V_k. \tag{7.4}$$

For stationarity of the process defined by Equation (7.4), it is necessary that the roots of

$$1 - \sum_{i=1}^{n} a_i D^i = 0 \tag{7.5}$$

lie outside the unit circle.

These observations provide the basic arguments for the use and applicability of autoregressive models both for power spectrum estimation and evaluation of dynamic response characteristics.

7.3 Estimation of an Optimal Autoregressive Model

7.3.1 Estimation of AR Parameters

Let the time series under observation be a realization of the autoregressive process defined by

$$y_k = \sum_{i=1}^{n} a_i y_{k-i} + V_k \quad , \quad k = 1, 2, \ldots \tag{7.6}$$

Let $\{V_k\}$ be a white noise sequence; that is, the V_k are uncorrelated with statistics

$$E[V_k] = 0 \text{ and } E[V_k^2] = \sigma^2 \text{ for all } k. \tag{7.7}$$

Define the autocovariance function of the stationary process $\{y_k\}$, for lag k, as

$$\gamma_k = E[y_t y_{t+k}]. \tag{7.8}$$

Since $\{y_k\}$ is a real process, the autocovariance function is symmetric, and

$$\gamma_k = \gamma_{-k} \text{ for all } k. \tag{7.9}$$

An important recurrence relation for the autocovariance function of a stationary autoregressive process is found by multiplying Equation (7.6) by y_{t-k} to obtain

$$y_{t-k}\, y_t = \sum_{i=1}^{n} a_i y_{t-i} y_{t-k} + y_{t-k}\, V_t. \tag{7.10}$$

Taking the expected value in (7.10) and noting that y_{t-k} is independent of y_t and $E[V_t] = 0$, we get

$$E[y_{t-k} y_t] = \sum_{i=1}^{n} a_i\, E[y_{t-i} y_{t-k}]. \tag{7.11}$$

Using definition (7.8), one obtains:

$$\gamma_k = \sum_{i=1}^{n} a_i\, \gamma_{k-i}\ , \quad k > 0. \tag{7.12}$$

Dividing (7.12) by γ_o, the correlation at lag zero, one obtains the normalized recursion relationship

$$\rho_k = \sum_{i=1}^{n} a_i \rho_{k-i},\ k > 0 \tag{7.13}$$

where

$$\rho_k = \gamma_k/\gamma_o,\ \rho_o = 1. \tag{7.14}$$

The correlations γ_k are computed from the observed time series as

$$\gamma_k = \frac{1}{N} \sum_{i=1}^{N-k} \tilde{y}_i\, \tilde{y}_{i+k} \tag{7.15}$$

$$\tilde{y}_i = y_i - \frac{1}{N} \sum_{k=1}^{N} y_k \tag{7.16}$$

where N is the number of measurements. If the data processing is made in blocks, then N is the length of a block. Equation (7.13) can be written for k = 1, 2, . . ., n giving

$$\rho_1 = a_1 + a_2 \rho_1 + \ldots + a_n \rho_{n-1}$$
$$\rho_2 = a_1 \rho_1 + a_2 + \ldots + a_n \rho_{n-2}$$
$$\vdots$$
$$\rho_n = a_1 \rho_{n-1} + a_2 \rho_{n-2} + \ldots + a_n. \qquad (7.17)$$

Equation (7.17) is called the Yule-Walker equations.[1] The parameters a_i, i = 1, 2, . . ., n are obtained by solving (7.17). Rewriting this in matrix notation, we obtain:

$$\begin{bmatrix} \rho_1 \\ \rho_2 \\ \vdots \\ \rho_n \end{bmatrix} = \begin{bmatrix} 1 & \rho_1 & \cdots & \rho_{n-1} \\ \rho_1 & 1 & \cdots & \rho_{n-2} \\ \vdots & \vdots & \ddots & \vdots \\ \rho_{n-1} & \rho_{n-2} & \cdots & 1 \end{bmatrix} \begin{bmatrix} a_1 \\ a_2 \\ \vdots \\ a_n \end{bmatrix} \qquad (7.18)$$

or $\underline{\rho} = P\,\underline{a}$. (7.19)

P is an nxn symmetric Toeplitz matrix.[7] Taking the inverse, one obtains the estimation

$$\hat{\underline{a}} = P^{-1}\,\underline{\rho}. \qquad (7.20)$$

In practice, the order n is less than 20. (See the numerical results of Section 7.7.) It can be shown that the Yule-Walker estimate is equivalent to the least square problem of

$$\min_{\underline{a}} \sum_{k=1}^{N} (y_k - \sum_{i=1}^{n} a_i \, y_{k-i})^2 \tag{7.21}$$

as $N \to \infty$. The key point here is that the autoregressive parameters are the same in a model for the normalized autocovariance function and in a model for the raw data.

7.3.2 Optimal Order of an AR Model

It is necessary to obtain an estimate of the optimal AR order. Akaike[8] obtained the following expression as the information criterion, and the optimal order n* corresponds to the minimum value of this criterion function

Information Criterion = - log(maximum likelihood function) + n.

As n increases, the first term decreases and an optimal order is obtained. The first term is a function of the squared error, and the addition of n takes care of the downward bias introduced in the estimation of the criterion function. The likelihood function can be evaluated by approximating the distribution of white noise as a Gaussian distribution. This restriction can in general be removed by using the result obtained by Caines,[9] that the strong consistency of the maximum likelihood estimation for the Gaussian log-likelihood is not dependent upon any Gaussian assumption concerning $\{V_k\}$.

If the estimate $\hat{\underline{a}}$ is available, the joint probability density for the Gaussian statistic may be used to find the likelihood function $\hat{L}$ as

$$\hat{L} = (2\pi\hat{\sigma}^2)^{\frac{N}{2}} \{\exp[-\frac{1}{2\hat{\sigma}^2} \sum_{k=1}^{N} \hat{V}_k^2]\} \tag{7.22}$$

where

$$\hat{V}_k = y_k - \sum_{i=1}^{n} \hat{a}_i y_{k-i} \quad , k = 1, 2, \ldots, N \tag{7.23}$$

is defined as the prediction error associated with the noise sequence. The noise variance is estimated from

$$\hat{\sigma}^2 = \frac{1}{N} \sum_{k=1}^{N} \hat{V}_k^2. \tag{7.24}$$

By varying the AR order n, an optimal value n* is obtained for which the information criterion, IC, is a minimum:

$$IC = - \log \hat{L} + n. \tag{7.25}$$

7.3.3 Estimation of Power Spectrum

With the knowledge of optimal autoregressive parameters, one can obtain the estimate of the power spectrum of the observed noise signal.

$$S_{yy}(f) = \frac{\hat{\sigma}_v^2 T}{|1 - \sum_{k=1}^{n} \hat{a}_k e^{-i2\pi fkT}|^2} \quad , |f| \leq \frac{1}{2T} \text{ Hertz}, \tag{7.26}$$

where

T = sampling time, sec

f = frequency, Hertz

σ_v^2 = variance of background white noise.

The power spectrum given by (7.26) will be periodic with folding frequency equal to 1/2T Hertz. $S_{yy}(f)$ obtained above is the smoothed spectrum and shows the salient features contained in the signal.

7.4 Model Verification

The final and important step in constructing a model is to determine whether the assumptions made in the analysis are satisfied within a specified confidence level.

The major assumption in the model is that the background noise is a white noise sequence. Such a noise process has the property that the adjacent points of the series are not correlated. The correlation function must have the characteristics of an impulse function. The spectrum of the noise sequence must be flat within the band limited by the folding frequency. Several statistical tests are enumerated below. For details, see references [5,10].

7.4.1 Autocorrelation Verification Using Prediction Error

If the parameters ($\underline{a}$) of the AR model were known exactly, it is shown by Anderson[11] that the estimated autocorrelation $\rho_k(\hat{V})$ of the noise sequence {V}, would be uncorrelated and distributed approximately normally about zero with variance $\frac{1}{N}$ and, hence, have a standard error of $\frac{1}{\sqrt{N}}$. In the case when $\underline{a}$ is not exactly known, an estimate of the noise sequence can be obtained using the prediction error

$$\hat{V}_k = y_k - \sum_{i=1}^{n} \hat{a}_i \, y_{k-i} \, , \; k = 1, 2, \ldots, N. \qquad (7.27)$$

Knowing $\{y_k\}$ and $\hat{\underline{a}}$, estimates of $\hat{V}_k$ are obtained. The autocorrelation is then determined and plotted. The standard error, $\frac{1}{\sqrt{N}}$, can be used as an estimate of the deviation of $\rho_k(\hat{V})$. It is shown by Box and Pierce[12] that this value may underestimate the error in $\rho_k(\hat{V})$ at low lags, but can be employed as a good estimate of the error at moderate or high lags. The whiteness of the noise is then checked by comparing a given number of $\rho_k(\hat{V})$ against a 95% confidence level given by $\frac{1.96}{\sqrt{N}}$. If less than 5% of the autocorrelation functions are within this limit, then the whiteness criterion is satisfied.

7.4.2 "Portmanteau" Lack of Fit Test

Since taking the $\gamma_k(\hat{V})$ individually and checking their boundedness is similar to testing a random sequence, an indication is often needed of whether or not the first few correlation functions taken as a whole indicate inadequacy of the model. Given the first M correlation functions from an AR(n) process, it is possible to show[12] that

$$Q = N \sum_{k=1}^{M} \gamma_k^2(\hat{V}) \tag{7.28}$$

is approximately Chi-squared distributed with (M-n) degrees of freedom if the driving function is white. If the model is inadequate, the average value of Q will be inflated.

7.4.3 Bandwidth of Residual Power Spectrum

If the noise sequence is pure white noise, its spectrum will be flat in the band $-\frac{1}{2T} \leq f \leq \frac{1}{2T}$. The flatness of the spectrum can be checked by calculating the spectrum of the estimates of $\{\hat{V}_k\}$ as follows:

a. Determine $\hat{V}_k = y_k - \sum_{i=1}^{n} \hat{a}_i \, y_{k-i}$

b. Determine $\gamma_k(\hat{V}) = \frac{1}{N} \sum_{i=1}^{N-k} \hat{V}_i \, \hat{V}_{i+k}$

c. Calculate the Fourier transform of $\gamma_k(\hat{V})$ using the equation

$$S_{vv}(f) = \sum_{k=-M}^{M} \gamma_k \, e^{-i2\pi fkt}, \quad |f| \leq \frac{1}{2T}. \tag{7.29}$$

Since γ_k is symmetric (7.29) becomes

$$S_{vv}(f) = \gamma_o + 2 \sum_{k=1}^{M} \gamma_k \cos 2\pi ftT \quad , \quad |f| \leq \frac{1}{2T}. \tag{7.30}$$

With the knowledge of $\gamma_k(\hat{V})$, $S_{vv}(f)$ may be calculated and plotted.

Satisfaction of all the above three diagnostic checks assures the appropriateness of the model and provides the needed confidence in the results.

7.5 Estimation of Response Characteristics

In this section, the impulse and step response of dynamic systems are derived using fitted autoregressive models.

7.5.1 A First Order System

The standard definition of the time constant is specified with reference to a first order system. Consider the following system:

$$\dot{x} + ax = u(t). \tag{7.31}$$

The unit step response for this system with $x(0) = 0$ is given by

$$x(t) = \frac{1}{a}(1 - e^{-at}). \tag{7.32}$$

Letting $t = \frac{1}{a}$ gives

$$x(\frac{1}{a}) = \frac{1}{a}(1 - \frac{1}{e}). \tag{7.33}$$

That is, when the time $t = \frac{1}{a}$, the value of $x(t)$ attains 0.632 of the steady state value. The time required for the step response of a stable first order system to attain 0.632 of the steady value ($\tau = \frac{1}{a}$ sec) is generally called the time constant of the system.

We observe that a closed form expression similar to (7.33) cannot be obtained for a system of order greater than one. However, one can always define τ as the time at which the response of the system to a step input will achieve 0.632 of its steady state value. Such a point on the response curve can be determined numerically.

7.5.2 Impulse and Step Responses from the Autoregressive Model

Consider the AR process determined for a given noise measurement

$$y_k = \sum_{i=1}^{n} a_i y_{k-i} + V_k \quad , \quad k = 1, 2, \ldots \tag{7.34}$$

The dynamics of (7.34) are obtained with the assumption that the driving force is a white noise sequence. Hence, it is not valid to replace V_k by the step input and evaluate the resulting response. However, the above model completely represents the dynamics of the system in terms of the AR parameters. Hence, the dynamic information (transient and steady state) is given by the poles of the equivalent Z-transform. By analogy to a continuous system, one can obtain the impulse response of (7.34) as an equivalent initial condition response.

7.5.3 Impulse Response Evaluation

Consider an nth order continuous system given by

$$\frac{d^n x}{dt^n} + a_1 \frac{d^{n-1} x}{dt^{n-1}} + \ldots + a_{n-1} \frac{dx}{dt} + a_n x(t) = u(t). \tag{7.35}$$

The unit impulse response of (7.35) is given by

$$X_I(t) = L^{-1}\left[\frac{1}{s^n + a_1 s^{n-1} + \ldots + a_{n-1} s + a_n}\right]. \tag{7.36}$$

Now, if one takes the Laplace transform of (7.35) with $u(t) = 0$ and all the initial condition equal to zero except $\frac{d^{n-1}x(0)}{dt^{n-1}}$, then one obtains

$$X(s) = \frac{x^{(n-1)}(0)}{s^n + a_1 s^{n-1} + \ldots + a_{n-1} s + a_n}. \tag{7.37}$$

The response to an initial condition of $x^{n-1}(0) = 1$ is

$$x_{IC}(t) = L^{-1}\left[\frac{(x^{(n-1)}(0) = 1)}{s^n + a_1 s^{n-1} + \ldots + a_{n-1} s + a_n}\right]. \tag{7.38}$$

Note that (7.36) and (7.38) are the same. In one case, the impulse response is obtained using a unit impulse input; in the other a non-zero initial condition on the (n-1)th derivative is used. A similar scheme applied to the discrete AR model to derive the impulse response is used.

A method which approximates the continuous case is obtained by using a differencing scheme. The derivatives are approximated as follows

$$
\begin{aligned}
x_k^1 &= y_k - y_{k-1} \\
x_k^2 &= x_k^1 - x^1_{k-1} \\
&\cdot \qquad\quad \cdot \\
&\cdot \qquad\quad \cdot \\
&\cdot \qquad\quad \cdot \\
x_k^{n-1} &= x_k^{n-2} - x_{k-1}^{n-2} \,.
\end{aligned} \tag{7.39}
$$

By letting $x^{n-1} \neq 0$ and all lower order differences equal to zero, the impulse response can be evaluated recursively. Note that (7.34) cannot be used directly. A new expression in terms of a_i, $i = 1, \ldots, n$, and $\{y_k, x^1_k, x^2_k, \ldots, x_k^{n-1}\}$ is derived. The resulting response has the form

$$
y_k = A_1\, y_{k-1} + A_2\, x^1_{k-1} + A_3\, x^2_{k-1} + \ldots + A_n\, x^{n-1}_{k-1}. \tag{7.40}
$$

The coefficients A_i are functions of AR parameters such that the relationships (7.39) are satisfied. The appropriate initial condition response is obtained by setting the initial value of $x^{n-1} = 1$ and all other terms in (7.40) equal to zero.

Computation of A_i is illustrated for a fourth order system. Consider

$$
y_k = \sum_{i=1}^{4} a_i\, y_{k-i}. \tag{7.41}
$$

Define the following:

$$
\begin{aligned}
x^1_k &= y_k - y_{k-1} \\
x^2_k &= x^1_k - x^2_{k-1} \\
x^3_k &= x^2_k - x^2_{k-1}
\end{aligned} \tag{7.42}
$$

$$x^1_{k-1} = y_{k-1} - y_{k-2}$$

$$y_{k-2} = y_{k-1} - x^1_{k-1} \tag{7.43}$$

$$x^2_{k-1} = x^1_{k-1} - x^1_{k-2} = x^1_{k-1} - (y_{k-2} - y_{k-3})$$

$$= x^1_{k-1} - (y_{k-1} - x^1_{k-1}) + y_{k-3}$$

$$y_{k-3} = y_{k-1} - 2x^1_{k-1} + x^2_{k-1} \tag{7.44}$$

$$x^3_{k-1} = x^2_{k-1} - x^2_{k-2}$$

$$= x^2_{k-1} - (x^1_{k-2} - x^1_{k-3})$$

$$= x^2_{k-1} - (y_{k-2} - y_{k-3}) + y_{k-3} - y_{k-4}$$

$$= x^2_{k-1} - (y_{k-1} - x^1_{k-1}) + 2(y_{k-1} - 2x^1_{k-1} + z^2_{k-1}) - y_{k-4}$$

$$y_{k-4} = y_{k-1} - 3x^1_{k-1} + 3x^2_{k-1} - x^3_{k-1}. \tag{7.45}$$

Using (7.43) - (7.45) in (7.41) gives

$$y_k = (a_1 + a_2 + a_3 + a_4)\, y_{k-1} - (a_2 + 2a_3 + 3a_4)\, x^1_{k-1}$$

$$+ (a_3 + 3a_4)\, x^2_{k-1} - a_4\, x^3_{k-1}. \tag{7.46}$$

Thus,

$$y_k = A_1\, y_{k-1} + A_2\, x^1_{k-1} + A_3\, x^2_{k-1} + A_4\, x^3_{k-1} \tag{7.47}$$

$$A_1 = a_1 + a_2 + a_3 + a_4,\ A_2 = -(a_2 + 2a_3 + 3a_4)$$

$$A_3 = a_3 + 3a_4,\ A_4 = -a_4.$$

It should be noted that results that agree quite well with results obtained by the above procedure for setting initial conditions are obtained by simply using (7.34) with $V_k = 0$ and y(initial) = 1. Of course, this does not have the analytical basis of the above method, and could not be relied upon universally.

7.5.4 Computation of Step Response

Once the impulse response is determined as outlined in (7.5.3), the step response is derived by integrating the impulse response

$$x(t) = \int_0^t x_I(\tau)\, d\tau. \tag{7.48}$$

A simple trapezoidal integration scheme is used to evaluate the step response since the integrand is available only at sample points.

7.6 Verification of the Method Using Simulated Systems

In this section, the methods discussed above are illustrated for three known systems.

7.6.1 Second Order System with Equal Poles

The following continuous system is considered:

$$G(s) = \frac{1}{(s+1)^2}. \tag{7.49}$$

The response is generated by sampling a continuous response due to an input to this system obtained from a random number generator at $\Delta t = 0.05$ sec. A total of 4000 samples was used.

Figures 7.1 through 7.6 show the results.

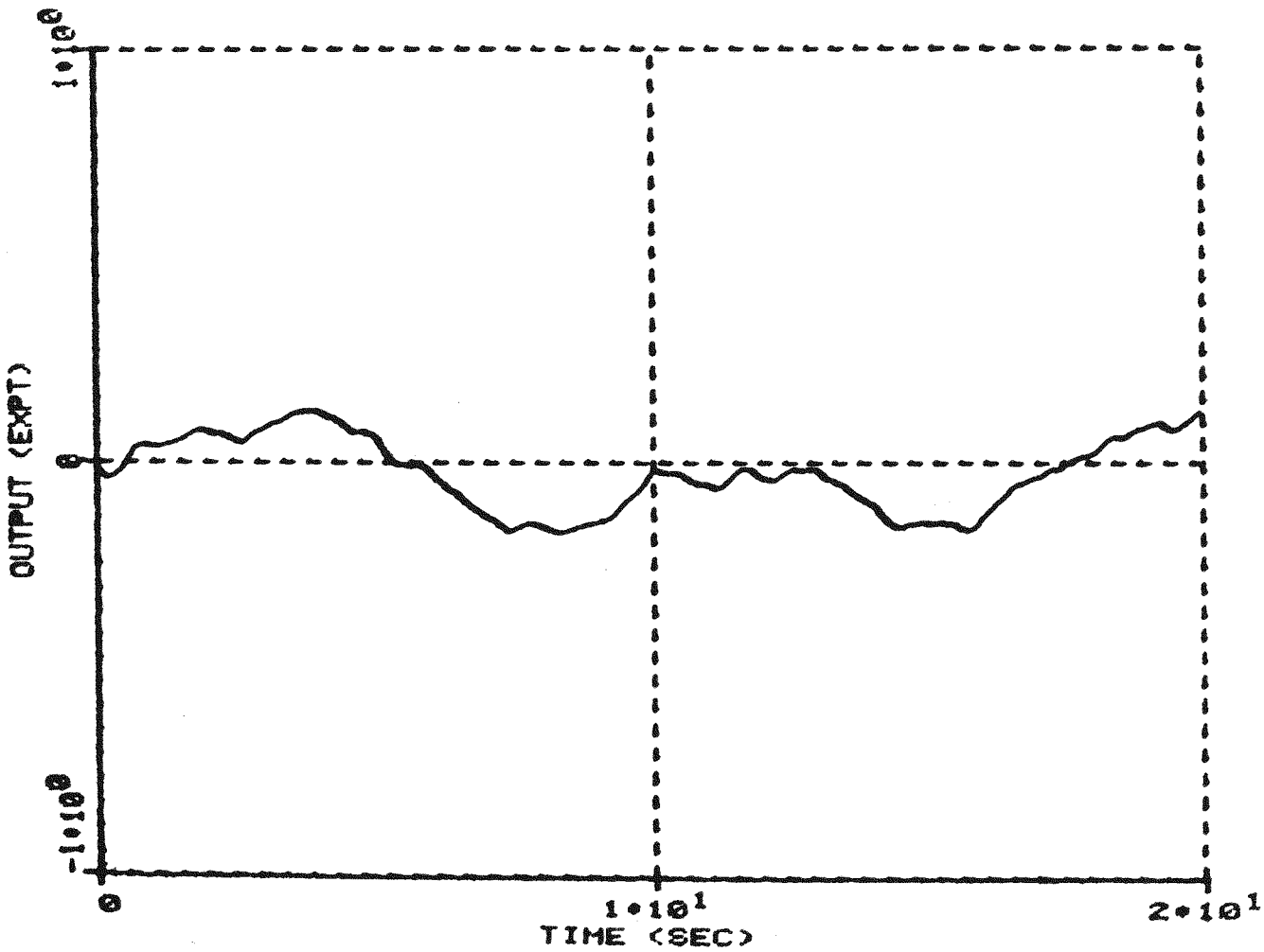

Figure 7.1 Output Noise for a Second Order System with Equal Poles.

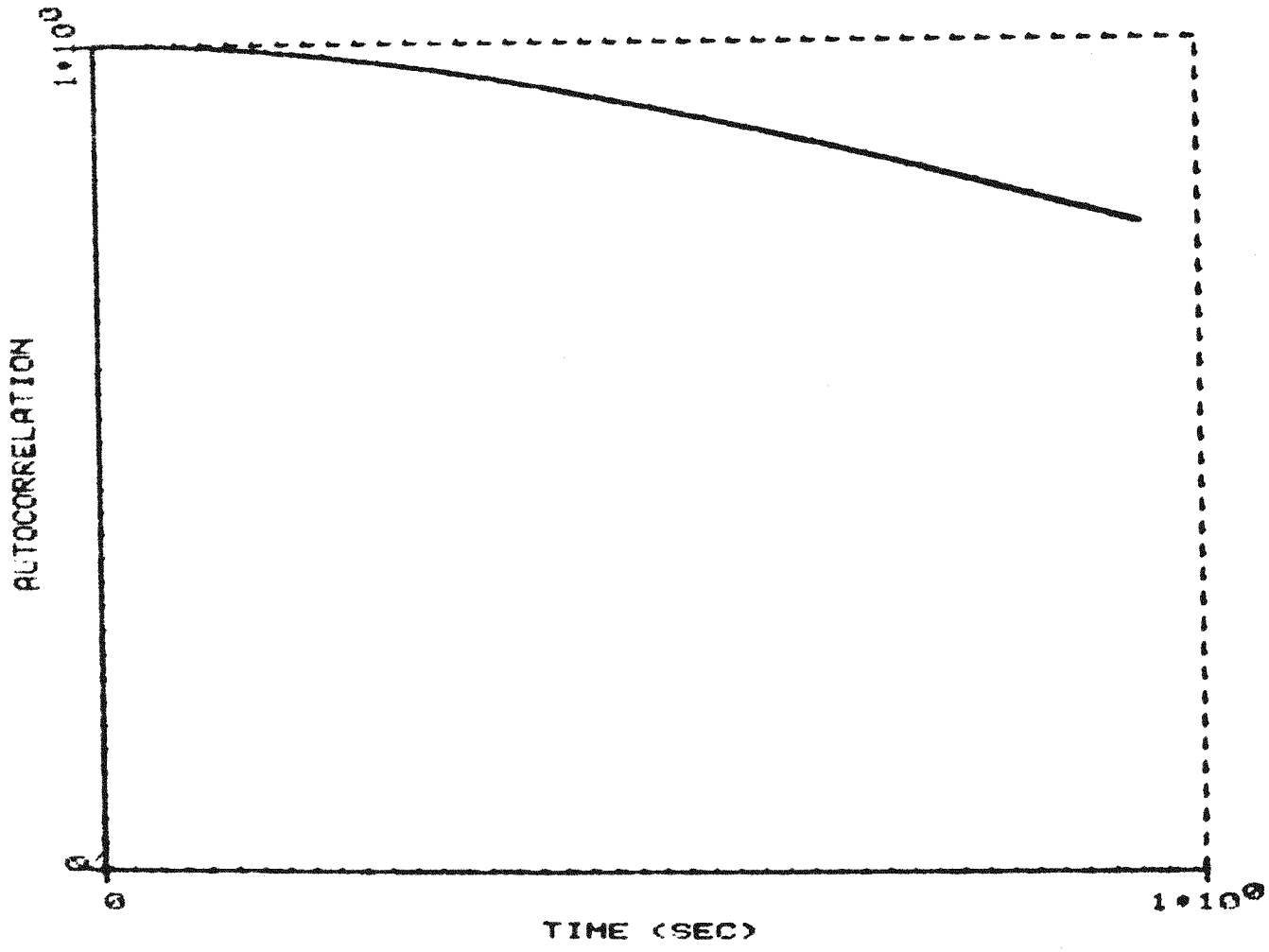

Figure 7.2 Autocorrelation Function for Data of Figure 7.1.

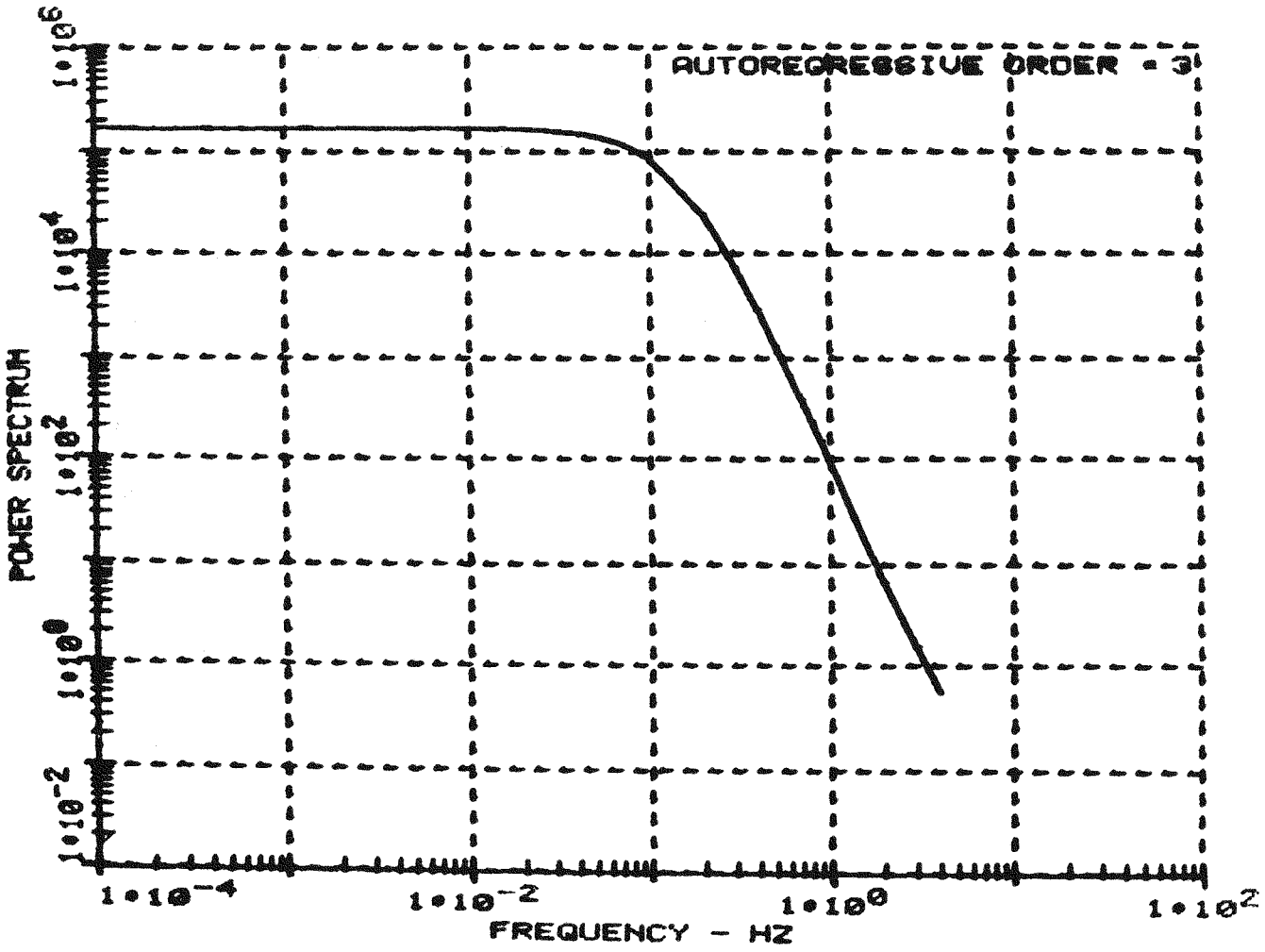

Figure 7.3 Power Spectrum Obtained Using AR (n=3) Parameters for Signal of Figure 7.1.

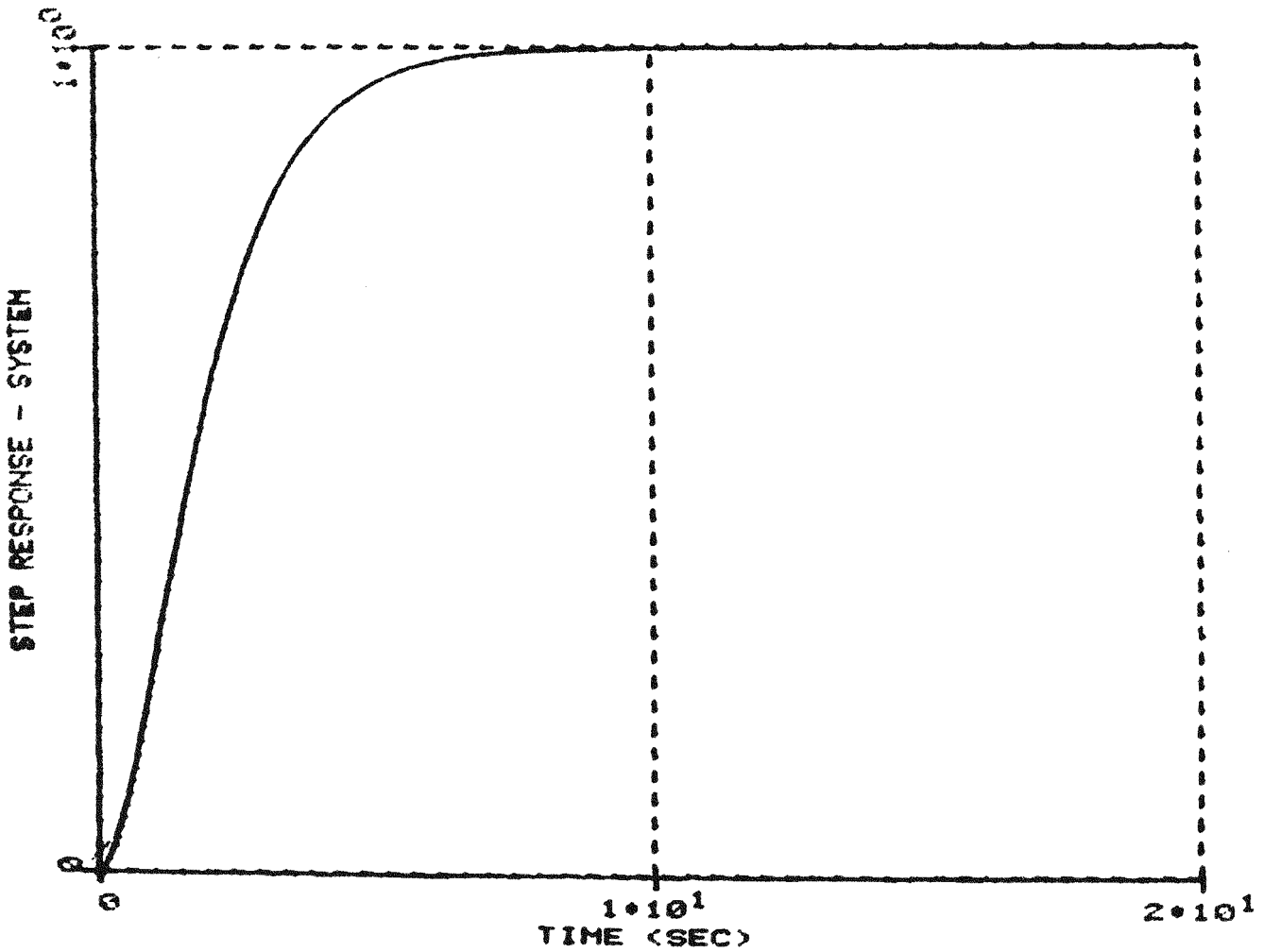

Figure 7.4 True Step Response for System with $G(s) = \frac{1}{(s+1)^2}$

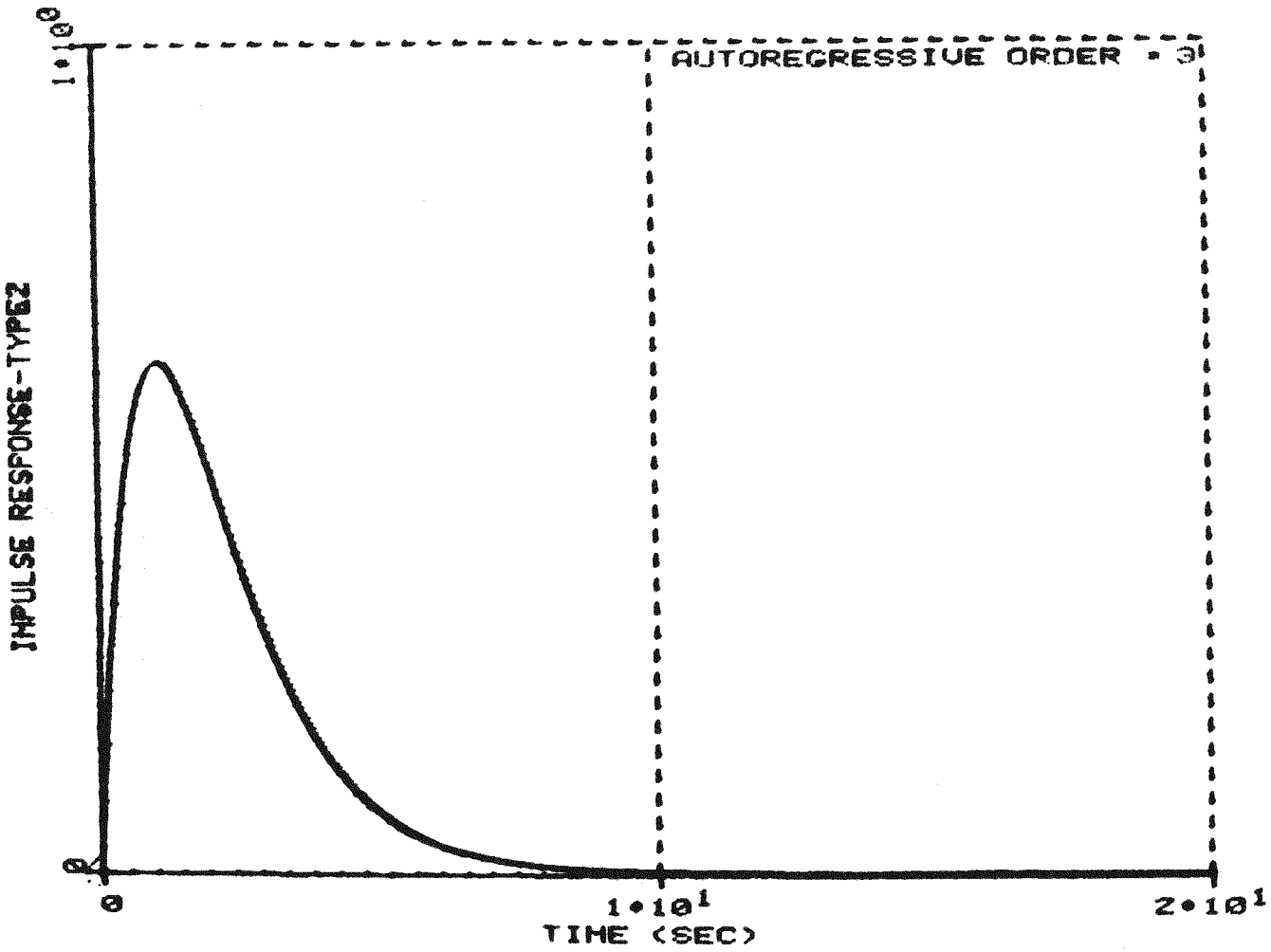

Figure 7.5 Impulse Response Calculated using AR (n=3) Parameters for the Signal of Figure 7.1.

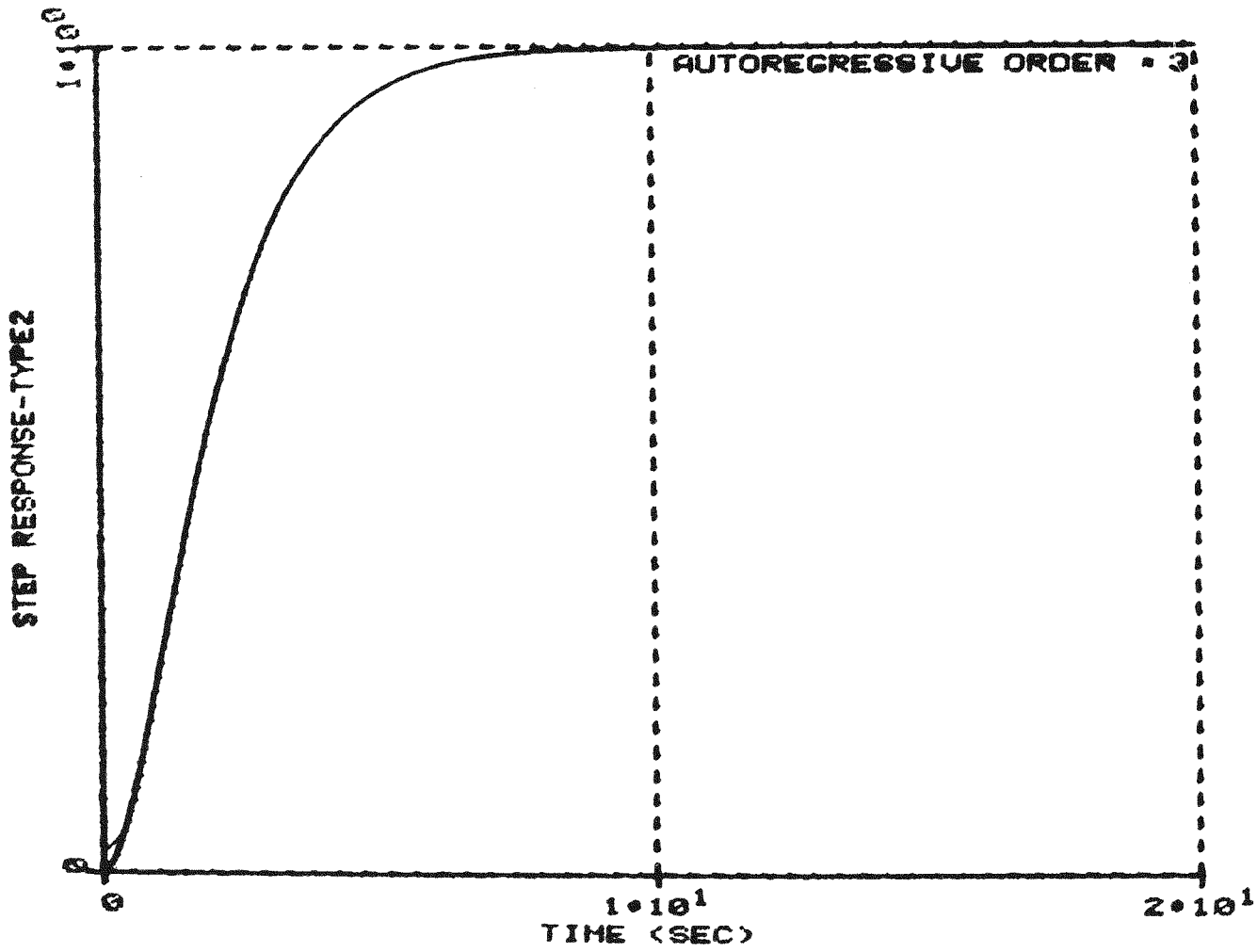

Figure 7.6 Step Response Calculated Using the AR (n=3) Parameters for the Data of Figure 7.1.

Results: The true system time constant is 2.1436 sec and the estimated time constant is 2.2058 sec. The optimal autoregressive model is:

$$Y_k = 1.8118\ y_{k-1} - 0.7295\ y_{k-2} - 0.08472\ y_{k-3} + V_k. \qquad (7.50)$$

7.6.2 Second Order System with Unequal Poles

$$G(s) = \frac{1}{(s+1)\ (s+2)}\ . \qquad (7.51)$$

Optimal AR order = 4. Figures 7.7 through 7.12 give the results for this case. The analysis was based on 4000 samples with a sampling interval of .05 sec.

Results: The true system time constant is 1.5848 sec and the estimated time constant is 1.6465 sec. The optimal autoregressive model is:

$$Y_k = 2.1218\ y_{k-1} - 1.4159\ y_{k-2} + 0.34375\ y_{k-3} - 0.05322\ y_{k-4} + V_k. \qquad (7.52)$$

7.6.3 Fifth Order System

$$G(s) = \frac{1}{(s+1)\ (s+2)\ (s+3)\ (s+4)\ (s+5)} \qquad (7.53)$$

Figures 7.13 through 7.18 show the results. The analysis was based on 4000 samples with a sampling interval of 0.05 sec.

Results: The true system time constant is 2.4341 sec and the estimated time constant is 2.3288 sec. The optimal autoregressive model is:

$$Y_k = 1.3616\ y_{k-1} - 0.07813\ y_{k-2} - 0.076424\ y_{k-3} - 0.07228\ y_{k-4} - 0.06207\ y_{k-5} - 0.02872\ y_{k-6}$$

(continued)

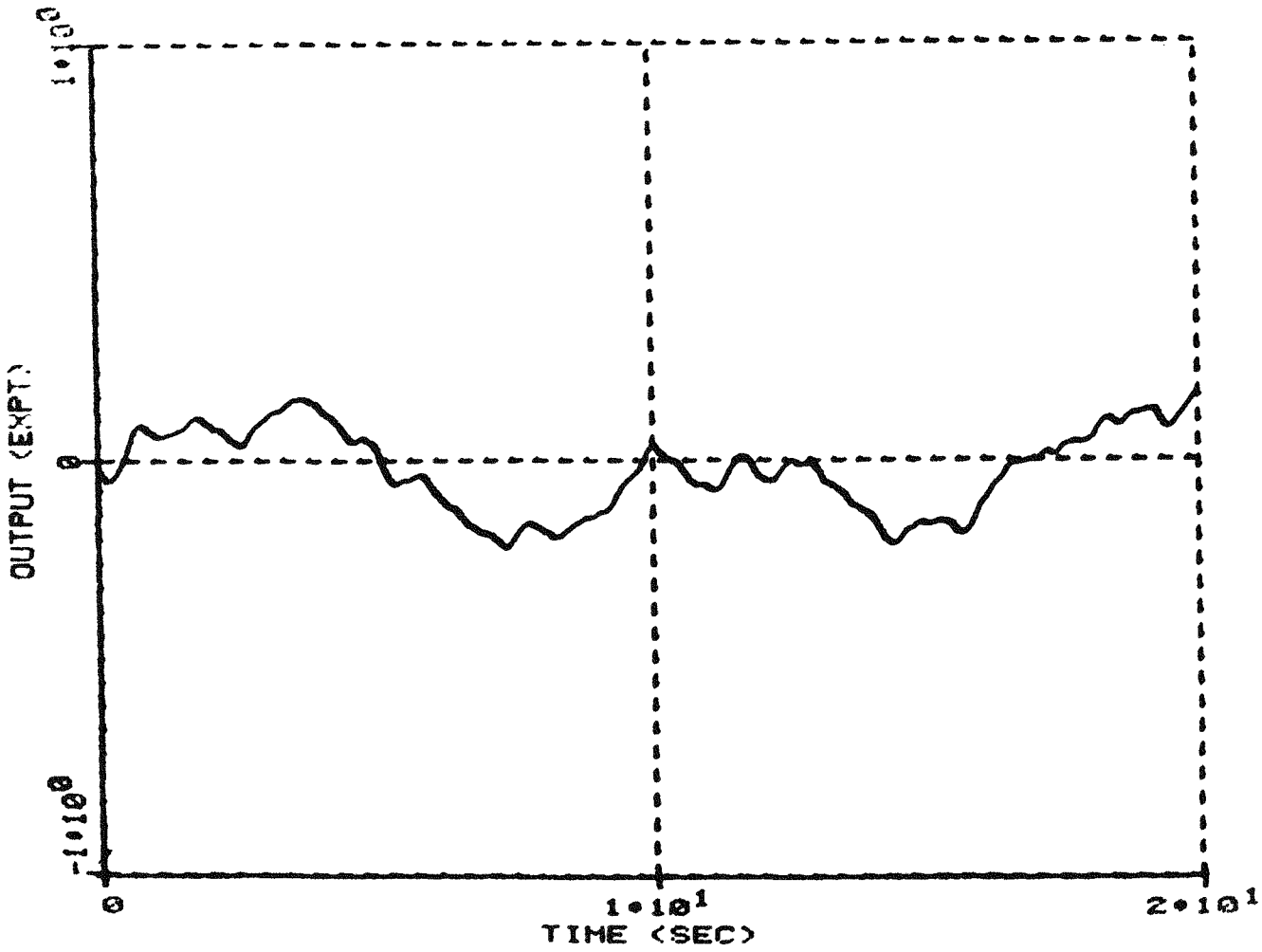

Figure 7.7 Output Noise Signal for a Second Order System with Transfer Function

$$G(s) = \frac{1}{(s+1)(s+2)} .$$

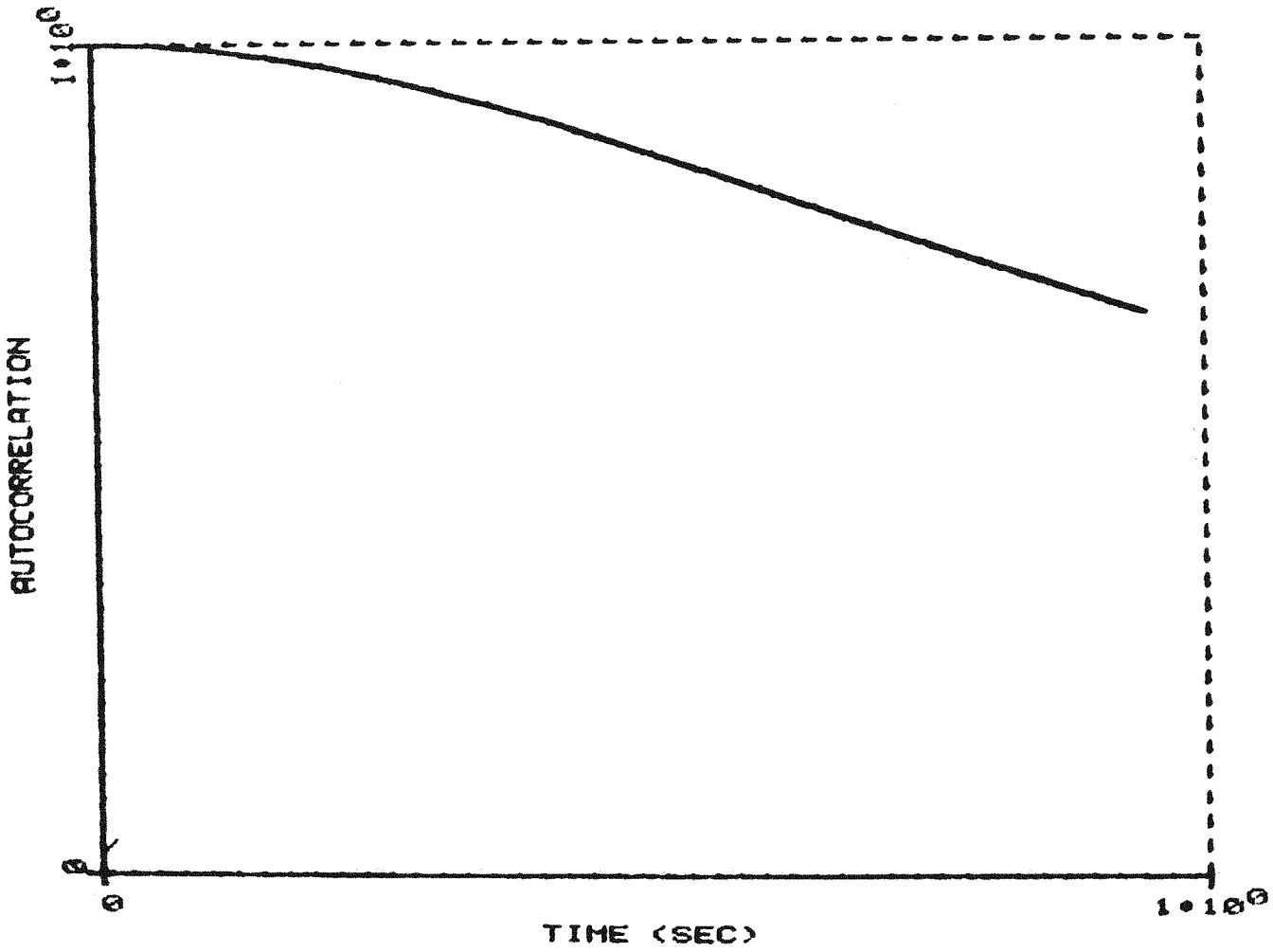

Figure 7.8 Autocorrelation Function for Data of Figure 7.7.

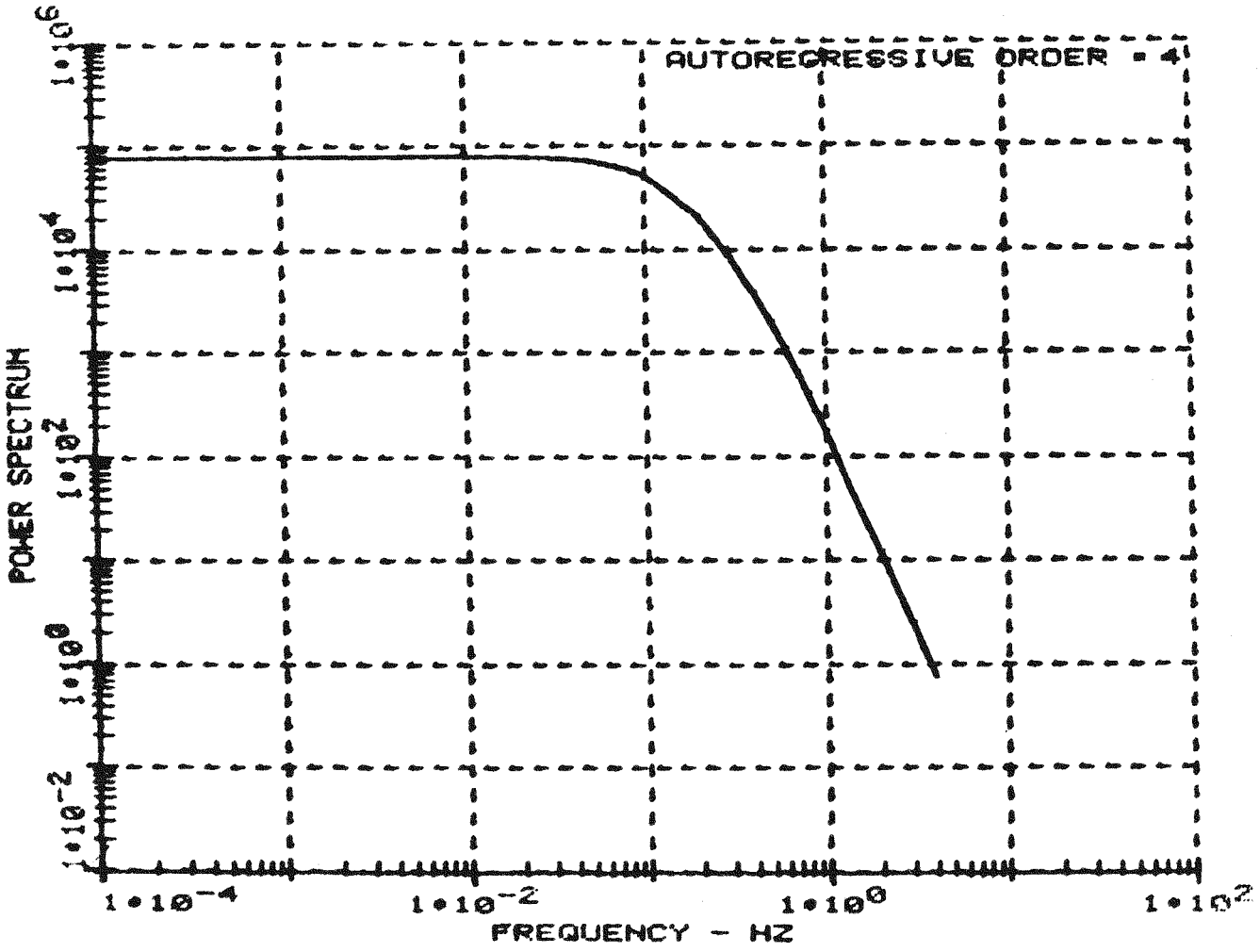

Figure 7.9 Power Spectrum Obtained Using AR(n=4) Parameters for Signal of Figure 7.7.

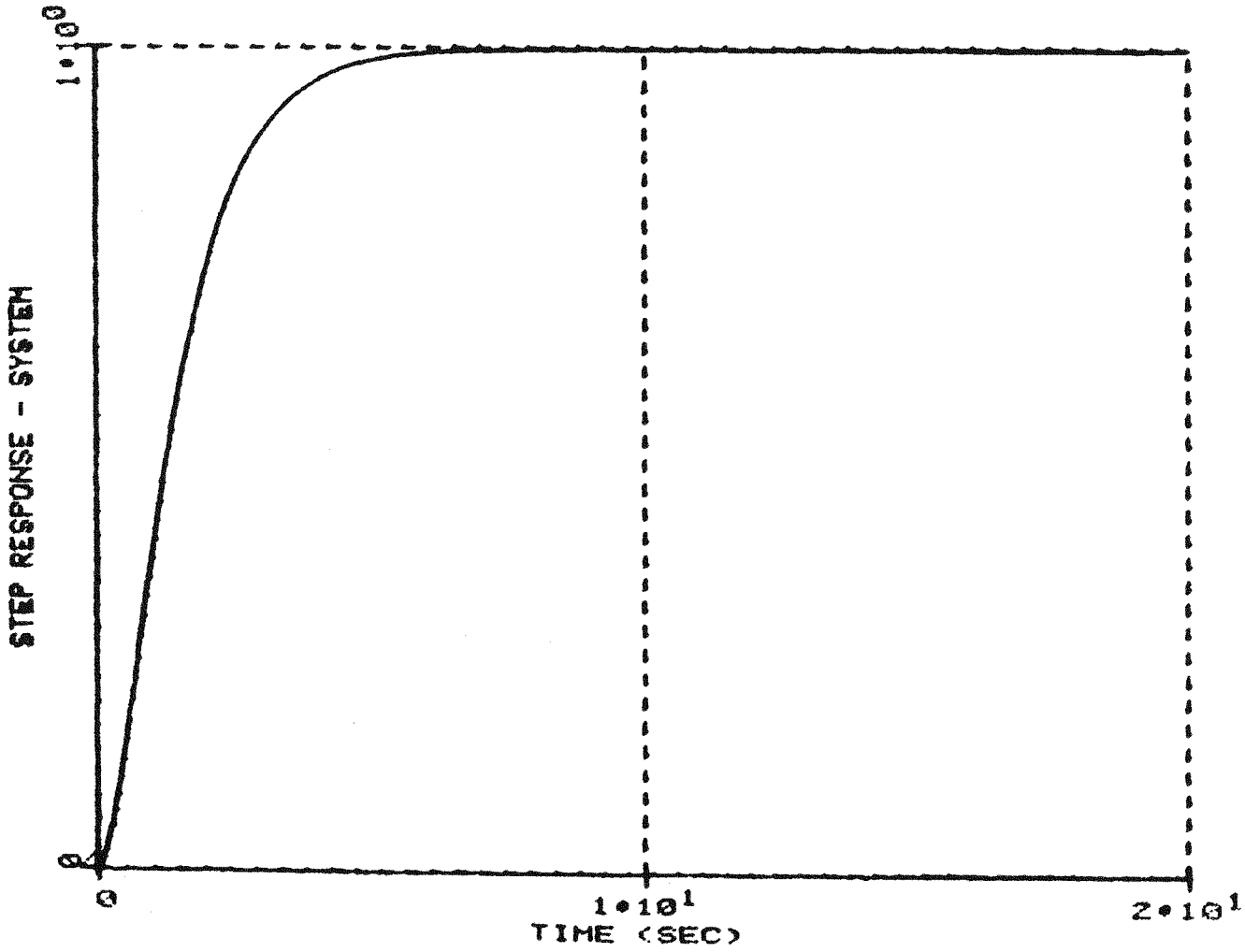

Figure 7.10 True Step Response for System with $G(s) = \frac{1}{(s+1)(s+2)}$.

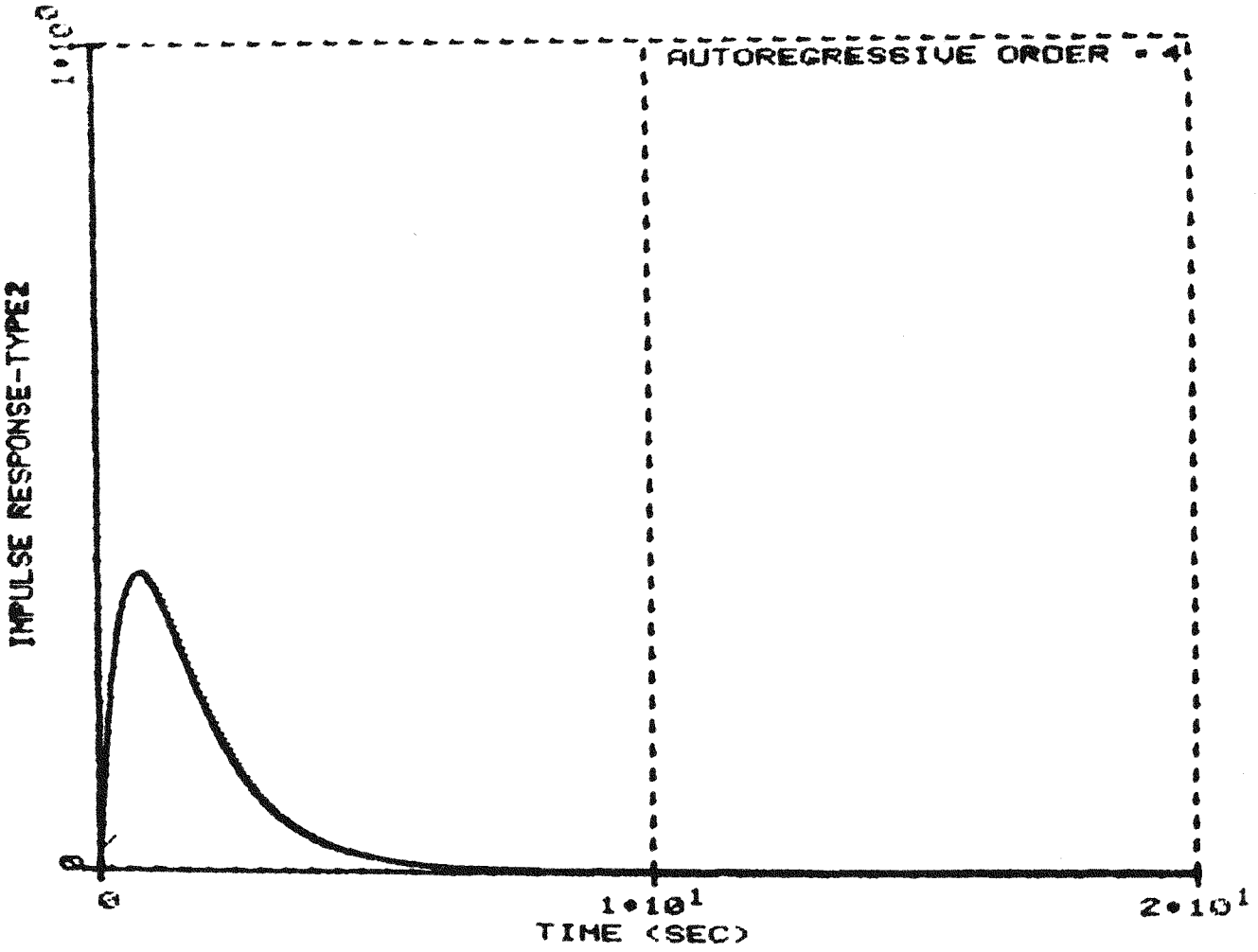

Figure 7.11 Impulse Response Calculated Using the AR (n=4) Parameter for the Data of Figure 7.7.

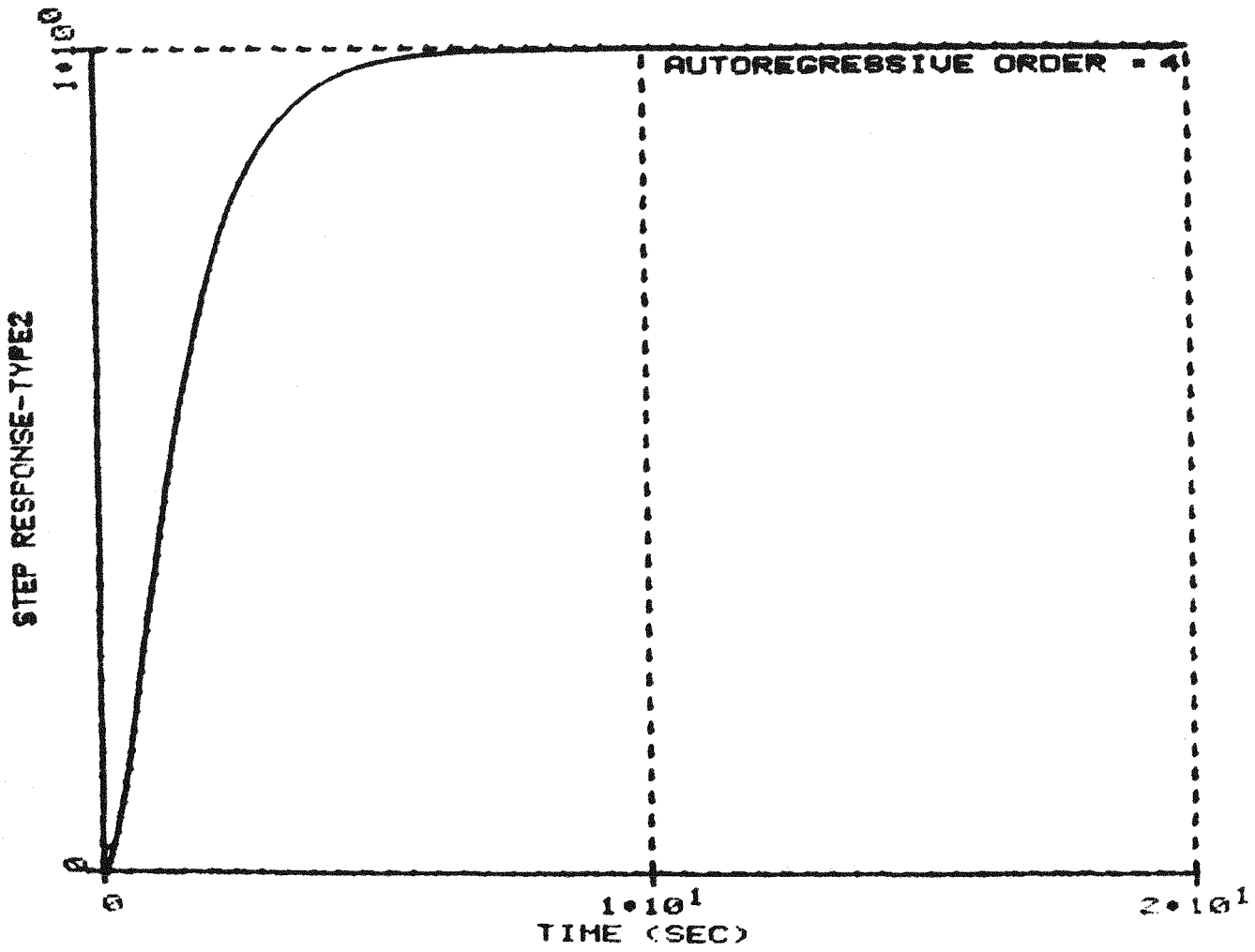

Figure 7.12 Step Response Calculated Using the AR (n=4) Parameters for the Data of Figure 7.7.

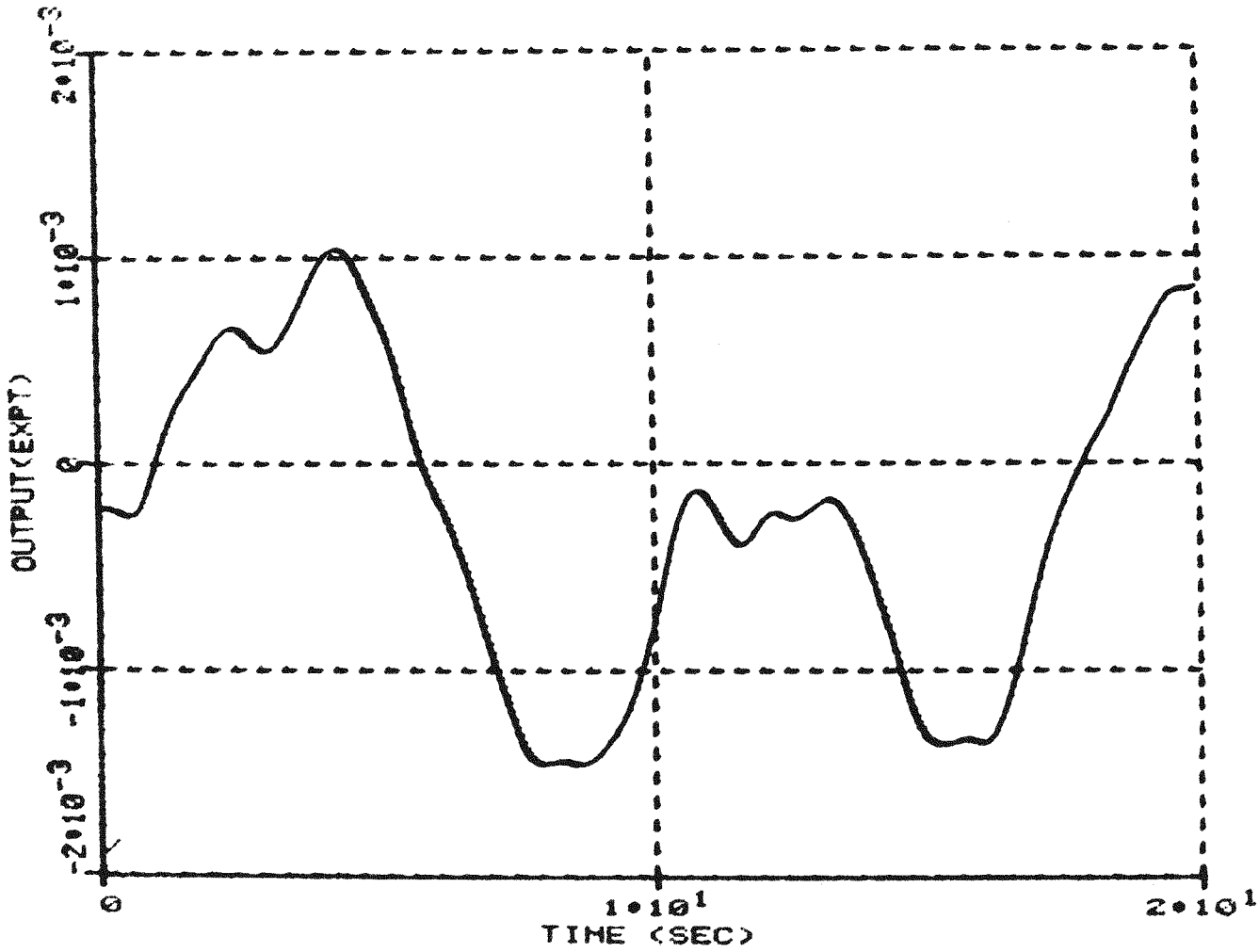

Figure 7.13 Output Noise Signal for a 5th Order System with Distinct Poles (Equation (7.53)).

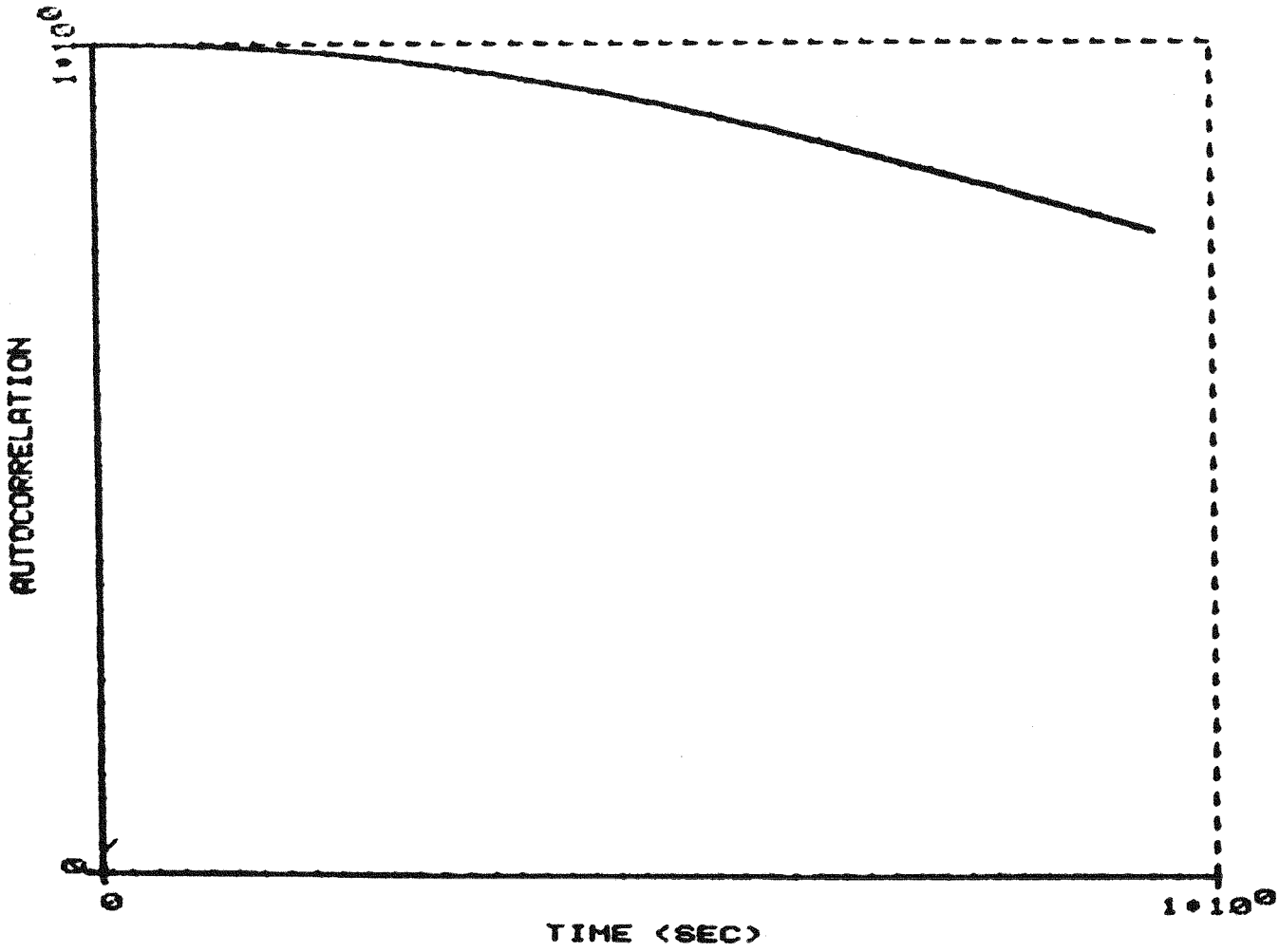

Figure 7.14 Autocorrelation Function for Data of Figure 7.13.

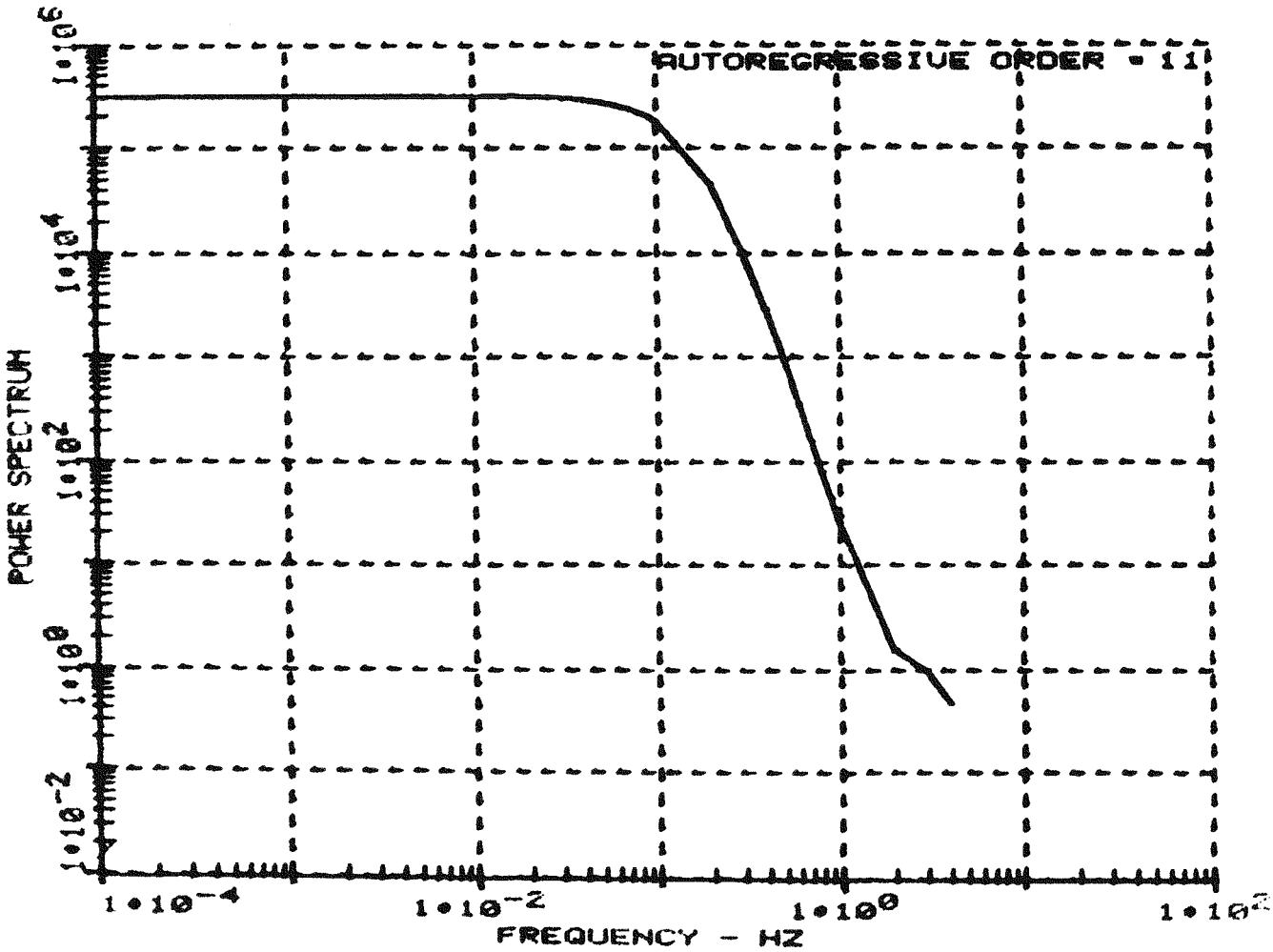

Figure 7.15 Power Spectrum Obtained Using AR (n=11) Parameters for Signal of Figure 7.13.

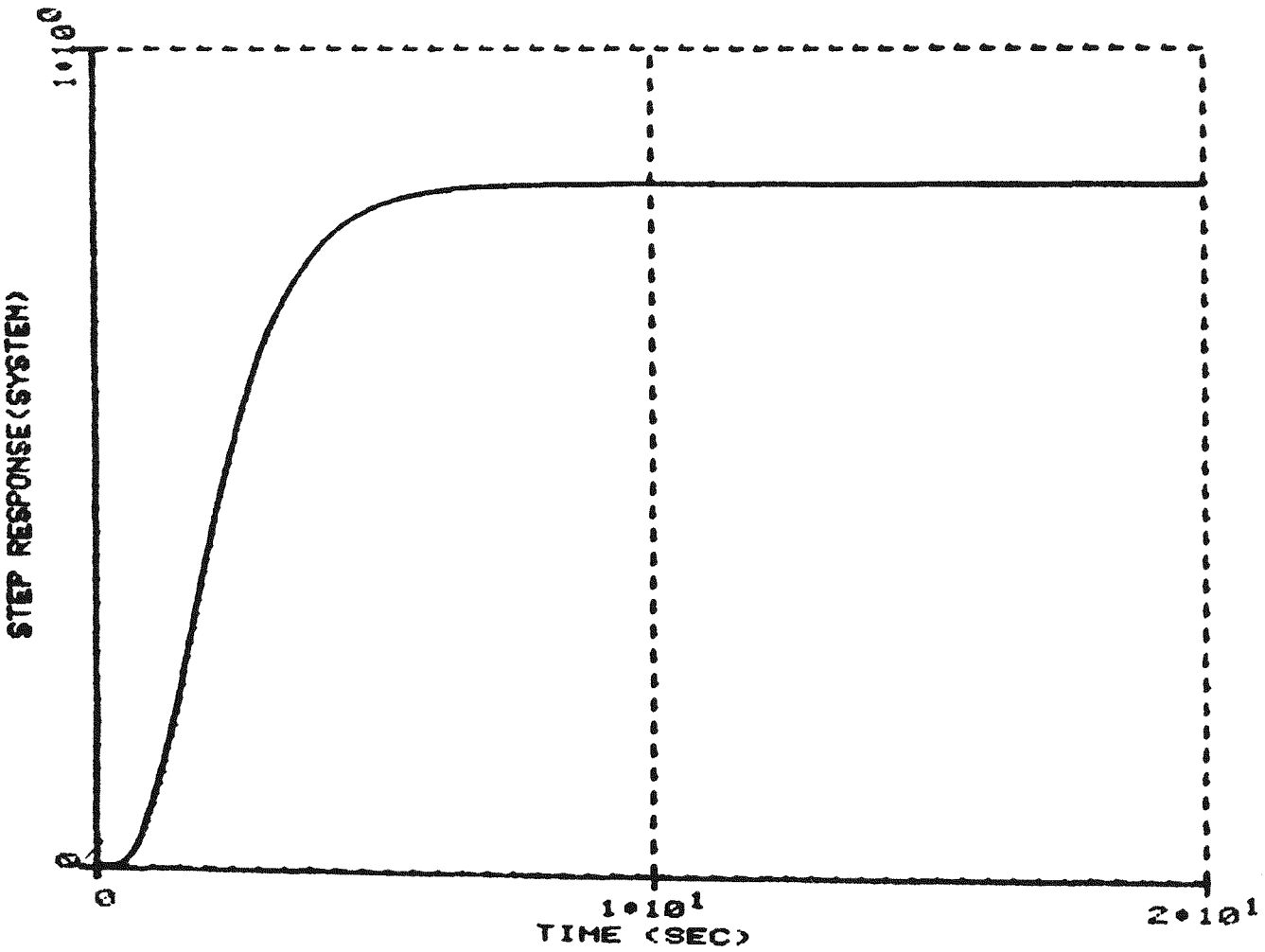

Figure 7.16 True Step Response for System with $G(s) = \frac{1}{(s+1)(s+2)(s+3)(s+4)(s+5)}$.

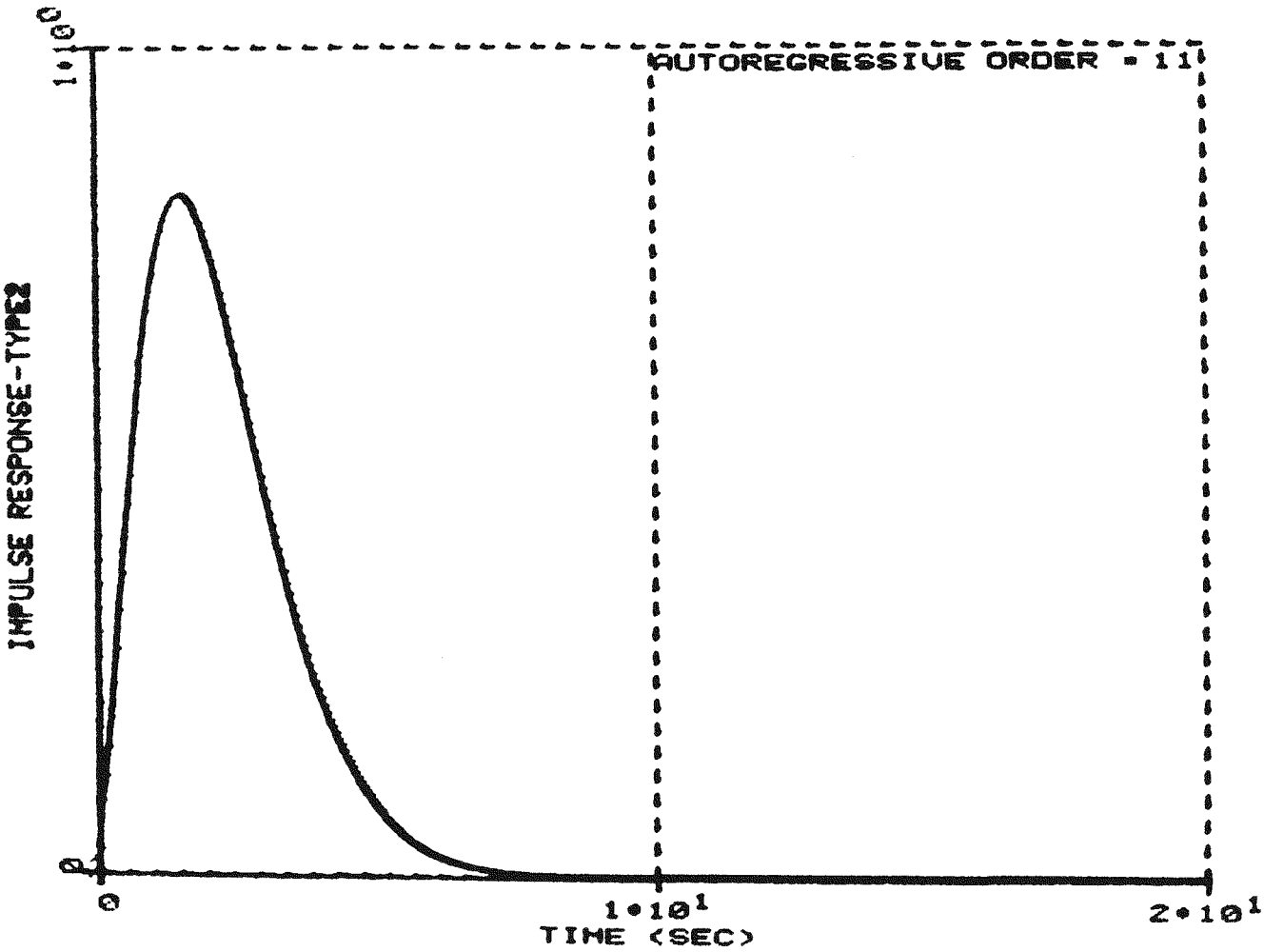

Figure 7.17 Impulse Response Calculated Using the AR (n=11) Parameter for the Data of Figure 7.13.

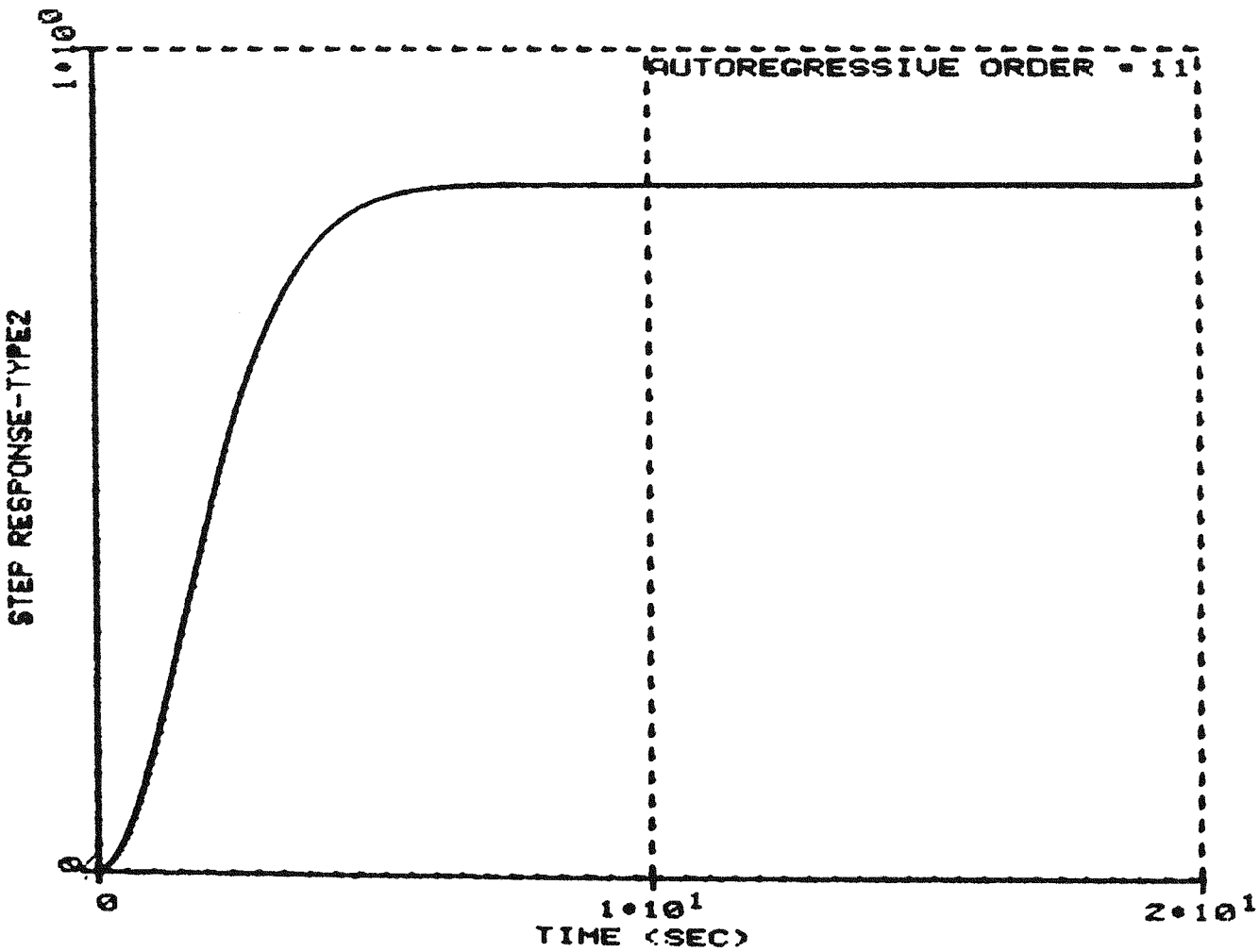

Figure 7.18 Step Response Calculated Using the AR (n=11) Parameters for the Data of Figure 7.13.

$$-0.06673\ y_{k-7} - 0.0186\ y_{k-8} - 0.007828\ y_{k-9}$$

$$-0.0354\ 7_{k-10} + 0.08276\ y_{k-11} + V_k. \qquad (7.54)$$

7.7 Response Characteristics of an RTD at Millstone 2

The results presented here are based on the RTD data obtained from data collected from the hot leg at the Millstone 2 PWR.

Figures 7.19 through 7.23 represent results similar to those discussed in Section 7.6 for AR order = 11. The analysis is based on 4000 samples with a sampling interval of 0.125 sec. The estimated time constant is 5.01 seconds. The optimal autoregressive model is:

$$y_k = 0.93955\ y_{k-1} - 0.14417\ y_{k-2} + 0.40174\ y_{k-3}$$

$$- 0.16557\ y_{k-4} + 0.11612\ y_{k-5} - 0.06816\ y_{k-6}$$

$$+ 0.07955\ y_{k-7} - 0.16772\ y_{k-8} + 0.03604\ y_{k-9}$$

$$- 0.09963\ y_{k-10} + 0.05784\ y_{k-11} + V_k. \qquad (7.55)$$

Model Validation: Verification of the AR model derived for the noise analysis is made using the tests discussed in Section 7.4.

Figure 7.24 shows the plot of prediction error

$$\hat{V}_k = y_k - \sum_{i=1}^{n} \hat{a}_i\ y_{k-i}.$$

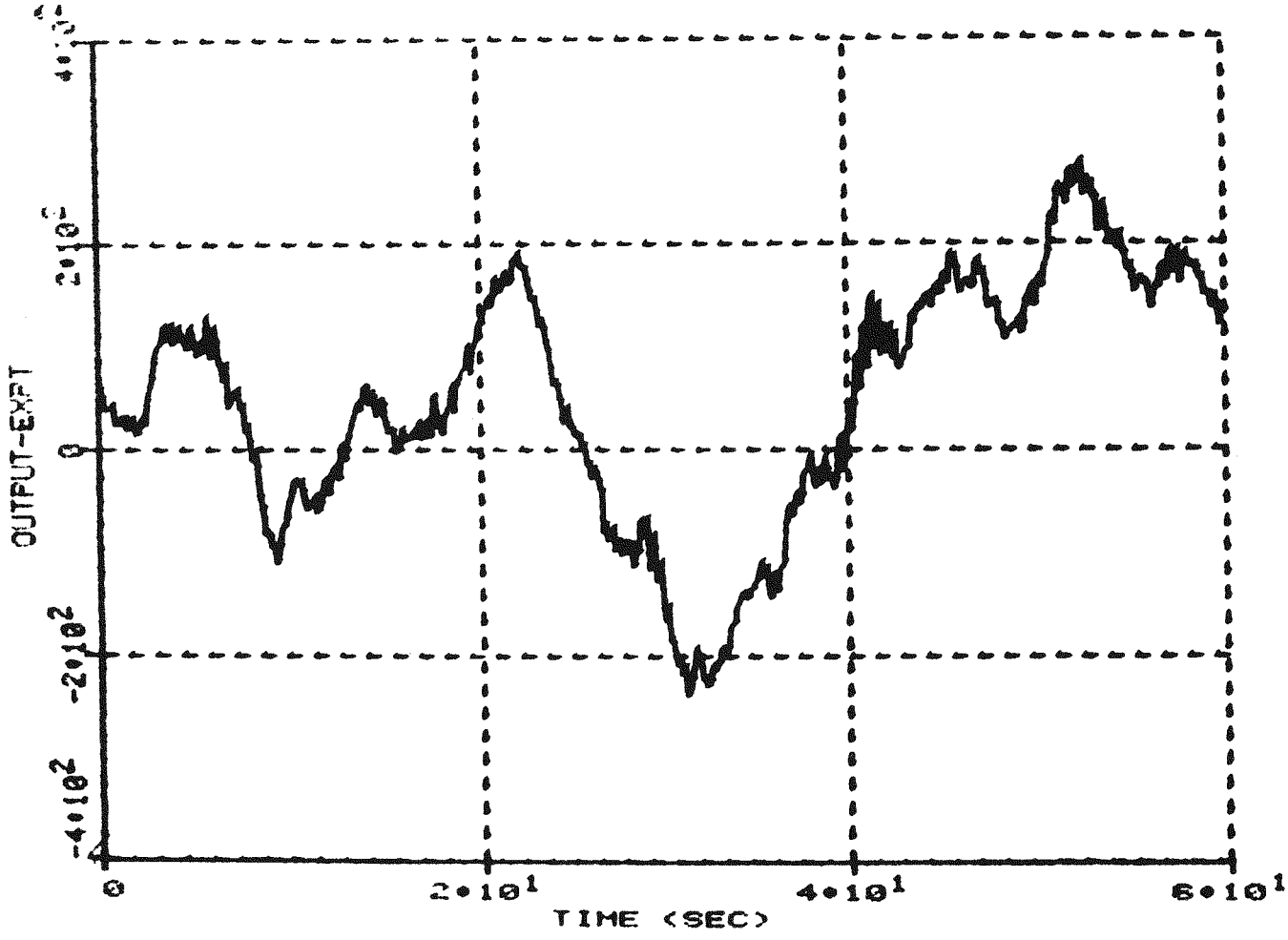

Figure 7.19 Output Noise RTD Data from Millstone 2.

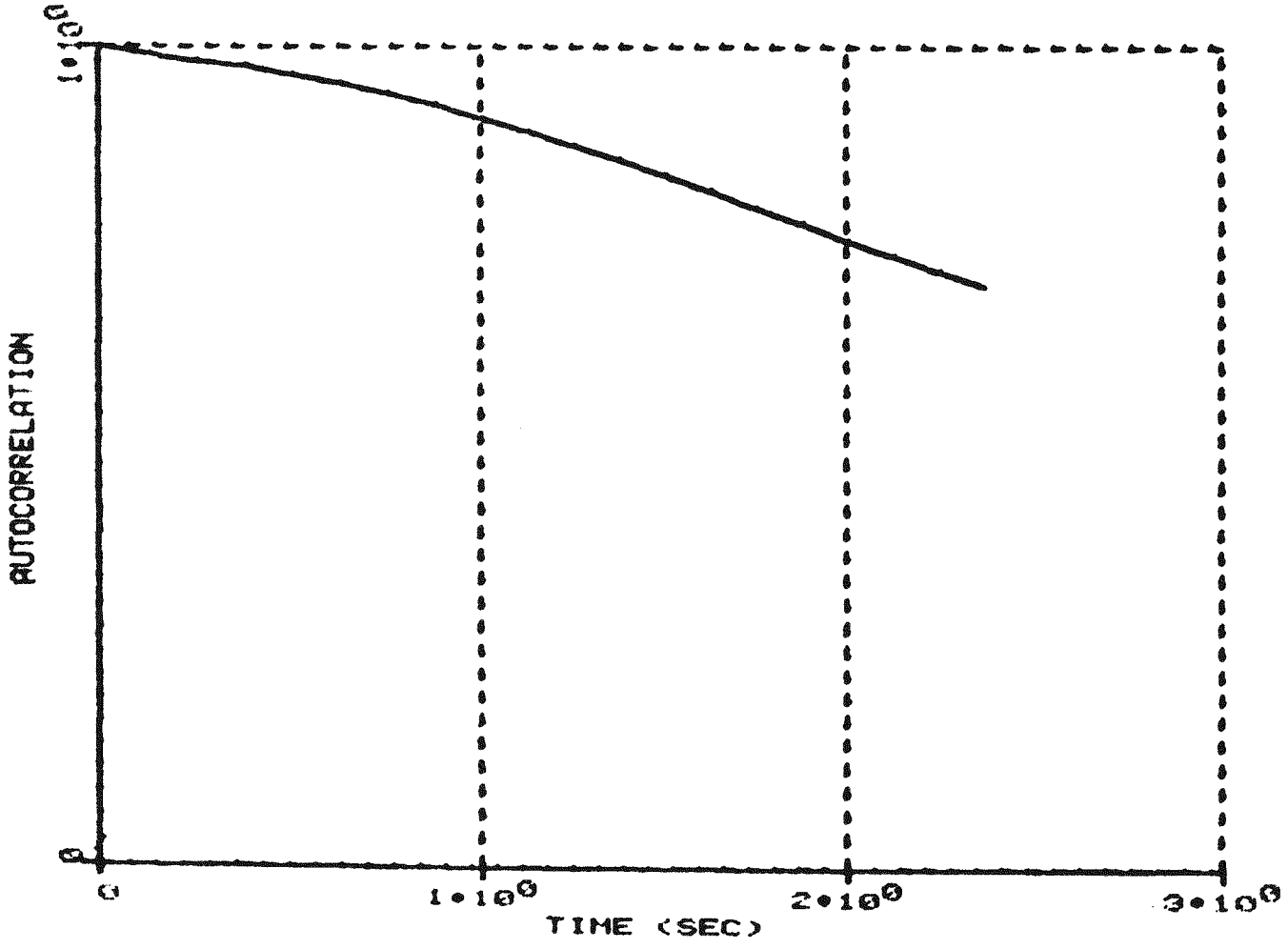

Figure 7.20 Autocorrelation Function for Data of Figure 7.19.

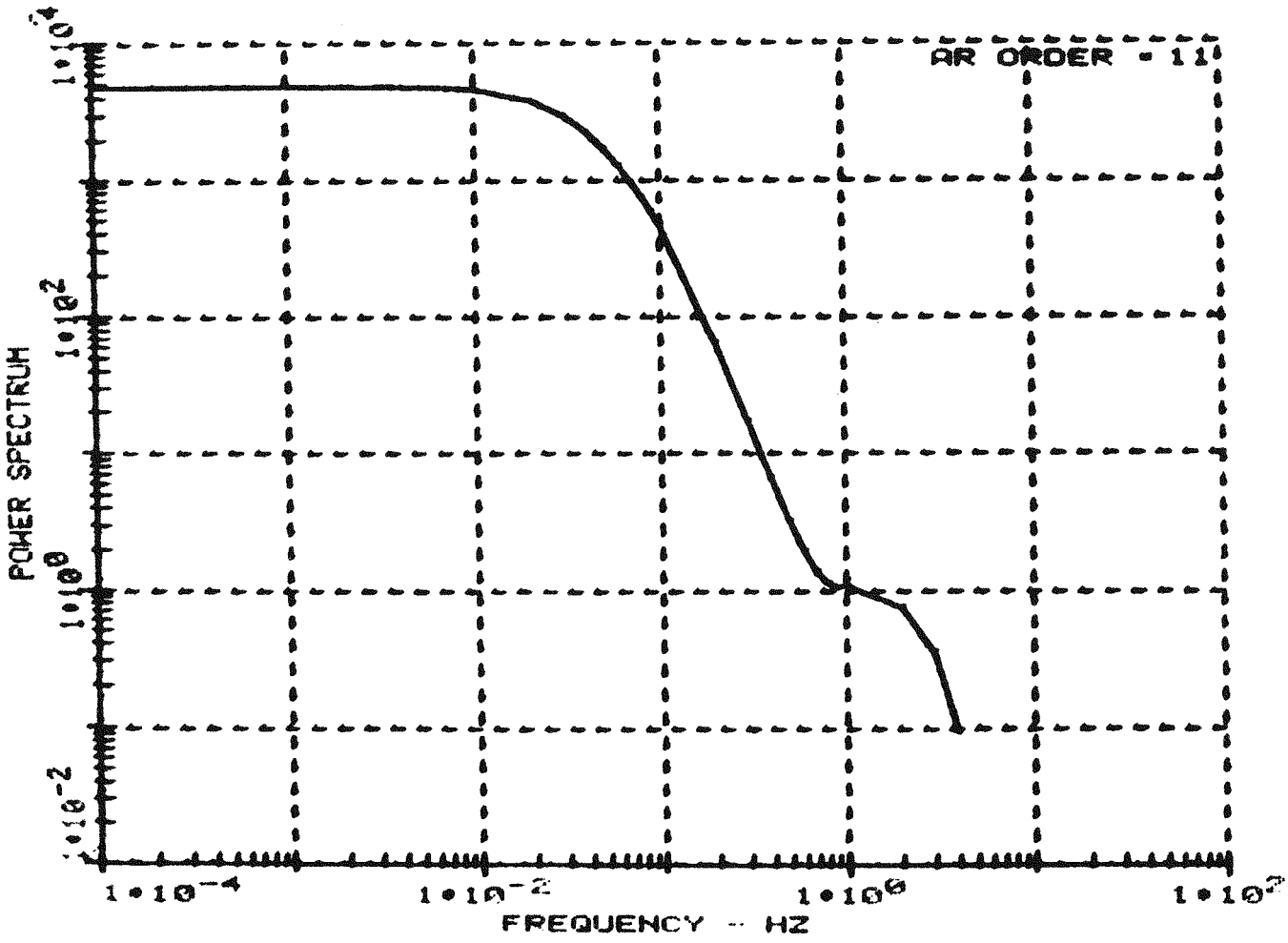

Figure 7.21 Power Spectrum Obtained Using AR (N=11) Parameters for Signal of Figure 7.19.

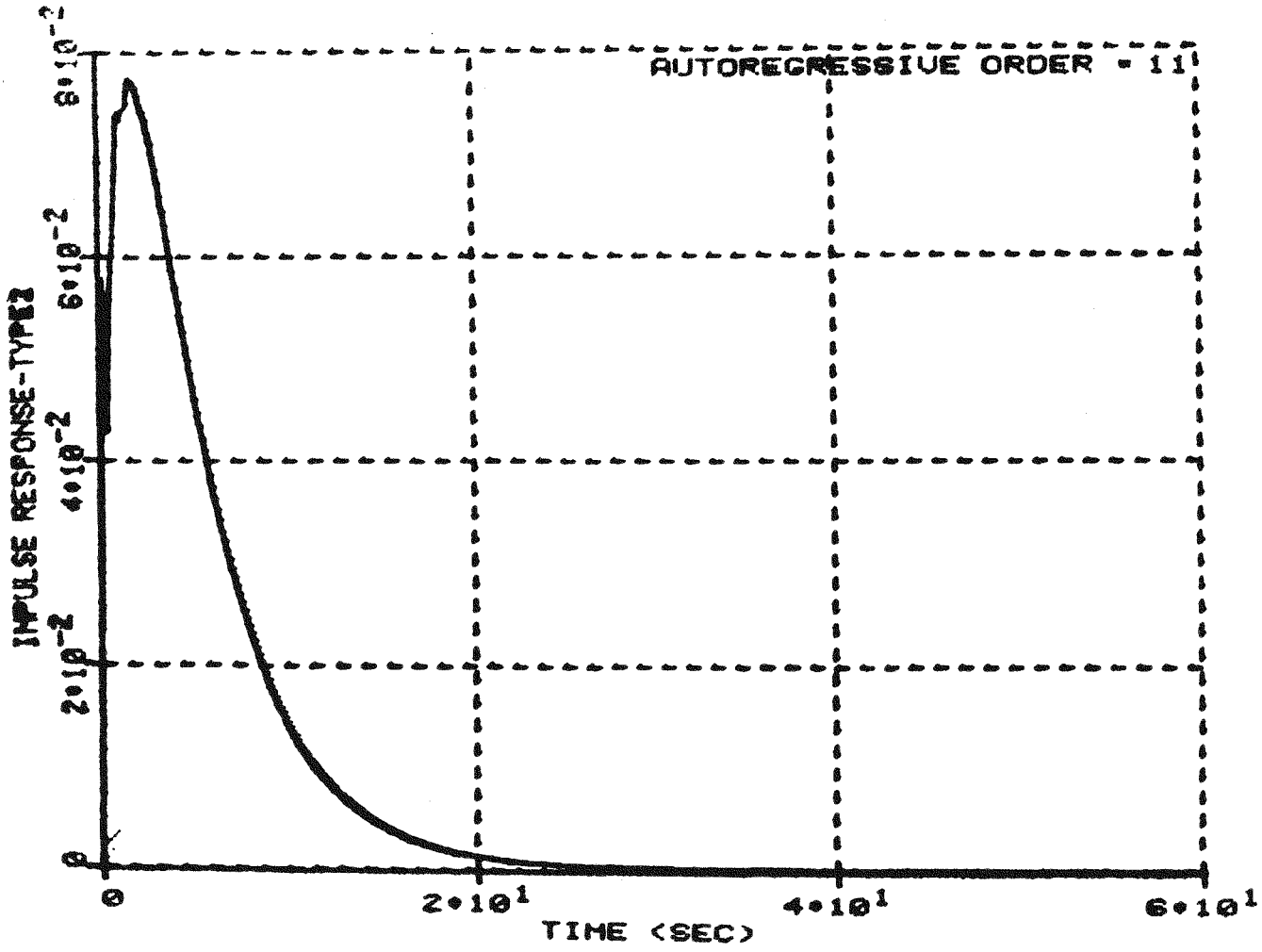

Figure 7.22 Impulse Response Calculated Using the AR (n=11) Parameters for the Data of Figure 7.10.

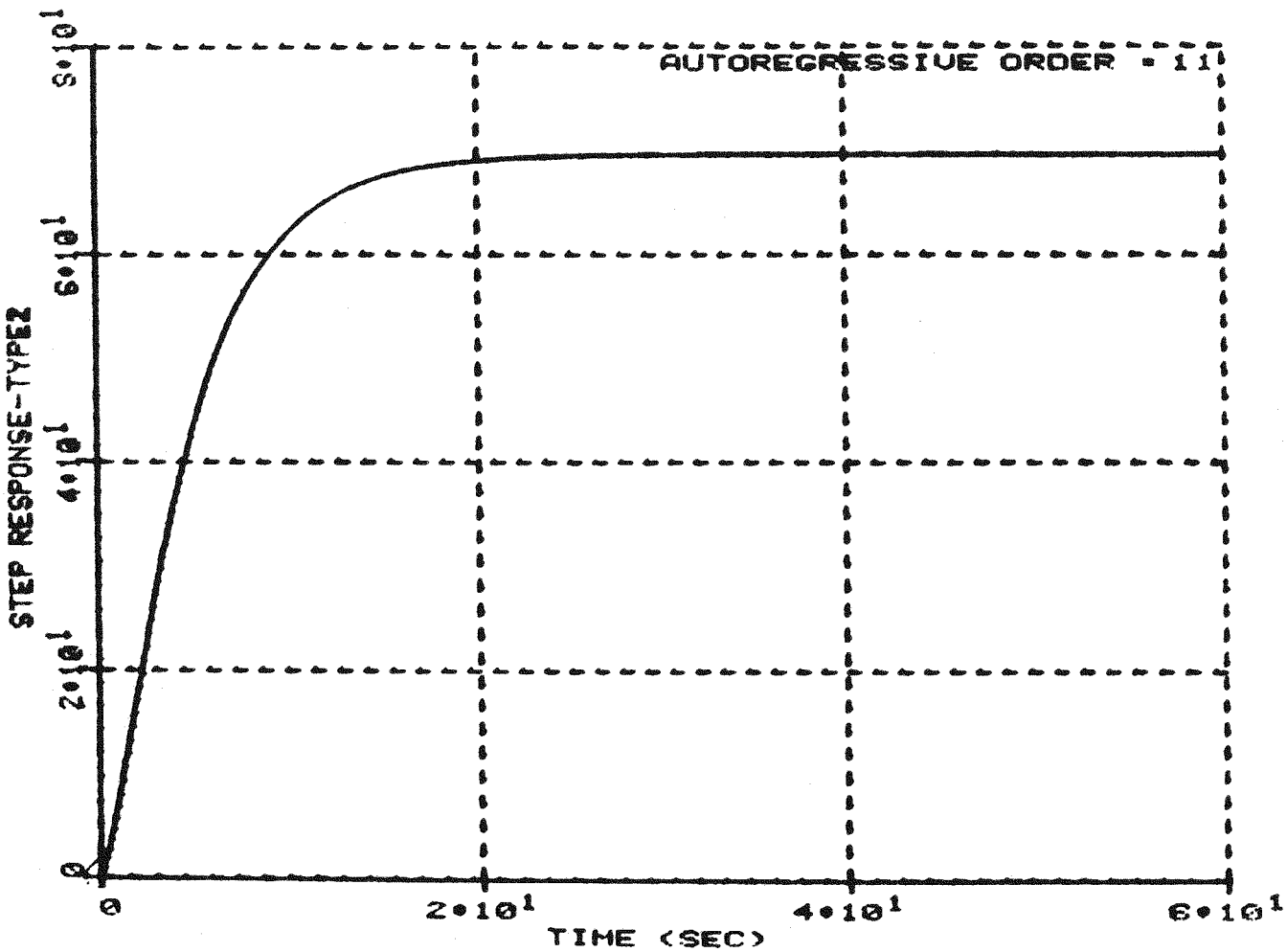

Figure 7.23 Step Response Calculated Using the AR (n=11) Parameters for the Data of Figure 7.19.

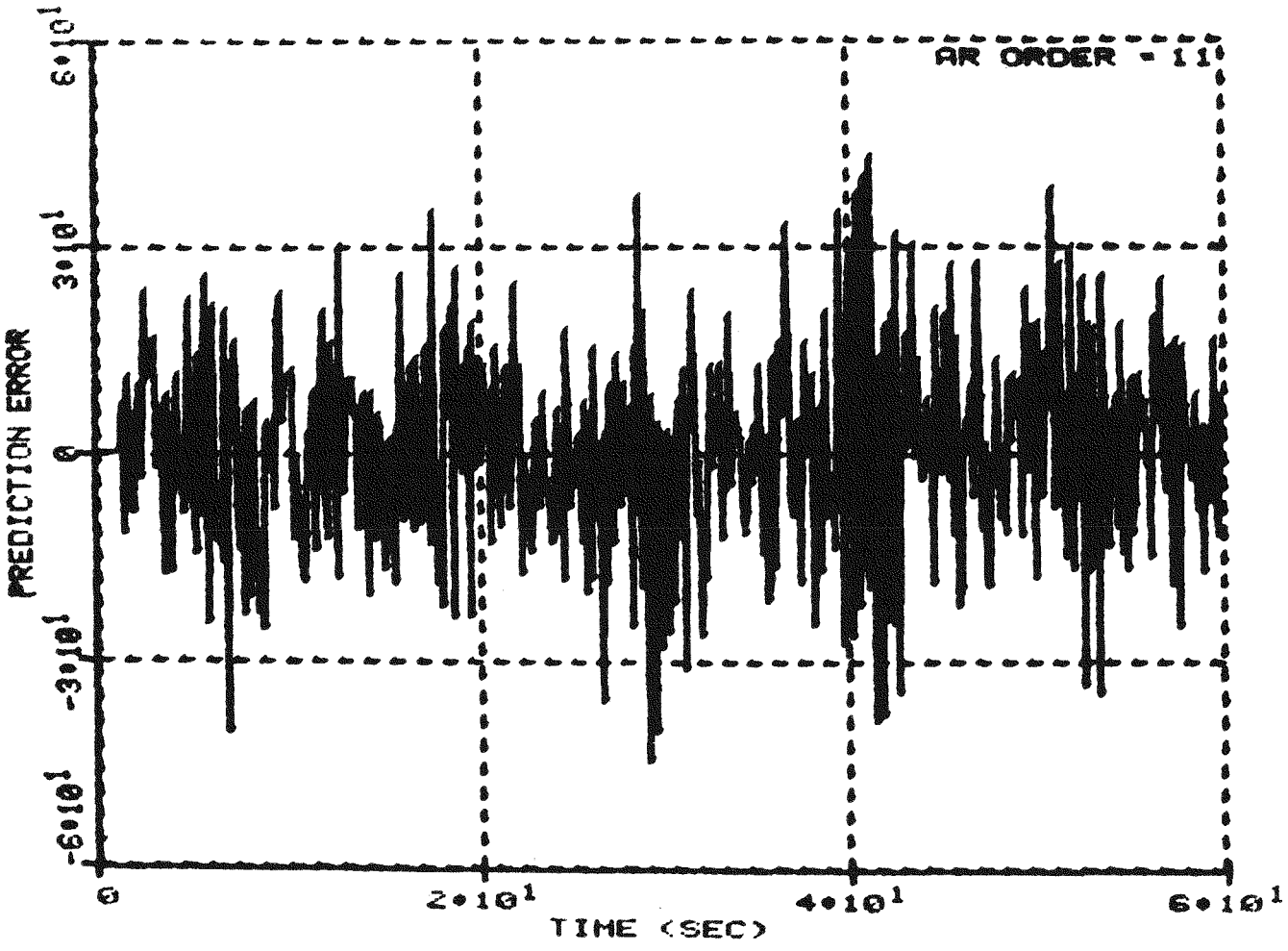

Figure 7.24 Prediction Error for Millstone 2 Data.

The variation in this estimate is within $\pm 1.96\,\hat{\sigma}$ where the estimated value of $\hat{\sigma} = 13.75$. Less than 5% of the residual sequence is outside this range.

Figure 7.25 shows the autocorrelation function of the prediction error based on N = 4000. The $\pm 1.96/\sqrt{N}$ bounds for a 95% confidence level is

$$\frac{1.96}{\sqrt{N}} = 0.031.$$

From the figure, one can determine that the autocorrelation functions lie within this range, thus verifying the whiteness of the noise disturbance.

The portmanteau test is applied for the first 60 correlation functions. The χ^2-test index

$$Q = N \sum_{i=1}^{60} \gamma_k(\tilde{V})^2 = 59.79.$$

The χ^2 value for degrees of freedom M - n = 60 - 11 = 49 is obtained from a table of percentage points of χ^2 values.

For 5% tail area, $\chi^2_{49} = 66.26$.

For 10% tail area, $\chi^2_{49} = 61.98$.

From the values of χ^2 for 90% and 95% levels, it is clear that the value of Q on an average will lie within the limits, thus satisfying the "portmanteau" test.

The power spectrum of the estimated noise sequence was computed and is shown in Figure 7.26; the flatness of this spectrum is a further indication that the assumption of whiteness is valid. The verification

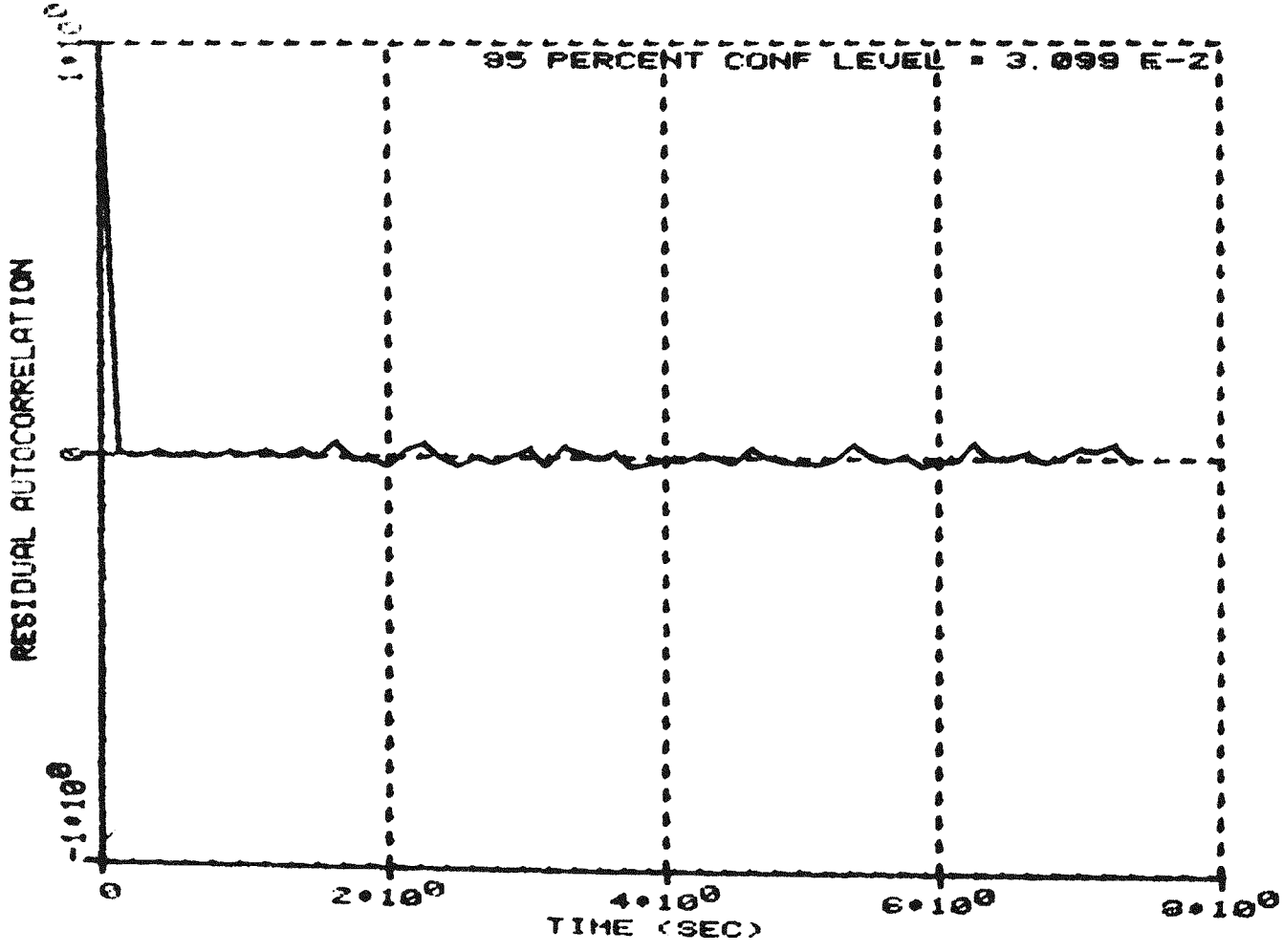

Figure 7.25 Autocorrelation Function of the Prediction Error for the Millstone 2 Data.

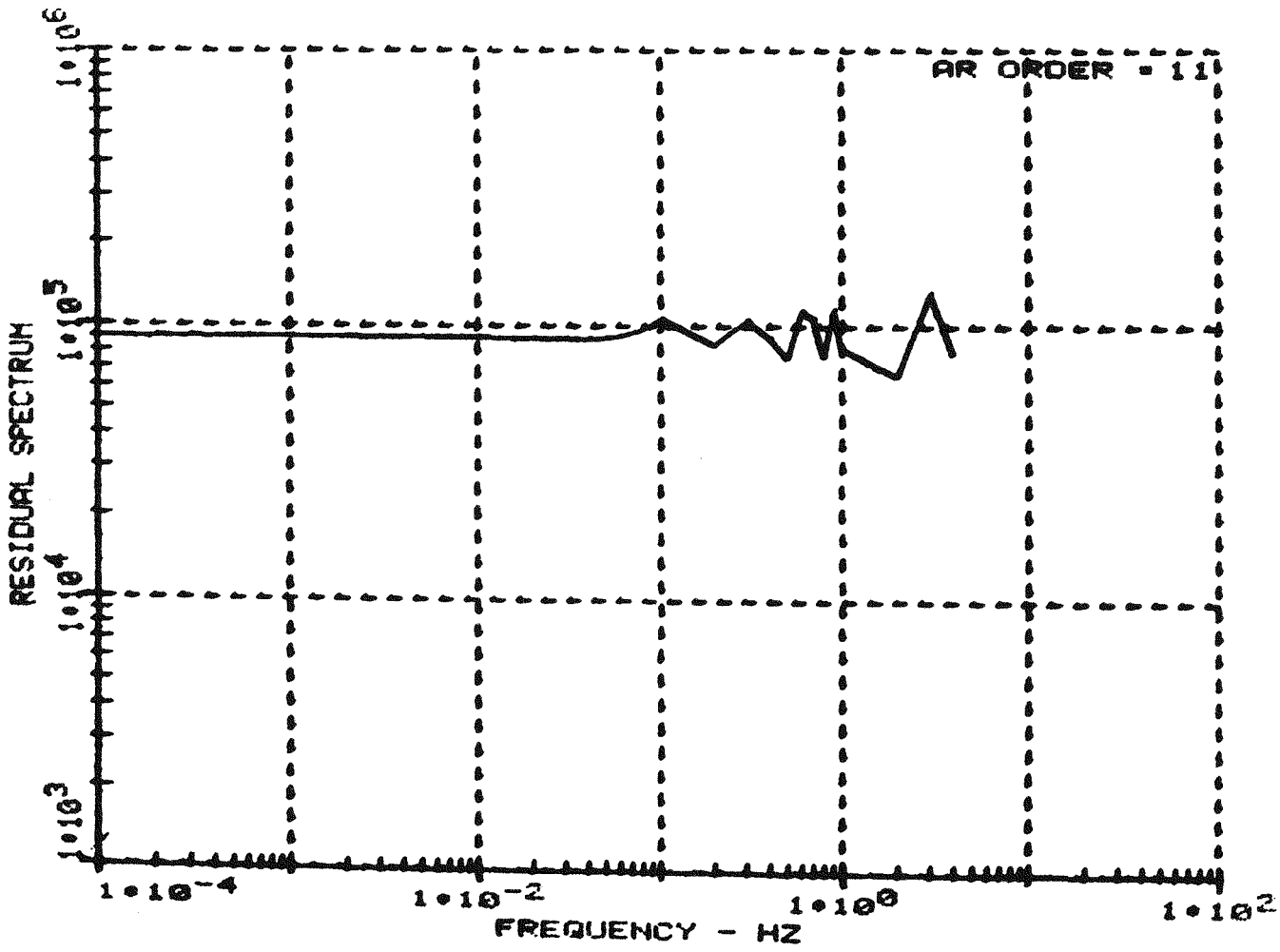

Figure 7.26 Power Spectrum of the Estimated Noise Sequence for the Millstone 2 Data.

of these tests provides confidence in the appropriateness of the autoregressive model and the associated response characteristics.

The comparison of the power spectrum obtained from direct FFT shows that the break frequency obtained by the intersection of low frequency and high frequency asymptotes coincides with the break frequency of the AR spectrum and is equal to 0.05 Hz. The AR spectrum is smooth and coincides with the overall spectrum obtained from FFT. The FFT computed spectrum for the Millstone 2 hot leg RTD appears in Figure 7.27.

It should be noted that the power spectral density for a Millstone 2 cold leg RTD shows strong evidence that the driving function is not white. Figure 7.28 shows the spectrum of the cold leg RTD signal. The result from a time series analysis gives a time constant, τ = 2.5 sec. This is much smaller than the hot leg RTD response time of τ = 5.01 sec. The calculated spectrum of the residual noise is shown in Figure 7.29. This indicates that the noise perturbation is not white. It is possible that the non-whiteness is caused by the feedwater controller and/or the primary pump. If the spectrum of the driving function is significantly non-white in the bandpass of the sensor dynamics, the method is invalid. Thus, it is assumed that the 2.5 second time constant obtained for the cold leg RTD is invalid.

7.8 Concluding Remarks

In the preceding sections, it has been shown that the time series obtained from systems driven by white noise can be successfully modeled by an autoregressive process of appropriate order. The computational requirement to find the AR(n) parameters is comparable

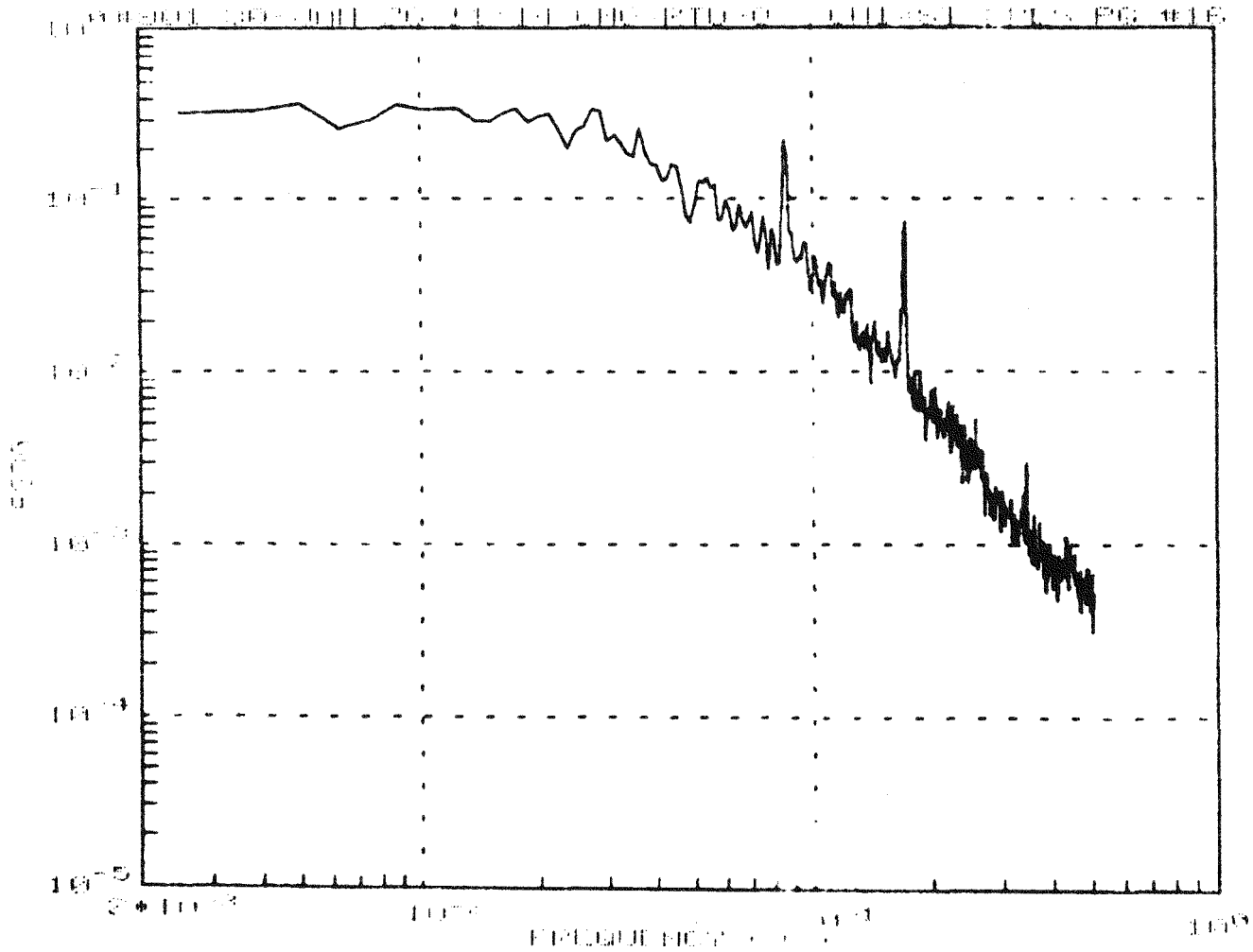

Figure 7.27 Power Spectral Density of the Hot Leg Temperature Signal.

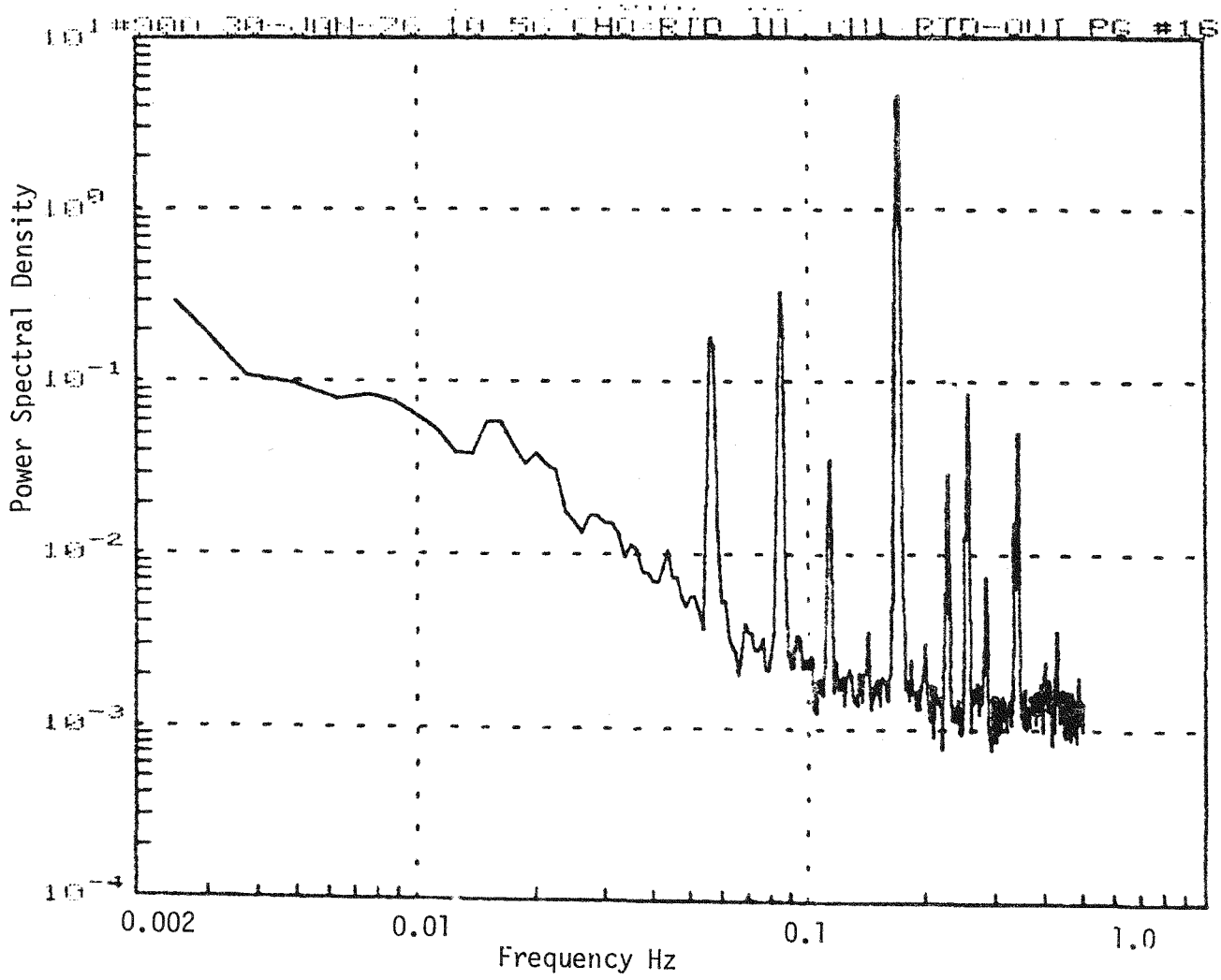

Figure 7.28 Power Spectral Density of the Cold Leg Temperature Signal.

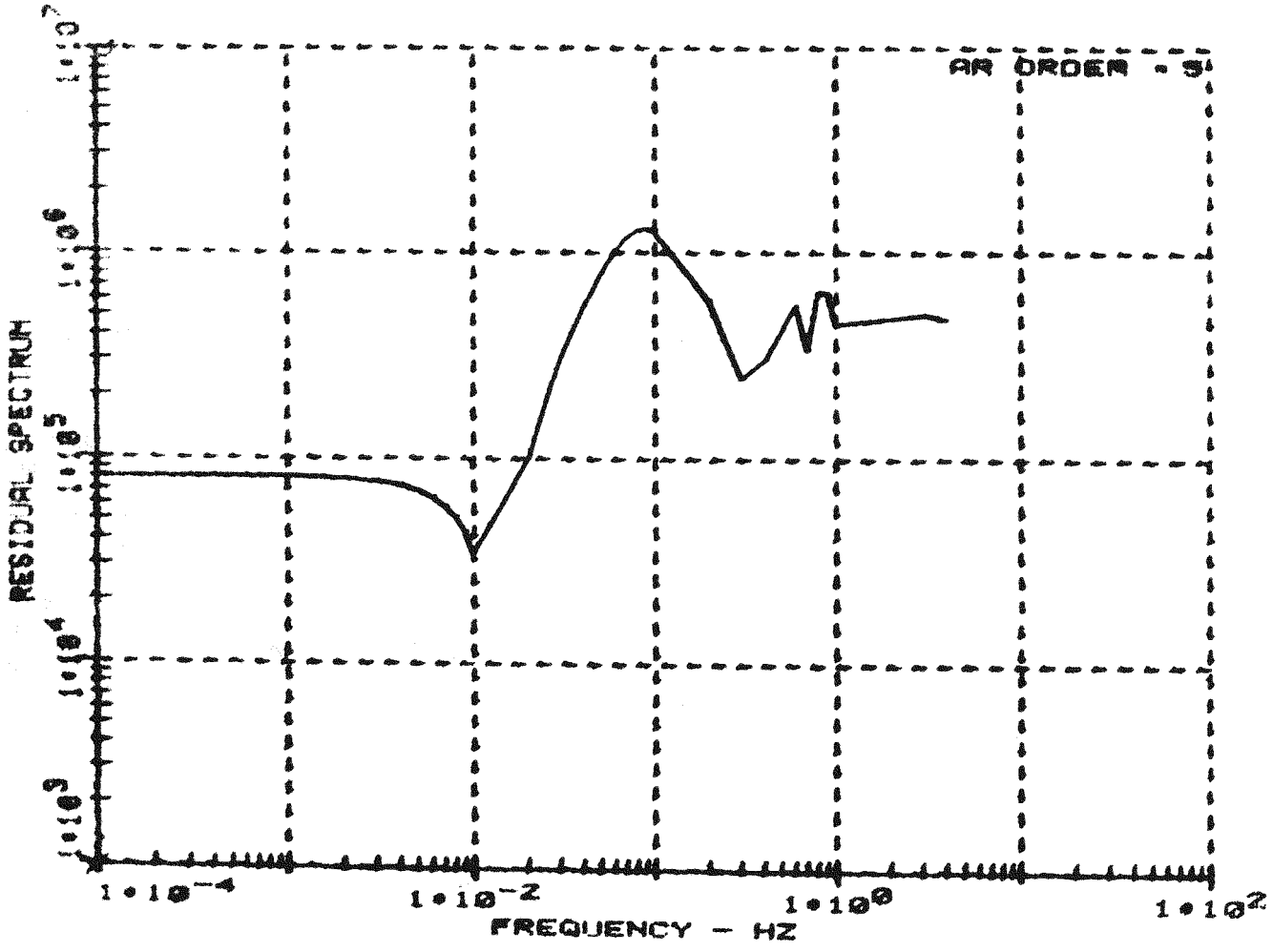

Figure 7.29 Spectrum of Residual White Noise for Cold Leg RTD.

to or better than other methods. For example, computations required for Fast Fourier Transform (FFT) techniques and the Yule-Walker equations are compared for a 10th order AR model as follows.

No. of multiplications for 10th order AR model = 10N.

No. of multiplications for FFT = $3N \log_2 N$.

where N is the block length. As N increases, the number of multiplications for FFT calculation increases as a nonlinear function of N.

The response characteristics derived in this chapter use digital numerical computations requiring no assumptions, other than that of white driving noise to construct the AR process. No geometric constructions or approximations are necessary. Hence, the technique developed can be adapted easily for on-line periodic checking of sensor response characteristics in nuclear power plants.

Further experience with this method will be obtained in the near future using noise data collected at the Oconee 3 plant for three different RTD's.

8. SUMMARY AND CONCLUSIONS

Three methods for measuring the response time of installed platinum resistance thermometers have been developed. These methods are: the loop current step response method, the self-heating method, and the noise analysis method. They have been tested in the laboratory and in two operating pressurized water reactors.

The loop current step response (LCSR) method involves analysis of the transient that occurs following a step increase in current through the sensor filament. Currents of 40 to 60 ma give temperature rises of 10 to 20 degrees Fahrenheit. These values are suitable for in-plant testing and result in no deleterious effect on the sensor.

The analysis of the LCSR data to obtain the desired response time for a fluid temperature step may be approached analytically or empirically. The analytical transformation has been developed and implemented, but has been found to have restricted utility because it depends on two essential assumptions:

1) predominantly one-dimensional heat transfer

2) centrally located filament.

These assumptions appear to be satisfied for sensors for the type that are common in PWR's manufactured by Combustion Engineering, Inc. and Babcock and Wilcox Company, but not for those commonly found in Westinghouse plants. Another problem with the analytical transformation is the accurate identification of the exponential coefficients that govern the LCSR transient and which are essential for constructing the estimate of the response time.

When the analytical transformation fails, it is possible to use an empirical transformation. Sensor degradation is simulated in the laboratory using artificial augmentation of the heat transfer resistance at the surface of the sensor. Plunge tests and LCSR tests are performed for a number of surface conditions, and a time constant is obtained for each. A plot of the plunge time constant as a function of the LCSR time constant provides an empirical correlation. For in-plant applications, LCSR tests could be performed, the LCSR time constant could be determined, and the plunge time constant could be read from the curve. The method depends on the following:

1. simulated sensor degradation using augmented surface heat transfer resistance adequately represents the degradation that is plausible in an operating sensor,
2. measurements made at room temperature and at low flow rate in the laboratory are suitable for establishing an empirical relation that is valid at PWR operating temperature and flow rate
3. experimental measurements of the LCSR time constant can be made accurately enough to indicate small changes in the plunge time constant.

The self-heating method involves measurement of the steady state temperature (resistance) increase as a function of I^2R power generated in the sensor filament. Increased time constants resulting from increased heat transfer resistance are indicated by a larger temperature rise for a given power generation. Implementation of this method involves

measurement of the slope of the self-heating curve (temperature rise vs. power generation) to obtain an empirical relationship between the plunge time constant and the slope of the self-heating curve. This relationship may be generated in the laboratory using augmented surface heat transfer resistances as with the LCSR empirical transformation. In-plant implementation could involve: (1) measurement of the change in electrical resistance as a function of power generation in the sensor filament, (2) evaluation of the slope of the self-heating curve, and (3) using the empirical transformation curve to estimate the plunge time constant. The method depends on the following:

1. simulated sensor degradation using augmented surface heat transfer resistance adequately represents the degradation that is plausible in an operating sensor,
2. measurements made at room temperature and at low flow rate in the laboratory are suitable for establishing an empirical relation that is valid at PWR operating temperature and flow rate,
3. experimental measurements of the slope of the self-heating curve can be made accurately enough to indicate small changes in the plunge time constant,
4. change in the effective heat capacity (which is not revealed by the self-heating test) is not a plausible degradation mode for a platinum resistance thermometer.

A successful self-heating test was performed in an operating PWR, suggesting that the measurement is experimentally feasible in operating plants.

The noise method involves analysis of the fluctuating part of the signal that occurs in normal sensor outputs. A method based on time series analysis has been developed and tested. It involves estimation of the impulse response then integration of the impulse response to obtain the step response. The time constant is simply read from the step response curve. The only assumption in the method is that the temperature fluctuations responsible for the fluctuating output is completely random (white noise). Measurements in an operating reactor indicate that this assumption is valid for a hot leg sensor, but not for a cold leg sensor. The cold leg temperature fluctuations are influenced by the steam generator and the primary pump.

In general, the work reported here shows that there are at least three methods that can give the required response time. They differ in terms of situations in which they are valid, complexity, and cost of implementation. However, the limitations of each method are well understood, and matching a testing method to a given plant appears to be possible. Early applications should probably involve redundant measurements using different methods, but experience should reduce the need for this approach.

REFERENCES

1. M. Edelmann, "Two On-Line Methods for Routine Testing of Neutron and Temperature Instrumentation of Power Reactors," Kernforschungszentrum Karlsruhe report KFF 2316, July 1976.

2. R. M. Carroll, R. L. Shepard, and T. W. Kerlin, "In-Situ Measurements of the Response Time of Sheathed Thermocouples," Trans. Amer. Nucl. Soc., 21, 427 (June 1975).

3. I. Warshawsky, "Heat Conduction Errors and Time Lag in Cryogenic Thermometer Installations," Trans. Instrum. Soc. Amer. 13 (4) 335 (1974).

4. T. W. Kerlin, "Analytical Methods for Interpreting In-Situ Measurements of Response Times in Thermocouples and Resistance Thermometers," Oak Ridge National Laboratory Report ORNL/TM-4912 (March 1976).

5. G. E. P. Box and G. M. Jenkins, Time Series Analysis - Forecasting and Control, Holden-Day, San Francisco, 1970.

6. H. Akaike, "Power Spectrum Estimation through Autoregressive Model Fitting," Ann. Inst. Stat. Math., Vol. 21, pp. 407-419, 1969.

7. U. Grenander and G. Szego, Toeplitz Forms and Their Applications, University of California Press, Berkeley, 1958.

8. H. Akaike, "A New Look at the Statistical Model Identification," IEEE Tran. Aut. Cont., Vol. AC-19, pp. 716-723, 1974.

9. P. E. Caines, "Prediction Error Identification Methods for Stationary Stochastic Processes," IEEE Tran. Aut. Cont., Vol. AC-21, pp. 500-505, 1976.

10. R. L. Kashyap and A. R. Rao, Dynamic Stochastic Models from Empirical Data, Academic Press, New York, 1976.

11. R. L. Anderson, "Distribution of the Serial Correlation Coefficient," Ann. Math. Stat., Vol. 13, p. 1, 1942.

12. G. E. P. Box and D. A. Pierce, "Distribution of Residual Autocorrelations in Autoregressive Integrated Moving Average Time Series Models," Jour. Amer. Stat. Assoc., Vol. 64, 1970.